



HAL
open science

Studies on O₂ plasma modification and fluoroalkyl functional siloxane (FAS) coating effects on natural lignocellulosic coir fibers and development of coir based polypropylene (PP)/ethylene-propylene-diene rubber (EPDM) composites

Praveen Kosappallyillom Muraleedharan

► **To cite this version:**

Praveen Kosappallyillom Muraleedharan. Studies on O₂ plasma modification and fluoroalkyl functional siloxane (FAS) coating effects on natural lignocellulosic coir fibers and development of coir based polypropylene (PP)/ethylene-propylene-diene rubber (EPDM) composites. Materials. Université de Bretagne Sud; Mahatma Gandhi University, 2018. English. NNT : 2018LORIS495 . tel-01994907

HAL Id: tel-01994907

<https://theses.hal.science/tel-01994907>

Submitted on 25 Jan 2019

HAL is a multi-disciplinary open access archive for the deposit and dissemination of scientific research documents, whether they are published or not. The documents may come from teaching and research institutions in France or abroad, or from public or private research centers.

L'archive ouverte pluridisciplinaire **HAL**, est destinée au dépôt et à la diffusion de documents scientifiques de niveau recherche, publiés ou non, émanant des établissements d'enseignement et de recherche français ou étrangers, des laboratoires publics ou privés.



THESE / UNIVERSITE DE BRETAGNE-SUD
sous le sceau de l'Université Bretagne Loire

pour obtenir le titre de
DOCTEUR DE L'UNIVERSITE DE BRETAGNE-SUD

Mention :
Ecole doctorale:

Présentée par : PRAVEEN KOSAPPALLYILLOM MURALEEDHARAN

Préparée à l'unité mixte de recherche
(n°) : IRDL, FRE-CNRS 3744

Etablissement de rattachement : Université of South Brittany

Nom développé de l'unité : Institut de Recherche Dupuy De Lomé

Studies on O₂ plasma modification and fluoroalkyl functional siloxane (FAS) coating effects on natural lignocellulosic coir fibers and development of coir based polypropylene (PP)/ethylene-propylene-diene rubber (EPDM) composites

Thèse soutenue le 29th June 2018

Devant le jury composé de :

Prof. Laurent Vonna

Rapporteur (Université de Haute Alsace, Mulhouse, France)

Prof. Pascal Carriere

Rapporteur (Université de Toulon Var, Toulon, France)

Prof. Nandakumar KALARIKKAL

Examineur (Mahatma Gandhi University, India)

Dr. Hanna J MARIA

Examineur (Mahatma Gandhi University, India)

Prof. Yves Grohens

Directeur de thèse (Université de Bretagne Sud, France)

Prof. Sabu Thomas

Co-Directeur de thèse (Mahatma Gandhi University, India)



Studies on O₂ plasma modification and fluoroalkyl functional siloxane (FAS) coating effects on natural lignocellulosic coir fibers and development of coir based polypropylene (PP)/ethylene-propylene-diene rubber (EPDM) composites

*A dissertation submitted in the partial fulfilment of the requirement for the degree of
Doctor of Philosophy*

by

PRAVEEN KOSAPPALLYILLOM MURALEEDHARAN

University of South Brittany

Department of Sciences & Engineering Sciences

&

International and Inter University Centre for Nanoscience and Nanotechnology

Mahatma Gandhi University, India

Defended on 29th June 2018, in front of the following commission:

Prof. Laurent Vonna	Reviewer (Université de Haute Alsace, Mulhouse, France)
Prof. Pascal Carriere	Reviewer (Université de Toulon Var, Toulon, France)
Prof. Nandakumar Kalarikkal	Examiner (Mahatma Gandhi University, India)
Dr. Hanna J Maria	Examiner (Mahatma Gandhi University, India)
Prof. Yves GROHENS	Director of Thesis (Université de Bretagne Sud, France)
Prof. Sabu THOMAS	Co-Director of Thesis (Mahatma Gandhi University, India)

Dedicated to my Family

ACKNOWLEDGEMENT

At the outset, I praise the God Almighty for showering all the blessings upon me throughout the research work and making this thesis a reality

On this occasion, I express my deep sense of gratitude to my Thesis Directors, Prof. Yves Grohens and Prof. Sabu Thomas for the profound help and support throughout my research career. I am thankful to Prof. Yves for the opportunity given to me to spend a good amount of time at University of South Brittany (Université de Bretagne Sud), Lorient, and France. During this period, the fulfilment of my experimental investigations and analysis was realized only because of your guidance and timely directions were given for the same. I also would like to thank Prof. Sabu Thomas, Mahtma Gandhi University for accepting my candidature for pursuing research under his guidance. It was a turning point in my life to open the doors of research under his training. Prof. Thomas has nurtured my skills of research through his amazing teaching methodologies. He helped me in raising my interpersonal skills and developed my managerial skills through his training strategies. I also extend my thanks to his family, especially, Dr Anne George for the kind words of support.

I would like to express my heartfelt thanks to Dr. Nandakumar Kalarikkal, Mahatma Gandhi University for his valuable guidance and kind support throughout my research stay at MGU. His immense care and love always created a harmony during these days.

Collaboration in scientific research will foster the exchange of ideas and utilization of experimental facilities between the research groups which in turn help to overcome the bottlenecks of research easily. I was fortunate to collaborate with premier research institutes of my scientific interest. First of all, I would like to express my sincere gratitude to Prof. Miran Mozetic from Jožef Stefan Institute, Slovenia for his active collaboration by providing me support on plasma based technologies and characterization facilities to carry out my research. I am also thankful to the support given by Dr. Gregor Primc & Dr. Ita Junkar from Jožef Stefan Institute, Slovenia and Prof. Marija Gorjanc and Prof. Barbara Simoncic, from University of Ljubljana, Slovenia. During the initial phases of my research the support given by Prof. Mohan Rao from Plasma Processing Lab, Indian Institute of Science was really helpful. I would like to acknowledge Prof. Rao and Dr. Rajesh for their immense support and guidance during this period.

I was also fortunate to meet and share scientific discussions with academicians and scientists of various fields of Materials Engineering. I would like to acknowledge Prof. Manfred Stamm and Dr. Jürgen Pionteck from IPF, Dresden, Prof. S. O. Oluwafemi from University of Johannesburg, Prof. Joanna Izdebska from Warsaw University of Technology, Poland, Prof. Ishak Ahmad from Universiti Kebangsaan Malaysia, Dr. Pramoda Kumari PALLATHADKA from Institute of Materials Research and Engineering (IMRE), Singapore, Prof. Uros Cvelbar from Jozef Stefan Institute, Slovenia, Prof. RNDr. Petr Špatenka, Technical University in Liberec, the Czech Republic for their kind support throughout my research career.

I am much obliged to Dr. Isabelle PILLIN and Mr. Antoine KERVOELEN for their active support and guidance throughout my research stay at UBS. Under the guidance of these experienced instructors, I was able to work with sophisticated instruments in the laboratory systematically.

I express my sincere gratitude to Ms. Khadedja for giving me all the support like a sister during my research stay at UBS. Even if we had very short time together, I am much obliged to Mickaël Riou for her kind advice and help.

I also would like to thank Mr. Anthony MAGUERESSE, Dr. Mickaël CASTRO, Mrs. Françoise PÉRESSE, Dr. Stéphanie LEPARMENTIER, Mr. Hervé BELLEGOU, Dr. Benjamin Saulnier, Dr. Bastien SEANTIER, Dr. Morgane Deroine, Mr. Tran Manh-Trung, Mr. Abhishek Sachan, Mr. Kevin Henry, Dr. Yves-Marie Corre, Mr. Samuel Requile and Mr. David Siniscalco for their technical supports and for making a very good ambience at UBS.

I am indebted to Mrs. Axelle Guitton and Mrs. Noluenn Chauvin for their sincerity and commitment in doing my entire doctoral official works in time. I express my gratitude towards Mrs. Nolwenn for her help and corporation in doing official works at UBS.

I am grateful to all the faculty members, Post docs, and PhD scholars of International and Inter University Centre for Nano science and Nanotechnology (IIUCNN) for their support. I also would like to express my sincere thanks to all the technicians and office staff of IIUCNN.

I would like to thank Mr. Sajith T A for his kind support and active co-operation especially in the BRNS project. I am grateful to Mr. Jemy James for the care and support given especially

during my stay at Lorient, France. I would like to express my sincere gratitude to T M Martin George for his immense support during my research period by giving specific research comments, jointly working with me in experiments and brotherhood. I would like to thank Dr. Aparna BEENA UNNI for her kind support especially during my research travel to Lorient, France. I also would like to extend my thankfulness to Dr.Hanna J Maria, Dr.Ajithkumar M P, Mr.Ajay rane, Ms.Aneesa P, Dr.Deepu Gopakumar, Dr.Yasir Beeran, Mr.Sreerag Gopi, Mrs. Blessy Prince, Mrs.Ajitha P, Ms.Abitha V K for their kind support during my research stay at MGU. It is with great pleasure I express my heartfelt thanks to all my colleagues and friends

I would like to extend my sincere gratitude to SAINTGITS COLLEGE OF ENGINEERING, KOTTAYAM for allowing me to pursue my research by granting 3 years of leave and relieving me from the academic duties during this time.

I would like to mention the financial support of Board of Research in Nuclear Sciences (BRNS), Govt. of India during my research stay at MGU.

The utmost appreciation and thanks are given to my parents K.S Muraleedharan Elayathu and N Ushadevi for their unconditional love, prayers and support throughout my research period and it is the only reason for what I am today. My eyes are filled with tears when I remember my grandmother, Late. Smt. Thankammal Antherjanam on this occasion. From my childhood onwards, I was fortunate to receive the immense care and emotional support from her. Though in her physical absence, I bow my forehead to her food prints for the blessings. The acknowledgment would have been incomplete without mentioning my second half, Surya Krishna and my sweet daughter, Pradithya. Words are helpless in attempting to bring out my indebtedness to both of you. Your support and motivation make me strong and capable to complete this thesis, without you I could never have accomplished this dream. I also would like to express my sincere gratitude to my elder sister Dhanya and Family, my younger sister Divya and Family, Parents-in-law & Family for their unconditional love and support.

PREFACE

In recent years, the development of advanced high performance composite materials made from natural fibers was mainly focussed on achieving high modulus and strength materials. However, the high strength is not sufficient, as some of the materials possess brittle nature (the overall elongation to fracture is small), and one of the more important performance criterion should be the ability to absorb energy and resist impact loadings. The manner in which a composite material deforms and subjected to fractures depends upon both the chemical and mechanical properties of three basic constituents: the fibers, the matrix and a fine interphase region (sometimes referred to as the interface) responsible for assuring the bond between the matrix and fiber. The relative energy absorbing capability of the composite fracture modes (such as delamination, intralaminar matrix cracking, longitudinal matrix splitting, fiber/matrix debonding, fiber pull-out and fiber fracture) depends upon the basic properties of the constituents as well as the loading mode. It is known that the failure modes that involve fracture of the matrix or interphase region result in low fracture energies whereas the failures involving fiber fracture points to significantly greater energy dissipation.

Blending of thermoplastic matrices with elastomers, tuning the interfaces of fibers and thermoplastic elastomeric matrices by using suitable compatibilisers and modifying the fibers as well as matrix using various surface modification techniques are emerging as solutions to the enhancement of impact response of polymer composites. In this work the natural lignocellulosic coir fiber was selected as reinforcement for binary blends of polypropylene (PP) and high-molecular grade ethylene-propylene-diene rubber (EPDM). The extremely hydrophobic nanocomposites coating based on fluoroalkyl functional siloxane (exhibits water as well as oil repellent properties) was given to the coir fiber surface using sol-gel technique. The coir fibers were treated with O₂ plasma before applying FAS sol gel coating the fiber. Binary blends of polypropylene (PP)/ ethylene-propylene-diene rubber (EPDM) at varying concentrations of EPDM of 2.5, 5, 7.5, 10, 20 and 30 parts per hundred (volume fraction, $\phi_a = 0.02, 0.04, 0.06, 0.08, 0.15$ and 0.2) were prepared first by dry blending followed by melt compounding using a Brabender Plasticorder mixer. The blend composition of 100 parts per hundred (pph) polypropylene and 7.5pph EPDM was selected for composite fabrication, because it registered highest impact strength and the maximum pull out stress with coir fiber used in this study. Composites of PP/EPDM/Coir were prepared by varying the

concentration of coir fiber of 10, 20, 30 and 40 pph (volume fraction $\phi_f = 0.07, 0.13, 0.19$ and 0.24) using dry blending followed by melt mixing and compression moulding technique.

The entire thesis is classified into 7 chapters

The chapter 1 starts with a brief introduction to polymer surfaces and interfacial problems by giving descriptions about surface phenomena in polymeric materials and adhesion phenomena in bonding of polymers. Following these discussions, it then outlines most recent developments in the area of surface engineering of polymeric interfaces with special reference to plasma surface modification technique. Then it explores further discussions on plasma treatment of synthetic and natural fibers. Thereafter it illustrates a short description about organofunctional siloxane with special reference to fluoroalkyl-functional siloxane. The topics lignocellulosic coir fiber and impact modification of polypropylene were discussed further. Finally the objectives of the thesis will be defined.

The chapter 2 provides the details of different materials used in this work, the experimental techniques and procedures followed for developing the samples etc. It also gives the details of the characterization techniques used for analysing the samples developed in this study.

The Chapter 3 investigates the O_2 plasma induced effects on the surface properties of lignocellulosic natural coir fibers. . It includes plasma surface modification of coir fibers, optical emission spectroscopy to characterise plasma, the analytical techniques to characterise the fibers such as water absorption studies, morphological investigations using scanning electron microscopy (SEM) analysis, topographic measurements using atomic force microscopy (AFM) analysis and determination of elemental composition on coir fiber surface using X-ray photoelectron spectroscopy (XPS) analysis.

Chapter 4 investigates the fluoroalkyl functional siloxane (FAS) based hydrophobic coating induced effects on surface properties of lignocellulosic natural coir fibers. It includes preparation of FAS solgel coating on coir fibers using spray dry cure method, wettability analysis, water absorption studies, scanning electron microscopy (SEM) analysis, atomic force microscopy (AFM) analysis and X-ray photoelectron spectroscopy (XPS) analysis

Chapter 5 discusses about optimizations of coir fiber characteristics and blend formulations for composite fabrication. It explains the breaking strength analysis of elementary as well as FAS coated fibers using tensile testing method. It further discusses the procedure for melt

blending of polypropylene (PP) and high-molecular grade ethylene-propylene-diene rubber (EPDM) with different constitutive ratios. The tensile, impact and flexural analysis results of all blend formulations are discussed in detail. The morphological examinations of cryofractured and impact fractured surfaces were done using SEM and HRTEM to identify mechanisms of toughening in PP/EPDM blends. The low shear rate rheology and dynamic viscoelastic properties of blends were carried out to study rheological behaviour of PP/EPDM blends. Non-isothermal crystallisation kinetics, nucleation activity and glass transition temperature of blends were investigated using DSC analysis. The maximum degradation temperature of blends was obtained by thermo gravimetric (TGA) analysis.

Chapter 6 provides details of preparation and characterisation of PP/EPDM/Coir composites. The critical length of fibers & the fiber pull-out test results of uncoated and FAS coated coir fibers on all the PP/EPDM blend formulations are tabulated and discussed. The mechanical, morphological, rheological and thermal properties of PP/EPDM 7.5/Coir composites are tabulated and the inferences are discussed. The tensile, impact and flexural analysis results of all composite formulations are discussed in detail. The morphological examinations of cryofractured surfaces were done using HRTEM and impact fractured surfaces were done using SEM to identify mechanisms of toughening in PP/EPDM/Coir composites. The low shear rate rheology and dynamic viscoelastic properties of composites were carried out to study rheological behaviour of PP/EPDM/Coir composites. Non-isothermal crystallisation kinetics, nucleation activity and glass transition temperature of composites were investigated using DSC analysis. The maximum degradation temperature of composite was obtained by thermo gravimetric (TGA) analysis.

Chapter 7 provides a summary of all the chapters and objectives for future research work.

TABLE OF CONTENTS

Chapter 1: Introduction.....1-27

1.1 Introduction

1.2 Polymer surfaces and Interfacial problems

1.2.1 Surface phenomena in polymers

1.2.2 Adhesion phenomena in bonding of polymers

1.3 Surface modification strategies in polymer multiphase systems

1.4 Plasma processing of polymeric materials

1.5 Plasma treatment of fibers

1.5.1 Plasma treatment of synthetic fibers

1.5.2 Plasma treatment of Natural fibers

1.6 Organo functional siloxanes

1.6.1 Fluoroalkyl functional siloxane (FAS)

1.7 Lignocellulosic coir fiber

1.8 Impact Toughening of Polypropylene

1.9 Objectives of the work

1.10 References

Chapter 2: Materials and methods.....28-46

2.1 Experimental

2.1.1 Materials used

2.1.2 Methodology

2.1.2.1 Preparation of fibers

2.1.2.2 Plasma modification of fibers

2.1.2.2.1 Optical emission spectroscopy

- 2.1.2.2.2 *Water absorption studies*
- 2.1.2.2.3 *Scanning Electron Microscope (SEM) Analysis*
- 2.1.2.2.4 *Atomic Force Microscope (AFM) Analysis*
- 2.1.2.2.5 *X-ray photoelectron spectroscopy (XPS) Analysis*
- 2.1.2.3 *Fluoroalkyl functional siloxane (FAS) Sol-Gel coating on coir fibers*
 - 2.1.2.3.1 *Wettability analysis*
 - 2.1.2.3.2 *Water absorption studies*
 - 2.1.2.3.3 *Scanning Electron Microscope (SEM) Analysis*
 - 2.1.2.3.4 *Atomic Force Microscope (AFM) Analysis*
 - 2.1.2.3.5 *X-ray photoelectron spectroscopy (XPS) Analysis*
- 2.1.2.4 *Melt blending*
- 2.1.2.5 *Preparation of test specimens*
- 2.1.2.6 *Breaking strength analysis and Pull-out stress of coir fibers*
 - 2.1.2.6.1 *Pull-out test of coir fibers*
- 2.1.2.7 *Mechanical property analysis*
 - 2.1.2.7.1 *Impact analysis*
 - 2.1.2.7.2 *Tensile analysis*
 - 2.1.2.7.3 *Flexural analysis*
- 2.1.2.8 *Morphological Analysis*
 - 2.1.2.8.1 *High resolution transmission electron microscopy (HRTEM)*
 - 2.1.2.8.2 *Scanning Electron Microscopy (SEM)*
- 2.1.2.9 *Differential Scanning Calorimetry*
 - 2.1.2.9.1 *Non-isothermal Crystallization Kinetics*
 - 2.1.2.9.2 *Determination of glass transition temperature (T_g)*
- 2.1.2.10 *Thermo gravimetric analysis*

2.1.2.11 Rheological Analysis

2.2 References

Chapter 3: Plasma surface modification of lignocellulosic natural coir

fibers.....47-67

3.1 Plasma surface treatment

3.2 Optical Emission Spectroscopy

3.3 Water Absorption Studies

3.4 Scanning Electron Microscope (SEM) Analysis

3.5 Atomic Force Microscope (AFM) Analysis

3.6 X-ray photoelectron spectroscopy (XPS) Analysis

3.7 Inferences

3.8 Conclusions

3.9 References

Chapter 4: Development and Characterisation of Fluoroalkyl functional siloxane (FAS)

based hydrophobic coating on lignocellulosic natural coir fibers.....68-86

4.1 FAS Sol-gel coating

4.2 Wettability analysis

4.3 Water Absorption Studies

4.4 Scanning Electron Microscope (SEM) Analysis

4.5 Atomic Force Microscope (AFM) Analysis

4.6 X-ray photoelectron spectroscopy (XPS) Analysis

4.7 Tensile Analysis of uncoated and FAS coated coir fibers

4.8 Conclusions

4.9 References

Chapter 5: Mechanical, morphological, rheological and thermal properties of PP/EPDM blends.....87-113

5.1 Polypropylene (PP) and high-molecular grade ethylene-propylene-diene rubber (EPDM) blends

5.2 Mechanical property (Impact, Tensile and Flexural) analysis of PP/EPDM blends

5.2.1 Impact analysis of PP/EPDM blends

5.2.2 Tensile analysis of PP/EPDM blends

5.2.3 Flexural analysis of PP/EPDM blends

5.3 Morphological analysis of PP/EPDM blends

5.3.1 High-resolution transmission electron microscopy (HRTEM)

5.3.2 Scanning Electron Microscopy (SEM) Analysis

5.4 Rheological analysis of PP/EPDM blends

5.4.1 Low shear rate rheology

5.4.2 Dynamic viscoelastic property analysis

5.5 Non-isothermal crystallisation kinetics of PP/EPDM blends

5.5.1 Nucleation Activity

5.5.2 Glass transition temperature

5.6 Thermo gravimetric (TGA) analysis

5.7 Conclusions

5.8 References

Chapter 6: Mechanical, morphological, rheological and thermal properties of PP/EPDM 7.5/coir composites.....114-142

6.1 Determination of critical length of coir fibers

6.2 Polypropylene (PP) / Ethylene-propylene-diene rubber (EPDM) / Coir composites

6.3 Mechanical property (Impact, Tensile and Flexural) analysis of PP/EPDM/Coir composites

6.3.1 Impact analysis PP/EPDM/Coir composites

6.3.2 Tensile analysis of PP/EPDM/Coir composites

6.3.3 Flexural analysis of PP/EPDM/Coir composites

6.4 Determination of pull-out stress

6.5 Morphological analysis of PP/EPDM/Coir composites

6.5.1 Morphology of impact-fractured samples

6.6 Rheological analysis of PP/EPDM/Coir composites

6.6.1 Low shear rate rheology

6.6.2 Dynamic viscoelastic property analysis

6.7 Non-isothermal crystallisation kinetics of PP/EPDM7.5/Coir composites

6.7.1 Nucleation Activity

6.7.2 Glass transition temperature

6.8 Thermo gravimetric (TGA) analysis

6.9 Conclusions

6.10 References

Chapter 7: Conclusions and Future work.....143-147

7.1 Conclusions

7.2 Future Work

CHAPTER 1

INTRODUCTION

ABSTRACT

With the advent of emerging technologies all over the world at the end of 20th century and in the beginning of 21st century, the polymers have played a huge role in transforming the conceptual ideas into structural integrities useful for the mankind. New polymers are synthesised and the existing polymers are modified in order to meet the manufacturing requirements of engineering industries all over the world. The behaviour of polymers at the interfaces is of fundamental importance in a wide range of technologies and applications. Adhesion problems exist with the bonding of polymers, the adhesion of coatings to the polymer surfaces and interface / interphase problems associated with melt blended polymers and polymer micro as well as nano composites are recurring and challenging areas in polymer based industries. By a thorough understanding of the surface and interface phenomenon in polymer multiphase systems, one can engineer the interfacial properties by controlling the interface/interphase region leading to the development of advanced materials with multifunctional properties. The first part of this chapter discusses most recent developments in the area of surface engineering of polymeric interfaces with special reference to plasma surface modification technique. Then it explores further discussions on plasma treatment of synthetic and natural fibers. Thereafter it illustrates a short description about organofunctional siloxane with special reference to fluoroalkyl-functional siloxane. The topics lignocellulosic coir fiber and impact modification of polypropylene were discussed further. Finally the objectives of the thesis were outlined.

1.1 Introduction

With the growing global energy crisis and ecological risks, polymers are playing a vital role in five major areas where the needs of society faces huge technological challenges. It includes energy, sustainability, health care, security and informatics, defence and protection [1]. In order to fulfil the aforesaid diverse societal needs, advanced polymeric materials are developed either by synthesising new polymers or through the modification of existing polymeric materials. In most of the cases researchers always opt for the modification of existing polymers rather than synthesising new polymers considering the cost aspects. Polymers are a major class of materials and possess a very wide range of mechanical, physical, chemical, and optical properties. Polymers have increasingly replaced metallic components in various applications. These substitution reflect the advantages of polymers in terms of corrosion resistance, low electrical and thermal conductivity , low density, high strength-weight ratio(particularly when reinforced), noise reduction, wide choice of colours and transparencies, ease of manufacturing and complexity of design possibilities and relatively low cost .The major classification of polymers include thermoplastics, thermosetting plastics, biodegradable plastics and elastomers (rubbers).

The behaviour of polymers at the interface/interphases is having prime importance when advanced materials are developed via polymer modification techniques. Adhesion problems exist with the bonding of polymers, the adhesion of coatings to polymer surfaces and interface problems between different phases of melt blended polymers and polymer composites are recurring and challenging areas in polymer based industries. By a thorough understanding of the surface and interface phenomenon in polymer multiphase systems, one can engineer the interfacial properties by controlling the interface/interphase region leading to the development of advanced materials with multifunctional properties.

The first part of this chapter covers concise introduction to polymeric materials, followed by a description on their structure, properties, and applications. Then it addresses the salient features of polymer surfaces and interfacial problems with a brief overview of surface phenomena and adhesion phenomena in bonding of polymers. Finally, the major part of this chapter covers the relevance of plasma processing on polymeric materials and interfaces. This part starts with a basic introduction, continues with discussions on mechanism of plasma surface modification and effects of plasma treatment on fibers. Thereafter this chapter covers about plasma treatment of synthetic and natural fibers, organofunctional siloxanes with

special reference to fluoroalkyl-functional siloxane, lignocellulosic coir fiber, impact modification of polypropylene and finally the objectives of the thesis were outlined.

1.2 Polymer surfaces and Interfacial problems

To meet specific applications in par with growing demands of polymer industries, the nature of the polymeric material formulations are too complex to allow for the simultaneous optimization of bulk and surface properties. Due to the complexity in polymer formulations, it is also difficult to obtain both bulk and surface properties through a single polymer processing operation. Pre/post treatment of polymeric surfaces has, therefore, become a common practice in the fabrication of many polymeric materials and its end products. The ultimate aim of polymer surface modification is, either increase the potential for surface interactions (e.g., adhesion promotion or to obtain a hydrophilic surface) or to decrease the degree to which the surface interacts with a given material (e.g., release or antifouling applications or to obtain a hydrophobic surface). Hydrophilicity, hardness, adhesion, antifouling, antifogging, lubrication, biocompatibility, and conductivity, among others, are considered to be the main properties in demand.

The surfaces and interfaces of polymers are known to have important role in the final properties and end use applications of polymeric products. In the case of inhomogeneous polymer blends and composites, the interfaces between different phases are the decisive factor for final mechanical properties [2]. Not only the strength properties, even the aesthetic properties of the polymer product which might critically influence the decision for the purchase of the product, corrosion or scratch resistance, texture etc. are determined by surface composition and structure.

Hydrophilicity of a solid surface is an important property because controlling the surface wettability is crucial in many practical applications [3]. Surfaces with water contact angles larger than 150° are termed as super hydrophobic (SH) surfaces. These type of surfaces have enormous applications in areas such as antisticking, anti-contamination [4] and self-cleaning [5] etc. Based on the observations inspired from nature, it can be inferred that, the special functionalities of polymeric surfaces are usually not governed by the intrinsic property of materials but are more likely related to the unique micro- or nanostructures. Latest researches in this domain trends are now focussing on responsive wettability of surfaces. By combining special topographic structures onto functional surfaces with responsive wettability helps in designing surfaces with responsive switching between superhydrophilicity and super

hydrophobicity. A thorough knowledge of surface phenomenon in polymers as well as adhesion phenomena in bonding of polymers is essential to design the surface modification strategies suitable for respective material surfaces with specific properties.

1.2.1 Surface phenomena in polymers

Last few years has witnessed the dedicated research on surface modification of polymeric materials because of its enormous applications in applied surface science and engineering. It includes applications in biomaterials, coatings and thin films, demanding the smooth, coloured or scratch resistant surfaces, appearance, durability and stability which are directly or indirectly linked with external interfaces. Also the gross behaviour (bulk properties) of material requires properties such as toughness or impact resistance of polymers, which are connected with defect, void or crack formation, which involves internal interfaces. The polymer surfaces are different in nature compare with its bulk part due to difference in molecular weight, addition of functional modifiers such as surfactants, compatibilizers, coupling agents, antioxidants, fire retardants etc., segregated lower energy components such as lubricants, and migration of additives across the interfaces while contacting with another surfaces. The most acceptable method to read the surface characteristics and to measure the surface energy state is the determination of surface tension. This is done by examining the outermost layers of atoms which is typically below 0.2nm depth [6]. The work which is required to increase the size of the surface of a phase is referred to as the surface tension. If the phase is a solid, the equivalent term surface free energy is commonly used. If the adjacent phase is a liquid or a solid, reference is made to interfacial tension. Compared with the bulk phase, a molecule at the surface of a material meets fewer molecules with which it can form interactions. Presence at the surface is therefore less beneficial from an energy point of view. However the property, surface tension, reflects the strength of bonding within the bulk material. The energy necessary to break these bonds is called the surface energy. In thermodynamics perspective, the surface tension can be define as the partial differential of the Gibbs free energy (G) of the system with the respect to the area (A), at the constant temperature (T) and pressure (P) [7].

$$\gamma = \left[\frac{\partial G}{\partial A} \right]_{T, P} \dots \dots \dots (1)$$

In the thermodynamic consideration of surface energy, the surface free energy can be defined as the excess of free energy associated with the surface (A), between the total free energy (G) of the system (G) and the one in the bulk (G^B) [7].

$$G^S = \frac{G - G^B}{A} \dots\dots\dots (2)$$

Hard solids are referred as ‘high energy surfaces’ (e.g. metals and their oxides, ceramics having surface tension $\sim 500\text{--}5000 \text{ mJ/m}^2$) due to its very different binding forces (covalent, ionic, metallic). Weak molecular solids and liquids are referred as low energy surfaces (surface tension $< 100 \text{ mJ/m}^2$) due to van der Waals forces and hydrogen bonding. Most of the polymers are considered as low energy surfaces where the interactions between the chains are dominated by van der Waals forces and hydrogen bonds. Surface and interfacial tensions of polymers significantly effect in wetting and coating processes, in melt blending of polymers and its composites, behaviour of colloidal dispersions, adhesion, friction, biocompatibility and also in corrosion and adsorption processes. The surface tension of polymers, in general, is determined from the contact angle analysis by positioning a liquid on the sample surface as shown in Fig. 1. On the other hand the interfacial tension between different polymers and between a polymer and a substrate is much more difficult to obtain than surface tension. The reason for difficulty in measurement of interfacial tension is due to high viscosities of materials, long time scales for achievement of equilibrium and sample decomposition etc. However the interface width and compatibility of polymer materials can be determined on the basis of model assumptions using mean field theory [6].

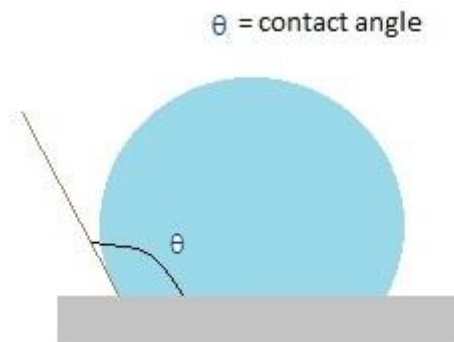


Fig.1.1 Schematic illustration of contact angle measurement

1.2.2 Adhesion phenomena in bonding of polymers

According to ASTM International, the 'adhesion' can be defined as a state in which two surfaces are held together by interfacial forces, which may consist of valence forces or interlocking forces or both [7]. Though adhesion is an interfacial phenomenon, the experimentally measured adhesion depends upon many factors in addition to events at the adherend-adherate interface. The material which adheres to the adherent is known as adherate. Thin films, thick films, coatings, and paints etc are common examples of adherate. An adhesive is a special type of adherate in which it adheres to two adherends [8]. The materials which are commonly used as adhesives fall under the category of polymeric materials. Only high molecular weight materials having long-chain molecules are expected to possess pronounced adhesive properties [9]. It is important to mention that, rather relating adhesion to wetting, where it is incorrectly approached the bonding as a thermodynamically reversible phenomenon, the testing of bond strength by analysing type of failure though determination of the type of separation is more practical approach for quantifying adhesive bond strength. Adhesion reflects not only fundamental adhesion (refers to the forces between atoms at the interface) but also the mechanical response of the adhesive, substrate and interfacial region (Practical adhesion-refers to the results of the various tests of adhesion of adhesive joint or coating or composites such as shear, peel, tensile strength obtained from the related tests). The prime requirement for a successful bond between two phases is to establish contact at a molecular or atomic level. It can be seen that there is no unique mechanisms of adhesion applicable to all adhesion cases and particular case of adhesive bonding needs to be studied and explained. In order to derive some useful predictions associated with adhesion phenomena at polymer-polymer interfaces, mechanical theory, adsorption theory, chemical theory, diffusion theory, electrostatic theory, rheological theory and weak boundary layer theory etc. are studied by various researchers. Mechanical theory of adhesion relates the interlocking (on a macro scale as well as on a micro scale) of the solidified adhesive material with the roughness and irregularities of the surface. However the attainment of good adhesion with smooth adherands (such as glass, where surface roughness is comparatively low) restricts the general validity of mechanical theory. The adsorption theory works based on the concept of adsorption and it proposes that the formation of a strong bond between adhesive and adherent is attained via intermolecular forces. On the basis of the magnitude of bond energy, the types of bonds are classified into primary bonds (ionic, covalent, metallic) and secondary bonds (van de Waals etc.). Chemical theory considers molecular bonding as the

most widely accepted mechanism for explaining adhesion between two surfaces in close contact. This theory explains intermolecular forces between adhesive and substrate are due to dipole-dipole interactions, van der Waals forces and chemical interactions (that is, ionic, covalent and metallic bonding). According to diffusion theory, diffusion of polymeric chains across the interface determines the adhesion strength. Appreciable diffusion does not take place in systems involving one or more hard solids (such as metals, glass, oxides, etc.) under normal conditions of temperature and time scale. According to Electrostatic theory, when two dissimilar polymeric materials are brought into contact, a charge transfer takes place which results in the formation of an electrical double layer. According to rheological theory adhesion occurs due to the interpenetration of substrates across an interface. Weak boundary layer theory (WBL) explains the premature adhesive failure due to the existence of WBL's at the surface [10]. The right blend of knowledge of the chemical composition of the polymer surfaces along with adhesion strength tests will uncover the correlations between the chemical bonding mechanism and adhesion. By modifying the surface chemical structures, the adhesion strength can be tailored for specific applications.

1.3 Surface modification strategies in polymer multiphase systems

One of the principal focus of research in polymer surface science and interfacial engineering has been on improving adhesion at the polymer-polymer interface in order to achieve useful polymer blends and tailored composites. Multiphase polymer blends or composites often have poor physical properties because of low adhesion at the polymer-polymer interface. It is known that, for compatibilization, the favourable enthalpic interactions between the segments of a block copolymer and a homopolymer substrate will enhance adhesion by virtue of interpenetration of the copolymer segments into that phase. As the availability of such preformed copolymers is limited, a potentially viable alternative is to form these copolymers in situ by reactive processing during blending, coextrusion, or thermal lamination using functionalized polymers. i.e., the functionally reactive groups can be attached directly to the two immiscible polymers of interest or attached to other polymers which form miscible mixtures with these phases. The chemical reactions at the polymer-polymer interface are also responsible for promoting adhesion. These principles were widely adopted for developing polymer blends/composites which shows toughness characteristics [11]. The surface modification of polymeric materials has been of great research interest in the last few years because of its importance in applications such as biomaterials and coatings [12]. Among the

various known techniques, three major surface modification principles which allow the optimization of functional polymer architectures are surface segregation, surface structure, and surface reorganization. These functional polymer architectures can be used for producing adhesive and release surfaces, the suppression of dewetting by the use of functional additives to lower the surface tension of a coating, and the creation of smart polymer surfaces with selective adhesion properties [13]. If the goal of surface modification is to create a hydrophobic surface, then the functional group usually has a lower surface free energy than the polymer backbone and if adhesion promotion is the objective of surface modification, then functional group will have higher surface energy than polymer backbone. In order to design functionalised polymers fundamental knowledge of different facets are required. It includes the appropriate selection of chemistry to introduce specific functional groups, different techniques to incorporate functional groups, processing, rheology, interfacial adhesion, mechanical properties, morphological analysis of blends, fracture characteristics etc.

1.4 Plasma processing of polymeric materials

Plasma-based technologies are emerging to be a proven technology which provides an efficient, economic and versatile solution to adhesion problems. Plasma technologies find increasing applications in the domain of polymer chemistry in terms of both materials processing and synthesis .Plasma based technologies can be used to synthesise new class of polymeric materials, with a unique set of properties from an organic or mixed organic–inorganic precursor , for which the structure-property relationships can be varied considerably depending on the final application .Using plasma as a surface modification technique, polymer surfaces can be activated with specific functional groups thereby design the surfaces for various applications of interest (i.e., for the treatment of polymer substrates by a reactive or inert gas aiming at a specific surface functionalization).

The plasma is defined as a partially ionized gas containing ions, electrons, various neutral species and photons at many different levels of excitation. Khelifa et.al proposed a more accurate definition of plasma based on the works of Grill and Bittencourt as “a quasi-neutral gas of charged and neutral particles characterized by a collective behaviour” [14]. When various plasma species interact with a polymer surface, a number of physical and chemical changes occur at the plasma-surface interface. If the objective is to modify the polymer surface using plasma, upon plasma treatment, the free electrons gain energy from an imposed

electric field, colliding with neutral gas molecules and transferring energy. These collisions and transfer of energy form free radicals, atoms and ions which then interact with the solid surfaces placed in the plasma. i.e., the energy and momentum of the plasma activated species will be transferred to the lattice atoms at the solid surface. This leads to drastic modifications of the molecular structure at the surface, providing the desired surface properties [15].

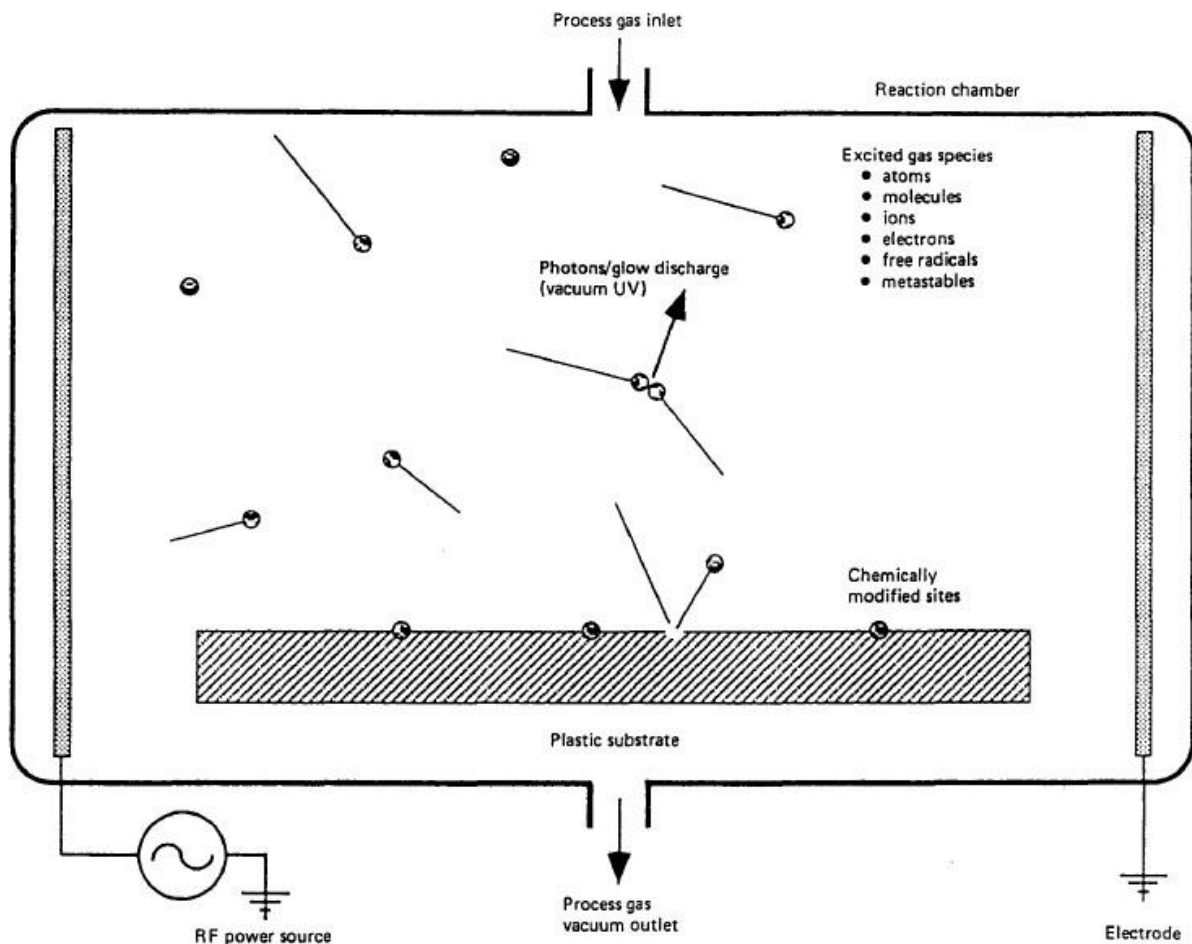


Fig.1.2.Schematic of the surface modification of plastic in a gas plasma reactor (Reproduced with permission from Elsevier)

The plasma process causes changes only to the few molecular layers from the surface of the material subjected to plasma treatment. The plasma treatment also changes the molecular weight of the surface layer by scissioning (reducing the length of molecules), branching and cross-linking. The type of gas used and the composition of the material surface have a major role in deciding the intended change in the surface of the material. The selection of the process gas decides how the plasma treatment will alter the surface of polymeric material.

The oxygen plasma treatment is regarded as the most commonly used plasma process to enhance adhesion. The oxygen plasma is aggressive, and forms numerous components such as O^+ , O^- , O_2^+ , O_2^- , O , O_3 etc. During plasma processing these components recombine and results in release of energy and photons. The photons in the ultra violet region have enough energy to break the polymer's carbon-carbon and carbon-hydrogen bonds. If the energy of the activated species is not sufficient to break the bonds at the surface, it will transfer a part of its energy onto the surface results in localised heating. In addition to this the incoming high energy ions also resulting in ion implantation by impinging into the material. When neutral atoms, having very low kinetic energy, are interacting with the material surface, the chemical changes are induced mostly by the recombination of activated species on the surface. The fluorinated plasmas are known to reduce the surface energy and increase the chemical inertness whereas the noble gas plasmas induce surface crosslinking. One of the great advantage of plasma treatment in comparison with chemical method is “plasma by-products” do not require special handling and are readily removed by the vacuum system. To understand the complex reaction between the plasma and the surface of the polymeric material, the understanding of the plasma parameters and their effect on the surface modification is essential. It is important to consider the effect of all the plasma properties including microscopic plasma parameters like ion energy, ion flux, degree of ionization, etc.in addition to macroscopic properties such as excitation source power and time of exposure to analyse the surface modification of polymers. Optical emission spectroscopy, Langmuir probe analysis etc are the commonly used techniques to characterise plasma and diagnose plasma parameters [16].

The three competing mechanisms which alter the polymers upon plasma treatment are ablation, cross linking and functionalization. The above three mechanisms occur simultaneously to initiate the required change. The extent of each mechanism depends on the chemistry and the process variables.

Ablation

Ablation results in the evaporation of surface material. Upon treatment, the plasma breaks the covalent bonds of the polymer backbone by bombardment with high-energy particles such as free radicals, electrons and ions. As a result, long molecules become shorter, their volatile oligomers and monomers boil off (ablate) and are swept away with the exhaust. The bond breaking occurs on the polymer surface usually with the oxygen plasma [15].

Crosslinking

Surface crosslinking is usually carried out with an inert process gas (oxygen-free argon or helium) and /or with noble gases. As there are no oxygen by-products in the plasma, the molecule can form a bond with a nearby free radical on a different chain (cross-link) [15].

Functionalization (activation)

In the activation process, the functional groups present on the surface of polymeric material are replaced with atoms or chemical groups from the plasma. In this process, upon plasma treatment the plasma breaks the polymer's backbone or groups from the backbone, creating free radicals on the surface. The new groups formed on the polymer surface can alter its adhesion characteristics. i.e., the type of atoms or groups substituted during plasma treatment determines how the surface will behave [15].

From the engineering point of view, the modified polymer surfaces are very important as they serve as interfaces of blends/composites which are used for high-performance applications [17].

1.5 Plasma treatment of fibers

Plasma surface modification is an effective approach to enhance the surface properties of fibers and fabrics in many applications. Natural fibers (such as cellulose based fibers, lignocellulose fibers etc), synthetic fibers such as glass fibers, carbon fibers etc, polymeric fibers and/ or even metallic fibers can be modified by plasma treatment technique. The plasma surface treatment modifies the chemical and physical properties of fibers which in turn compatibilises their reinforcements in composite systems. Since the fibers and matrices are chemically different strong adhesion at their interface is needed for the effective transfer of stress and bond distribution throughout the interface. The plasma surface modification improves the bonding strength between fibers and matrix without affecting their bulk properties. The plasma treatment of fibers can increase its surface energy by modifying the surface chemistry. Greater surface energy corresponds to greater chemical reactivity and compatibility.

1.5.1 Plasma treatment of synthetic fibers

The synthetic fibers such as carbon fiber, glass fiber, aramid fiber, kevlar fiber, graphite fiber etc are known to possess good mechanical properties and also having a well-developed

manufacturing base. However these fibers having a ‘weak’ outer layer which causes reduction in mechanical properties when embedded in polymer matrices. The surface modification techniques are employed to remove the ‘weak’ outer layer of the material which in turn increase the number of surface active groups, thus providing a more intimate contact between the fiber and the polymer, either by enhancing the level of van der Waals forces, or to facilitate covalent bond formation [18]. The chemical surface modification techniques usually poses health and safety and environmental risks. Also it is easy to over-treat and damage parts. The plasma surface modification is emerged as an environmental friendly technique for the surface engineering of both synthetic as well as natural fibers. The plasma treatment of carbon fibers have been studied by various research groups [19-22] in order to obtain better adhesion ,interfacial properties with polymer matrices and resulting mechanical properties of the composites. Oxygen plasma treatment in case of carbon and polymeric fiber materials increase the degree of nano-roughness on the surface and removes contaminant substances. The surface of the plasma treated fibers was rougher than that of pristine fibers leading to more mechanical interlocking. After plasma treatment, different polar functional groups such as carboxyl and hydroxyl groups were observed on the surface of carbon fibers. Lee et.al. reported that obtained surface characteristics by plasma treatment will help to overcome the drawbacks of recycled CF by restoring mechanical and chemical properties comparable to those of fresh carbon fiber reinforced plastics (CFRP) [23]. Okajima et al reported that the plasma activated carbon fibers (ACFs) were used as the electrodes of an electric double-layer capacitor and showed an enhanced capacitance effect after a RF-plasma treatment [24].

Plasma surface treatment of glass fibers shows the improvement of interfacial shear strength (IFSS) properties [25-26]. Lim et.al investigsted that plasma surface modification of glass and glass fibers enhanced the surface resistance rate and dielectric property. Surface modification process of plasma-treated glass fiber is shown below [27].

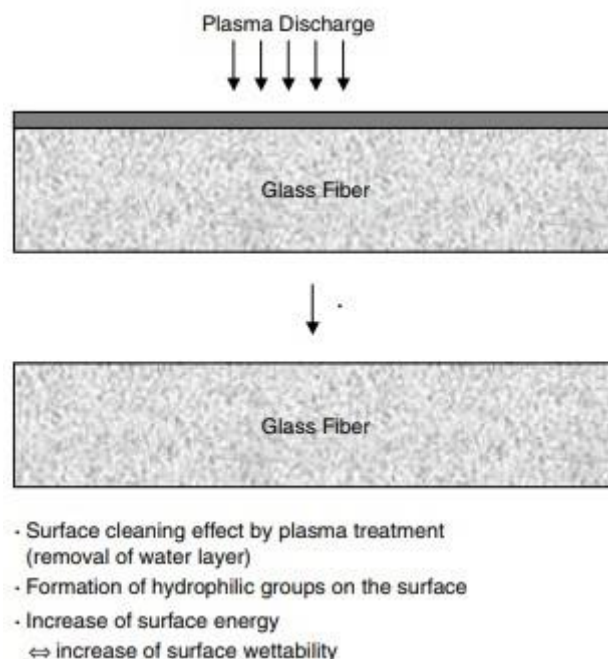


Fig.1.3. Surface modification process of plasma treated glass fibers

Plasma treatment of glass fibers leads to the generation of numerous free radicals, the cleaning action of removing water layers on the glass fiber surface and the prevention of a weak boundary layer. Plasma treatment results in improvement of the surface wettability, the surface activation energy and forms desirable interfacial binding of glass fibers with epoxy resins.

Kevlar fiber, characterized by high tenacity, high modulus and strength, and low electrical conductivity compared with metallic and carbon fibers, is widely used in the manufacturing of advanced high performance composites[28]. Tribological properties between kevlar fibers and most resins is poor because of the high crystallinity and smooth surface of the kevlar fiber resulting in chemical inertness. Guo et al investigated that the plasma treatment generates oxygenic and nitrogen based functional groups on the surface of the fabric, together with an increase of the surface roughness, strengthening the bond between the kevlar fabric and phenolic adhesive resin and hence improving the tribological properties of the Kevlar fabric/phenolic composites. Su et al found that oxygen-plasma treatment significantly changed the interfacial adhesion by changing the chemistry and morphology of the surfaces of the kevlar fibers which in turn results in improved interlaminar shear strength, water resistance and dielectric properties of the final composite material[29]. Wang et al investigated that the aramid fiber surface was roughened by plasma treatment enhancing the

mechanical bond with the poly(phthalazinone ether sulfone ketone) resin [30]. Park et al indicated that modified the surface roughness of aramid fiber increased mechanical interlocking between the fiber surface and vinyl ester resin [31].

1.5.2 Plasma treatment of Natural fibers

The growing global energy crisis and ecological risks lead to the growing interest on natural and sustainable materials, like natural fibers, in order to replace synthetic or non-renewable sources of materials. Natural fibers are known to be the prime source for cellulose content around the globe. The natural fibers are composed of cellulose as the major component with some non-cellulosic components. The non-cellulosic components include lignin, hemicelluloses, protein, pectin, ash, waxes, sugars, pigments etc. Due to the poor adhesion between the hydrophilic natural fibers and hydrophobic polymer matrix, large moisture uptake, and poor flame-retardant properties questions its viability in many applications. Due to the environmental friendly nature, plasma surface modification is emerged as a new technique to modify the natural fibers. Many research groups have studied the influence of low-pressure plasma treatment on cellulose fibers to improve the adhesion between a polymeric matrix and natural fibers. Farias et al investigated that low pressure oxygen plasma surface modification of coir fibers partially etched the amorphous layer which covers most of the fibers pointing to the surface lignin removal. As a result, the surface roughness has increased and partially exposed the crystalline cellulose underneath [32]. Praveen et al also investigated that low pressure oxygen plasma converts coir fiber surface to extremely hydrophilic. Chapter 3 explained the details of this work. Enciso et al reported that low pressure plasma treatment of flax fiber improves adhesion between flax fiber surface and polyethylene matrix [33]. Sarikanat et al investigated that the mechanical properties of flax fiber-reinforced polyester composites such as flexural strength, flexural modulus, ILSS, tensile strength, and tensile modulus were improved successfully by modifying the flax fiber surface via atmospheric air and argon plasma treatments [34]. Oliveira et al found that the plasma treatment of coir fibers causes an increase in hydrophilicity and surface roughness, enabling them better sorption properties [35]. Volokitin et al efficiently used low-temperature plasma to create a protective-decorative coating on the surface of wood species. After processing with plasma, the material retains its environmental quality, while improving its physical, mechanical and decorative properties. When the surface of wooden products is exposed to low-temperature plasma the polished layer having high performance properties,

such as decreased permeability, destruction of fungal diseases and timber mold, a wonderful manifestation of the texture of wood and color (golden brown), and increased resistance to abrasion is formed. [36]. Acda et.al showed that plasma modification resulted in significant improvement in work of adhesion for the three wood species [37]. Cho et al treated wood with hydrophobic plasma polymers to reduce the water penetration [38].

Seki et. al investigated that RF plasma system is more effective in improving the interfacial adhesion between the jute fiber and polyester matrix [39]. O₂ plasma treatment also improved the tensile and flexural strengths of jute fiber/ polyester composites. Gibeop et al investigated that etching effect of the plasma treatment creates the rough surface for the jute fiber, enabling good interlocking between jute fiber and PLA matrix [40]. Sever et al found that when RF plasma system was used, the interlaminar shear strength (ILSS) values of the Jute/HDPE composites increased with increasing plasma power [41]. Oliveira et al found that the plasma treated banana fibers showed significant improvement in hydrophilicity and spreading of distilled water after treatment in the fiber's surface [42]. Gorjanc et al investigated that the CF₄ plasma treatment caused substantial etching of the fibers and led to a dramatic increase in the surface roughness, which, in turn, led to higher adsorption of silver nanoparticles [43]. Vasiljevic et al. investigated that the plasma pre-treatment increased the effective concentration of the FAS network on the cotton fabric, which resulted in enhanced water repellency before and after repetitive washing, compared with that of the FAS-coated fabric sample without the plasma pre-treatment [44].

1.6 Organo functional siloxanes

Polysiloxanes are a large and most important group of various inorganic-organic (hybrid) compounds and materials, composed of silicon and oxygen atoms in their main chain and organic substituents bound to silicon..Organofunctional siloxanes are hybrid compounds that combine the functionality of a reactive organic group and the inorganic functionality of an alkyl silicate in a single molecule. Organofunctional silanes act as molecular bridges between organic polymers and inorganic materials. A schematic diagram is shown in figure Fig.4.

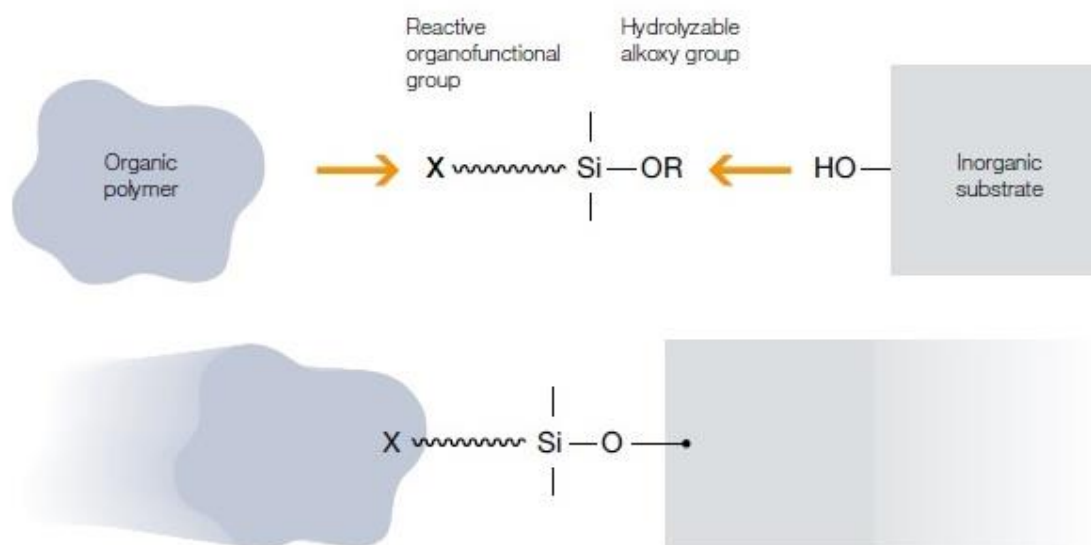


Fig.1.4. Organofunctional siloxanes as molecular bridges

(Reproduced with permission from Wacker Chemie AG, München, Germany) [45]

The choice of functional group X will depend ultimately on the nature of the organic polymer. Commercially available silanes contain amino, epoxy and glycidoxy, mercapto and sulfido, isocyanate, methacryloxy and vinyl groups. Bonding to the inorganic material is effected by way of the hydrolyzable functional groups –OR. The most common of these are the methoxy and ethoxy substituents. The silane’s alkoxy groups hydrolyze in the presence of moisture to form reactive silanols. These either react with themselves to form oligomeric siloxanes, or else react with the inorganic substrate [45].

1.6.1 Fluoroalkyl functional siloxane (FAS)

If the functional group ‘X’ denotes an organic polymer having formula $(\text{CH}_2)_n\text{C}_m\text{F}_{2m+1}$, it belongs to the class of fluoroalkyl-functional siloxane. The complete structure is shown in figure Fig.5. It exhibits benefits such as extremely low surface tension, incompatibility with aqueous and non-aqueous media and aesthetics. Due to its low surface tension characteristic, it can be used for producing release surfaces. It also finds applications in stain resistant and easy clean coatings, non-aqueous antifoams, crude oil, solvent borne coatings, coatings for special effects, hammer finish, oil resistant elastomers, auto parts and where oil resistance/chemical resistance is required [46].

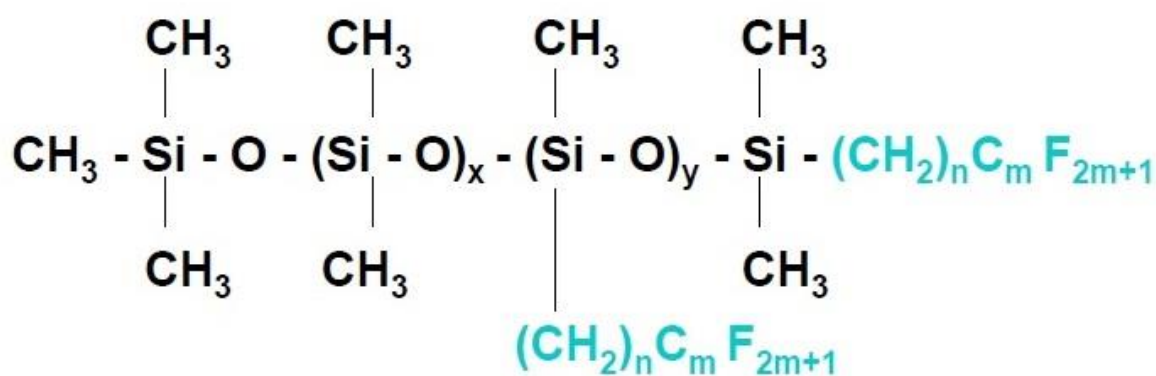


Fig.1.5.Chemical structure of fluoroalkyl functional siloxane [47]

1.7 Lignocellulosic coir fiber

Coir is known to be an inexpensive fiber among the various natural fibers available in the world. Coir is a natural lignocellulosic fiber obtained from the fibrous mesocarp of coconut, the fruit of coconut tree (*Cocos nucifera*) cultivated extensively in the tropical countries. Coir fiber is obtained by dehusking the coconut fruit. The major step involved in dehusking is a bacteriological process known as retting. Retting involves soaking the husks in saline backwaters for about 4 to 12 months. During this process, the phenolic material is removed, which gives strength to the outer covering of the husk. It loosens the fiber interior and as a result the fibers can be easily extracted [47]. Coir is a hard fiber having length varying from 150 to 300 mm and diameter of 250 to 350 μm depending on the type of the coconut. The physical properties and chemical composition of coir fiber are tabulated in Table 1.9

Table 1.1 Physical properties and chemical composition of coir fiber

Constituents	Composition (%)	Diameter(μm)	Micro fibrillar angle ($^{\circ}$)
Cellulose	36-43	250-350	30-49
Lignin	41-45		
Hemicellulose	0.15-0.25		
Pectins	3-4		
Water soluble materials	7-8		

A typical cross section of coir fiber viewed under scanning electron microscopy (SEM) is shown in figure Fig.6

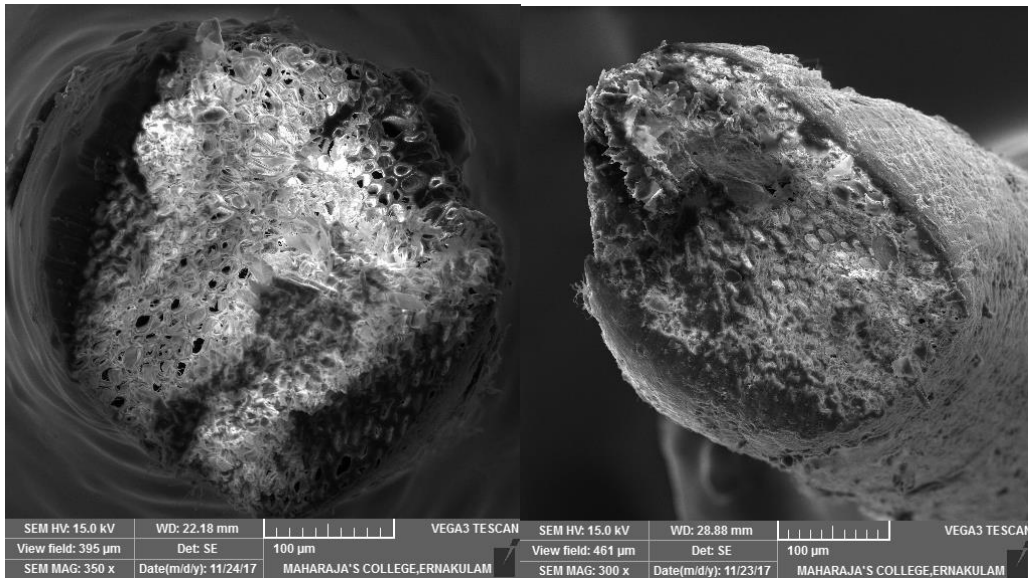


Fig.1.6. Cross sectional view of coir fiber

Coir is a multicellular fiber which contains 30 to 300 or more cells in its cross section, which is polygonal to round in shape. These cells are 12-14 µm in diameter and are arranged around the central pore that is called lacuna. Like other natural fibers, the microstructure of coir fiber comprises of different hierarchical structures. Each fiber cell is constituted by four concentric layers, with the “primary” layer on the outside and three “secondary” layers inside (viz. outer secondary wall, middle secondary wall and inner secondary wall). Primary layer is porous in nature and these pores act as diffusion paths of water through the layer. It is initially cellulosic but become lignified on growth. It also consists of pectin and other nonstructural carbohydrates. The secondary layer is developed on to the inner surface of the primary layer, which comprises of a number of cylindrical, long, sheath-like and anisotropic cellulosic micro-fibrils. These cellulosic microfibrils are surrounded and joined by a macromolecular network of lignin-hemicellulose matrix.

All the secondary walls are fibrillar in nature and vary in composition and microfibrillar angle (orientation of the micro-fibrils, i.e., micro-fibrils present in the middle secondary wall are spirally arranged about the fiber axis at an angle). The lumen in the centre of the fiber contributes to the water uptake properties of the fiber [48].

Cellulose is a linearly aligned polymer which contains anhydro-β-D-glucopyranose units linked by 1,4-oxygen linkages. Cellulose is polymorphic and exist in two crystalline forms cellulose-I and cellulose-II. The cellulose-I is highly crystalline with about 80% crystallinity whereas cellulose-II is comparatively less crystalline (60%). The crystallinity of the fiber is

due to the presence of crystalline cellulose. But cellulose-I is more commonly used to represent cellulose. It is stiff and straight due to intra chain hydrogen bonds formed between the hydroxyl groups and oxygen atoms of neighbouring ring molecules which stabilises the cellulose chains.

Hemicellulose belong to a group of heterogeneous polysaccharides which are formed through biosynthetic routes different from that of cellulose and it forms hydrogen bonding to cellulose and acts as cross-linking molecule between the cellulose micro-fibrils. Unlike cellulose, hemicellulose are low molecular weight polymers. Most hemicellulose have a degree of polymerization of only 200. The solubility and susceptibility to hydrolysis of hemicellulose are comparatively greater than cellulose. Hemicellulose consists of hexosans such as glucosan, galactan and mannan, pentosans like araban, xylan and polyuronides of gluconic acid [49].

Pectin is located between the cellulose microfilaments of the cell wall. Pectins are polyuronides and consist exclusively of galacturonic units. Pectins decrease as plant tissues mature and it may undergo transformation to hemicellulose and lignin.

Lignin is a complex amorphous cementing material, which consists of phenyl propane derived structural units nonlinearly and randomly linked. The structure of lignin is complicated by the various ways in which these units are joined. The lignin content increases as the plant matures and the fiber becomes stiffer and tougher [50].

1.8 Impact Toughening of Polypropylene

Polypropylene (PP), a thermoplastic polymer is known to be one of the widely used commodity plastic due to its good mechanical, electrical, and chemical properties and good resistance to tearing. The toughening has been one of the most active and relevant area in the field of the modification for polypropylene plastics. Bucknall et al. reported that the incorporation of a secondary rubbery phase in PP is usually achieved both by propylene–ethylene block copolymerization and by melt blending of PP with ethylene–propylene rubber (EPR) and ethylene–propylene–diene terpolymer (EPDM) [51]. These blends are rarely miscible and often form a multiphase morphology [52-53]. Yokoyama et al. investigated that, for a constant level of the total rubber content, the incorporation of EBR as the elastomeric component improved the fracture toughness of PP blends. Improvement of the fracture resistance was also obtained by increasing the molecular weight of the elastomers [54].

Only few researches have been done to examine the rubber toughening mechanisms in semi crystalline polymers. Because of the complex polycrystalline nature, additional possible mechanisms may be anticipated for toughening crystalline polymers. Jang et al. reported that by acting as a nucleus for the crystallization of matrix polymer, the rubber particles may serve to reduce the average spherulite size, thereby increasing the impact resistance of polymer [55]. In addition to this, other morphological changes induced by the rubbery phase may also occur.

Though the impact response of polypropylene can be increased considerably by elastomer addition, the enhancement of the toughness is obtained at the expense of the stiffness, elastic modulus, and thermal resistance. According to latest research trends in recent years, ternary phase blends of PP containing soft elastomer and rigid fillers are of ever-increasing interest because both their stiffness and toughness can be partly controlled and materials with balanced mechanical properties can be formulated [56]. Considering the growing ecological risks and cost aspects, researchers have studied the effect natural fibers [57-60] as rigid fillers in of PP containing soft elastomer systems. Though natural fibers possess several advantages over synthetic fillers, adhesion between the fiber and matrix, moisture repellence, flame retardant properties etc are still challenging areas to be addressed.

1.9 Objectives of the work

1. To develop fluoroalkyl-functional siloxane (FAS) as a hydrophobic coating to natural coir fibers with enhanced water repellent properties
2. To develop plasma surface modification technique as a viable method to improve wettability characteristics of lignocellulosic natural coir fibers
3. To develop an efficient method to optimize critical length of natural coir fiber with PP/EPDM matrix.
4. To develop hydrophobic coir based PP/EPDM composite with high impact resistance properties
5. To study the mechanical properties of PP/EPDM blends using tensile, impact and flexural analysis.
6. To study the morphological features of PP/EPDM blends using scanning electron microscopy (SEM) and High-resolution transmission electron microscopy (HRTEM)
7. To study the low shear rate rheology and dynamic viscoelastic properties of PP/EPDM blends using rheological analysis.

8. To study the non-isothermal crystallisation kinetics of PP/EPDM blends with the aid of differential scanning calorimetry (DSC) analysis
9. To study the (maximum degradation temperature of PP/EPDM blends with the aid of thermo gravimetric (TGA) analysis
10. To study the mechanical properties of PP/EPDM/Coir composites using tensile, impact and flexural analysis.
11. To study the morphological features of PP/EPDM/Coir composites using scanning electron microscopy (SEM)
12. To study the low shear rate rheology and dynamic viscoelastic properties of PP/EPDM/Coir composites using rheological analysis.
13. To study the non-isothermal crystallisation kinetics of PP/EPDM/Coir composites with the aid of differential scanning calorimetry (DSC) analysis
14. To study the maximum degradation temperature of PP/EPDM/Coir composites with the aid of thermo gravimetric (TGA) analysis

1.10 REFERENCES

1. Kalpakjian, S., & Schmid, S. (2006). *Manufacturing, Engineering and Technology SI 6th Edition*-Serope Kalpakjian and Stephen Schmid: Manufacturing, Engineering and Technology. Digital Designs.
2. Ober, C. K., Cheng, S. Z., Hammond, P. T., Muthukumar, M., Reichmanis, E., Wooley, K. L., & Lodge, T. P. (2008). Research in macromolecular science: challenges and opportunities for the next decade. *Macromolecules*, 42(2), 465-471.
3. Sun, T., Feng, L., Gao, X., & Jiang, L. (2005). Bioinspired surfaces with special wettability. *Accounts of chemical research*, 38(8), 644-652.
4. Blossey, R. (2003). Self-cleaning surfaces--virtual realities. *Nature materials*, 2(5), 301.
5. Vasiljević, J., Gorjanc, M., Tomšič, B., Orel, B., Jerman, I., Mozetič, M., ... & Simončič, B. (2013). The surface modification of cellulose fibers to create super-hydrophobic, oleophobic and self-cleaning properties. *Cellulose*, 20(1), 277-289.
6. Stamm, Manfred. "Polymer surface and interface characterization techniques." *Polymer Surfaces and Interfaces* (2008): 1-16.
7. Kovačević, Vera. "SURFACE AND INTERFACE PHENOMENON IN POLYMERS." (2008).

8. Mittal, K. L. "The role of the interface in adhesion phenomena." *Polymer Engineering & Science* 17.7 (1977): 467-473.
9. Voyutskii, S. S., and V. L. Vakula. "The role of diffusion phenomena in polymer-to-polymer adhesion." *Journal of Applied Polymer Science* 7.2 (1963): 475-491.
10. Awaja, F., Gilbert, M., Kelly, G., Fox, B., & Pigram, P. J. (2009). Adhesion of polymers. *Progress in polymer science*, 34(9), 948-968.
11. *Polymer-Polymer Interfaces in Blends and Composites*, D. R. Paul and J. W. Barlow, The University of Texas at Austin, Dept. of Chemical Engineering and Center for Polymer Research
12. Chen, J., Zhuang, H., Zhao, J., & Gardella, J. A. (2001). Solvent effects on polymer surface structure. *Surface and interface analysis*, 31(8), 713-720.
13. Koberstein, J. T. (2004). Molecular design of functional polymer surfaces. *Journal of Polymer Science Part B: Polymer Physics*, 42(16), 2942-2956.
14. Khelifa, F., Ershov, S., Habibi, Y., Snyders, R., & Dubois, P. (2016). Free-radical-induced grafting from plasma polymer surfaces. *Chemical reviews*, 116(6), 3975-4005.
15. Kaplan, S. L., & Rose, P. W. (1991). Plasma surface treatment of plastics to enhance adhesion. *International journal of adhesion and adhesives*, 11(2), 109-113.
16. Guruvenket, S., Rao, G. M., Komath, M., & Raichur, A. M. (2004). Plasma surface modification of polystyrene and polyethylene. *Applied Surface Science*, 236(1), 278-284.
17. Praveen, K. M., Thomas, S., Grohens, Y., Mozetič, M., Junkar, I., Primc, G., & Gorjanc, M. (2016). Investigations of plasma induced effects on the surface properties of lignocellulosic natural coir fibers. *Applied Surface Science*, 368, 146-156.
18. Koutroumanis, Nikos, Anastasios C. Manikas, Panagiotis Nektarios Pappas, Faidonas Petropoulos, Lamprini Sygellou, Dimitrios Tasis, Kostas Papagelis, George Anagnostopoulos, and Costas Galiotis. "A novel mild method for surface treatment of carbon fibers in epoxy-matrix composites." *Composites Science and Technology* (2018).
19. Yuan, L. Y., Chen, C. S., Shyu, S. S., & Lai, J. Y. (1992). Plasma surface treatment on carbon fibers. Part 1: Morphology and surface analysis of plasma etched fibers. *Composites science and technology*, 45(1), 1-7.

20. Li, C. Q., Dong, H. B., & Zhang, W. W. (2018). Low-temperature plasma treatment of carbon fiber/epoxy resin composite. *Surface Engineering*, 1-7.
21. Scheffler, C., Wölfel, E., Förster, T., Poitzsch, C., Kotte, L., & Mäder, G. (2016, July). Influence of microwave plasma treatment on the surface properties of carbon fibers and their adhesion in a polypropylene matrix. In *IOP Conference Series: Materials Science and Engineering* (Vol. 139, No. 1, p. 012046). IOP Publishing.
22. Park, O. K., Kim, W. Y., Kim, S. M., You, N. H., Jeong, Y., Lee, H. S., & Ku, B. C. (2015). Effect of oxygen plasma treatment on the mechanical properties of carbon nanotube fibers. *Materials Letters*, 156, 17-20.
23. Lee, H., Ohsawa, I., & Takahashi, J. (2015). Effect of plasma surface treatment of recycled carbon fiber on carbon fiber-reinforced plastics (CFRP) interfacial properties. *Applied Surface Science*, 328, 241-246.
24. Okajima, K., Ohta, K., & Sudoh, M. (2005). Capacitance behavior of activated carbon fibers with oxygen-plasma treatment. *Electrochimica Acta*, 50(11), 2227-2231.
25. Cech, V., Prikryl, R., Balkova, R., Grycova, A., & Vanek, J. (2002). Plasma surface treatment and modification of glass fibers. *Composites Part A: Applied Science and Manufacturing*, 33(10), 1367-1372.
26. Hoferek, L., Janecek, P., & Cech, V. (2010). Plasma coating of glass fibers used for polymer composites. In *12th international conference on plasma surface engineering*, September (pp. 13-17).
27. Lim, K. B., & Lee, D. C. (2004). Surface modification of glass and glass fibers by plasma surface treatment. *Surface and interface analysis*, 36(3), 254-258.
28. Guo, F., Zhang, Z. Z., Liu, W. M., Su, F. H., & Zhang, H. J. (2009). Effect of plasma treatment of Kevlar fabric on the tribological behavior of Kevlar fabric/phenolic composites. *Tribology International*, 42(2), 243-249.
29. Su, M., Gu, A., Liang, G., & Yuan, L. (2011). The effect of oxygen-plasma treatment on Kevlar fibers and the properties of Kevlar fibers/bismaleimide composites. *Applied Surface Science*, 257(8), 3158-3167.
30. Wang, J., Chen, P., Xiong, X., Jia, C., Yu, Q., & Ma, K. (2017). Interface characteristic of aramid fiber reinforced poly (phthalazinone ether sulfone ketone) composite. *Surface and Interface Analysis*, 49(8), 788-793.

31. Park, S. M., Kwon, I. J., Kim, M. S., Kim, S. S., Choi, J. Y., & Yeum, J. H. (2012). Surface Modification Effect and Mechanical Property of para-Aramid Fiber by Low-temperature Plasma Treatment. *Textile Coloration and Finishing*, 24(2), 131-137.
32. de Farias, J. G. G., Cavalcante, R. C., Canabarro, B. R., Viana, H. M., Scholz, S., & Simão, R. A. (2017). Surface lignin removal on coir fibers by plasma treatment for improved adhesion in thermoplastic starch composites. *Carbohydrate polymers*, 165, 429-436.
33. Enciso, B., Abenojar, J., & Martínez, M. A. (2017). Influence of plasma treatment on the adhesion between a polymeric matrix and natural fibers. *Cellulose*, 24(4), 1791-1801.
34. Sarikanat, M., Seki, Y., Sever, K., Bozaci, E., Demir, A., & Ozdogan, E. (2016). The effect of argon and air plasma treatment of flax fiber on mechanical properties of reinforced polyester composite. *Journal of Industrial Textiles*, 45(6), 1252-1267.
35. de Oliveira, D. M., Cioffi, M. O. H., de Carvalho Benini, K. C. C., & Voorwald, H. J. C. (2017). Effects of plasma treatment on the sorption properties of coconut fibers. *Procedia Engineering*, 200, 357-364.
36. Volokitin, G. G., Skripnikova, N. K., Sinitsyn, V. A., Volokitin, O. G., Shekhovtsov, V. V., Vaschenko, S. P., & Kuz'min, V. I. (2016). Plasma treatment of wood. *Thermophysics and Aeromechanics*, 23(1), 119-124.
37. Acda, M. N., Devera, E. E., Cabangon, R. J., & Ramos, H. J. (2012). Effects of plasma modification on adhesion properties of wood. *International journal of adhesion and adhesives*, 32, 70-75.
38. Cho, D. L., & Sjoebloom, E. (1990). Plasma treatment of wood. *Journal of Applied Polymer Science*, 46, 461-472.
39. Seki, Y., Sarikanat, M., Sever, K., Erden, S., & Gulec, H. A. (2010). Effect of the low and radio frequency oxygen plasma treatment of jute fiber on mechanical properties of jute fiber/polyester composite. *Fibers and Polymers*, 11(8), 1159-1164.
40. Gibeop, N., Lee, D. W., Prasad, C. V., Toru, F., Kim, B. S., & Song, J. I. (2013). Effect of plasma treatment on mechanical properties of jute fiber/poly (lactic acid) biodegradable composites. *Advanced Composite Materials*, 22(6), 389-399.
41. Sever, K., Erden, S., Gülec, H. A., Seki, Y., & Sarikanat, M. (2011). Oxygen plasma treatments of jute fibers in improving the mechanical properties of jute/HDPE composites. *Materials Chemistry and Physics*, 129(1-2), 275-280.

42. Oliveira, F. R., Erkens, L., Fangueiro, R., & Souto, A. P. (2012). Surface modification of banana fibers by DBD plasma treatment. *Plasma chemistry and plasma processing*, 32(2), 259-273.
43. Gorjanc, M., Bukošek, V., Gorenšek, M., & Mozetič, M. (2010). CF₄ plasma and silver functionalized cotton. *Textile research journal*, 80(20), 2204-2213.
44. Vasiljević, J., Gorjanc, M., Tomšič, B., Orel, B., Jerman, I., Mozetič, M., ... & Simončič, B. (2013). The surface modification of cellulose fibers to create super-hydrophobic, oleophobic and self-cleaning properties. *Cellulose*, 20(1), 277-289.
45. Wacker Chemie A.G., Product Brochure, Geniosil Organofunctional Silanes: "For Powerful Connections"
46. Avril Surgenor (2006) Organofunctional Siloxanes: The Best of Both Worlds. Dr Avril Surgenor. Dow Corning Ltd. Chemsources Symposium
47. Geethamma, V. G., Joseph, R., & Thomas, S. (1995). Short coir fiber-reinforced natural rubber composites: effects of fiber length, orientation, and alkali treatment. *Journal of Applied Polymer Science*, 55(4), 583-594.
48. Satyanarayana, K. G., Kulkarni, A. G., & Rohatgi, P. K. (1981). Structure and properties of coir fibers. *Proceedings of the Indian Academy of Sciences Section C: Engineering Sciences*, 4(4), 419-436.
49. Geethamma, V. G. (2004). Short coir fiber reinforced natural rubber composites.
50. Chen, H. (2014). Chemical composition and structure of natural lignocellulose. In *Biotechnology of lignocellulose* (pp. 25-71). Springer, Dordrecht.
51. Bucknall, C. B., *Toughened Plastics*. Applied Science, London, 1977.
52. D'orazio, L., Mancarella, C., Martuscelli, E., Sticotti, G., & Massari, P. (1993). Melt rheology, phase structure and impact properties of injection-moulded samples of isotactic polypropylene/ethylene-propylene copolymer (iPP/EPR) blends: influence of molecular structure of EPR copolymers. *Polymer*, 34(17), 3671-3681.
53. Rondin, J., Bouquey, M., Muller, R., Serra, C. A., Martin, G., & Sonntag, P. (2014). Dispersive mixing efficiency of an elongational flow mixer on PP/EPDM blends: Morphological analysis and correlation with viscoelastic properties. *Polymer Engineering & Science*, 54(6), 1444-1457.
54. Yokoyama, Y., & Ricco, T. (1998). Toughening of polypropylene by different elastomeric systems. *Polymer*, 39(16), 3675-3681.

55. Jang, B. Z., Uhlmann, D. R., & Vander Sande, J. B. (1985). Rubber-toughening in polypropylene. *Journal of Applied Polymer Science*, 30(6), 2485-2504.
56. Gao, X., Mao, L. X., Jin, R. G., Zhang, L. Q., & Tian, M. (2007). Structure and mechanical properties of PP/EPDM/attapulgate ternary blends. *Polymer journal*, 39(10), 1011.
57. Machado, L., Arroyo, M., Biagiotti, J., & Kenny, J. M. (2003). Enhancement of mechanical properties and interfacial adhesion of PP/EPDM/flax fiber composites using maleic anhydride as a compatibilizer. *Journal of Applied Polymer Science*, 90(8), 2170-2178.
58. Anuar, H., & Zuraida, A. (2011). Improvement in mechanical properties of reinforced thermoplastic elastomer composite with kenaf bast fiber. *Composites Part B: Engineering*, 42(3), 462-465.
59. Ruksakulpiwat, Y., Sridee, J., Suppakarn, N., & Sutapun, W. (2009). Improvement of impact property of natural fiber–polypropylene composite by using natural rubber and EPDM rubber. *Composites Part B: Engineering*, 40(7), 619-622.
60. Pigatto, C., Santos Almeida, J. H., Luiz Ornaghi, H., Rodríguez, A. L., Mählmann, C. M., & Amico, S. C. (2012). Study of polypropylene/ethylene-propylene-diene monomer blends reinforced with sisal fibers. *Polymer Composites*, 33(12), 2262-2270.

CHAPTER 2 MATERIALS AND METHODS

2.1 Experimental

2.1.1 Materials used

The polymer matrix used for this study was Repol H350FG polypropylene supplied by Reliance Industries Ltd., Mumbai, India, with a melt flow index of 38g/10 min (230°C/2.16 kg). The property profiles of polypropylene calculated experimentally are displayed below.

Table 2.1 Properties of Polypropylene

Typical Characteristics			
Property	Test Method	Unit	Value
Notched izod impact strength (23 °C)	ASTMD256	kJ/M ²	1.9
Tensile Strength at Yield (1 mm/min)	ASTMD638	MPa	22
Elongation a yield (1 mm/min)	ASTMD638	%	3
Melt flow (230°C/2.16 kg)	ASTM D1238	g/10 min	38
Heat deflection temperature (455 kPa)	ASTM D648	°C	104
Flexural Modulus	ASTMD790A	MPa	1508

High-molecular grade ethylene-propylene-diene rubber (EPDM), Keltan 9565Q DE is selected as material for dispersed phase was supplied by Ramcharan Co. Pvt Ltd, India an authorised representative of LANXESS Deutschland GmbH, Germany. It is a semi crystalline ethylene-propylene rubber, with medium ENB (ethylidenenorbornene) content and a very high Mooney viscosity at 50phr colourless oil extension. The exceptional high molecular weight in combination with the relatively low oil content offers the best dynamic performances in very polymer rich formulations, such as for (engine) mounts, (torsional) dampers and air springs. The semi-crystalline nature balances low temperature performances with mechanical properties and process behaviour. This grade is very suitable for dynamic applications, soft solid parts as well as thermoplastic elastomers (TPV). The specialty of

EPDM grade (Keltan 9565Q) used here is characterized by its exceptionally high molecular weight, which gives the synthetic rubber its extremely high NR-type strength and resilience. This grade also still features the heat, weathering and ozone resistance typical of EPDM rubber. Keltan 9565Q is thus not only superior to natural rubber in terms of heat aging but can also offer this benefit in highly dynamic applications. In addition, this new ultra-high-molecular Keltan grade opens up new potential for more economical EPDM processing compared with NR [1]. The property profiles obtained from datasheet are depicted below.

Table 2.2 Properties of Keltan 9565Q DE

Property	Nominal Value	Unit	Test Method
Mooney Viscosity ML (1+8)	67	MU	ASTM D 1646
Ethylene content	62	wt%	ASTM D 3900
ENB content	5.5	wt %	ASTM D 6047
Molecular weight distribution	Narrow		LANXESS
Oil content	50	phr	ASTM D 5774

The coir fibers used in this study were collected from Central Coir Research Institute (CCRI), Alappuzha, Kerala, India. It has an average diameter of 300 μ m and a specific gravity of 1.15g/cm³.

Table 2.3 Properties of Coir fibers

Constituents	Composition (%)
Cellulose	36-43
Lignin	41-45
Hemicellulose	0.15-0.25
Pectins	3-4
Water soluble materials	7-8

2.1.2 Methodology

2.1.2.1 Preparation of fibers

The coir fibers collected from the supplier is washed thoroughly with water to remove dust and impurities from these fibers. The cleaned fibers dried in a vacuum oven at 100⁰C for 24 hours to remove moisture content of the fibers.

2.1.2.2 Plasma modification of fibers

The oxygen plasma pre-treatment was performed to enhance the hydrophilic behaviour of coir fibers which in turn increase the effective concentration of the FAS network on the coir fiber surface (discussed in section 2.1.2.3). The schematic illustration of oxygen plasma treatment of coir fiber surface is shown in figure Fig.2.1.

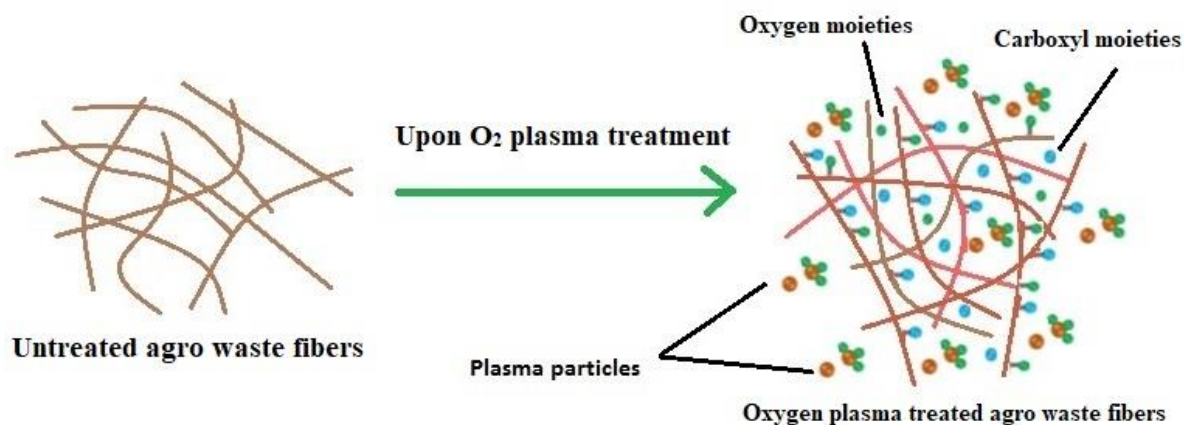


Fig.2.1 Schematic illustration of oxygen plasma treatment of coir fiber surface

The plasma experiments were conducted in two different discharge chambers having chamber volumes, say 17 litres and 3.1 litres respectively. These two chambers are known to be large and small chamber respectively. This is illustrated in the following as two different cases.

Case 1

Coir fibers were mounted into large discharge chamber of plasma system as shown in Fig.1. Weakly ionized oxygen plasma was created in discharge chamber of volume 17 litres by an inductively coupled radiofrequency (RF) discharge. The RF generator operates at a

frequency of 27.12 MHz and at power of about 500W. The plasma generated in this chamber is uniform all over the volume (Figure 1). The power density is estimated to be $500 \text{ W} / 17 \text{ L} = 30 \text{ W} / \text{L}$. The treatment for further analysis was done at two different treatment conditions. The pressure was set to 75 Pa and the treatment time was 20 and 30s.

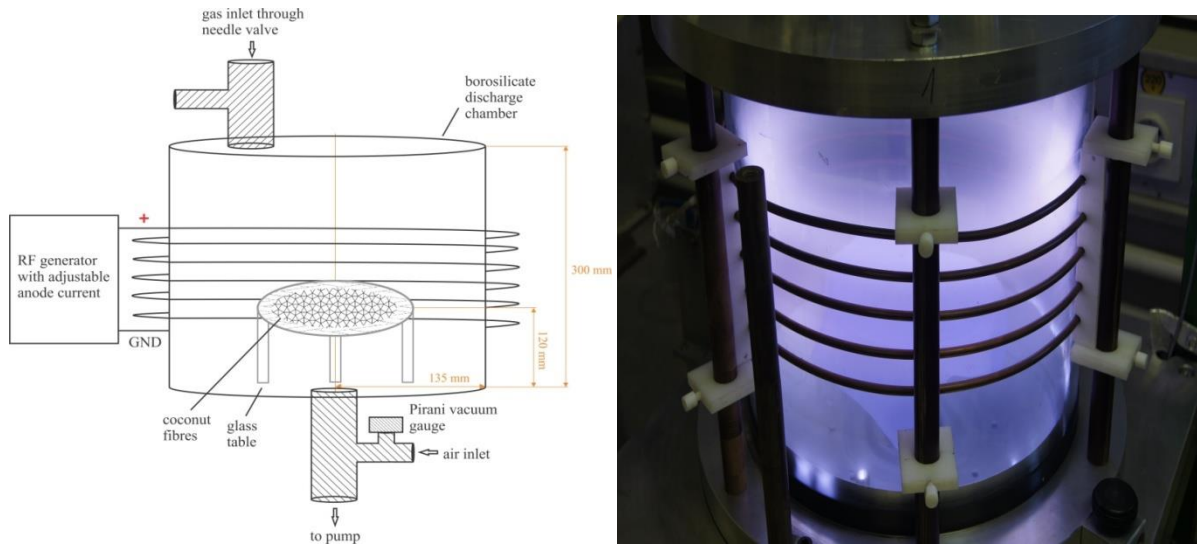


Fig.2.2 Large Plasma chamber used for treatment of coconut fibers.

Case 2

Coconut fibers were mounted into the small discharge chamber of plasma system as shown in Fig.2. Weakly ionized oxygen plasma was created in discharge chamber of volume 3.1 L by an inductively coupled radiofrequency (RF) discharge. The RF generator operates at a frequency of 27.12 MHz and at power of about 500W. The power density is estimated to be $500 \text{ W} / 3.1 \text{ L} = 160 \text{ W} / \text{L}$. The plasma in the smaller reactor is confined to the lower half of the reactor (where plasma glows). Since there is no visible glowing in the upper part, this volume is not affected. It can be stated that, as plasma is confined to only one half of the glass tube (Fig.2), therefore the “real” power density is estimated to be $300 \text{ W} / \text{L}$ (Accounting about half of the geometrical volume of the discharge tube, i.e., $500\text{W} / (3.1\text{L} / 2) \sim 300\text{W/L}$).

The treatment for further analysis was done at two different pressures; 75 Pa and 50 Pa and at 5 different treatment times; 1, 3, 5, 10 and 15s.

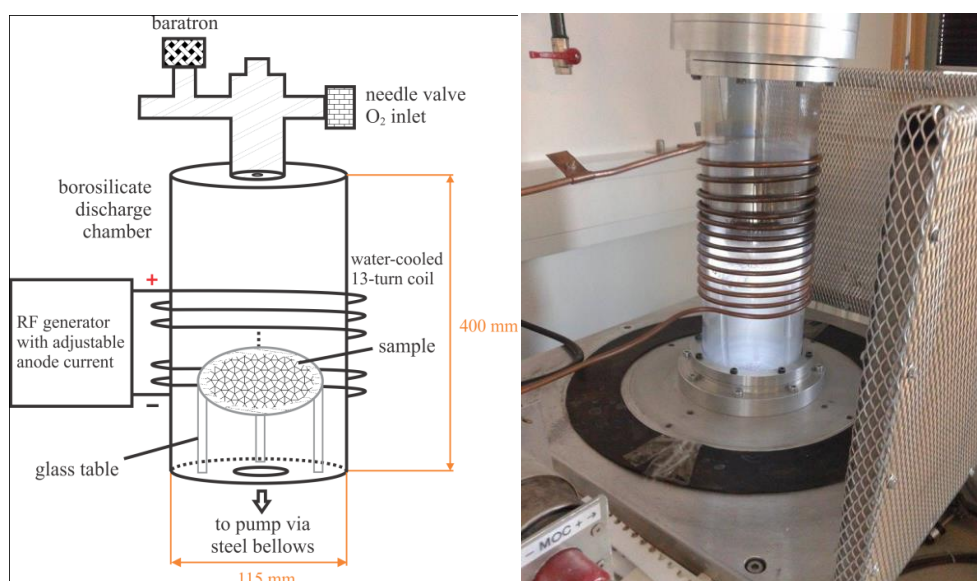


Fig.2.3 Small Plasma chamber used for treatment of coconut fibers. The inner diameter of the glass tube is 100 mm. Due to specific discharge mode plasma is concentrated just next to the sample (white glow in attached photo).

2.1.2.2.1 Optical emission spectroscopy

Optical emission spectroscopy was used to characterise plasma in the empty discharge chamber and in the chamber containing fibers. Fibers were placed approximately 1 cm from the glass tube at the height of 19 cm measured from the bottom of the glass tube. Optical emission spectra were recorded by Avantes Ava Spec 3648 spectrometer. The device is based on Ava Bench 75 symmetrical Czerny Turner design with a 3648 pixel CCD detector with the focal length of 75 mm. The range of measurable wavelengths is from 200 nm to 1100 nm and the wavelength resolution is 0.5 nm. The spectrometer has USB 2.0 interface, enabling high sampling rates of up to 270 spectra per second. Signal to noise ratio is 350:1. Integration time is adjustable from 10 s to 10 min. At integration times below 3.7 ms, the spectrometer itself performs an internal averaging of spectra before transmitting them through the USB interface. For our particular case, the spectra were averaged over three sub-sequent measurements.

2.1.2.2.2 Water absorption studies

The water absorption capacity of the untreated and plasma-treated coir fibers was performed according to the standard ISO9073-6:2003 by measuring the water absorbency time and water absorptive capacity. The water absorbency time test measures the time required for the complete wetting of a specimen which is rolled into a cylindrical wire basket and is dropped on the surface of the liquid from 25 mm height. The water absorptive capacity method provides a measure of the amount of liquid held within a test piece after specified times of immersion and drainage. To perform the measurements the untreated and plasma-treated fibers were prepared according to standard. A sample of coir fibers (5 g) was inserted into wire basket of defined dimensions (height 80 mm, diameter 50 mm, thickness of wire 0.4 mm, mesh 20 mm). The basket with the sample was released sideways from 25 mm height into the round vessel of 110 mm diameter containing distilled water with temperature 20°C and height 100 mm. The time taken for the basket to completely sink to the bottom of the vessel was measured. The samples were left in the water for 60 s and afterwards hung freely and vertically to drain for 120 s. Without squeezing the water from the sample, the sample was weighted. For each sample, fresh conditioned water was set. The water absorptive capacity (LAC) of fibers was calculated according to the equation:

$$LAC = \frac{m_w - m_d}{m_d} \times 100 [\%] \dots\dots\dots (2.1)$$

Where, m_w is the mass of a wet sample and m_d is the mass of a dry sample.

2.1.2.2.3 Scanning Electron Microscope (SEM) Analysis

Surface features of pristine and plasma-treated coir fibers were analysed by scanning electron microscopy, Jeol JSM 7600 FEG. Coir fibers were sputtered with gold and operated at 8 kV. The samples were examined at 500× and 1000× magnification, and the changes of morphology were examined after 30 s and 60 s of plasma treatment in a large discharge chamber. The changes of morphology were examined after 10 s of plasma treatment for the case when small chamber was used for plasma generation.

2.1.2.2.4 Atomic Force Microscope (AFM) Analysis

Topographic features of fibers were monitored by atomic force microscopy (AFM, Solver PRO, NT-MDT, Russia) technique in the tapping mode in air. Samples were scanned with the standard Si cantilever with a force constant of 22 N/m and at a resonance frequency of 325

kHz (tip radius was 10 nm and the tip length was 95 μ m). The imaging was done on $5 \times 5 \text{ m}^2$ and $2 \times 2 \text{ m}^2$ areas on the untreated sample and the one treated in oxygen plasma for 30 s for the case where large chamber was used.

2.1.2.2.5 X-ray photoelectron spectroscopy (XPS) Analysis

Surface of fibers were analysed with an XPS instrument TFA XPS Physical Electronics. The base pressure in the XPS analysis chamber was about 6×10^{-8} Pa. The samples were excited with X-rays over a $400 \mu\text{m}$ spot area with a monochromatic Al $K_{\alpha 1, 2}$ radiation at 1486.6 eV. The photoelectrons were detected with a hemispherical analyser positioned at an angle of 45° with respect to the normal of the sample surface. The energy resolution was about 0.5 eV. Survey scan spectra were obtained at a pass energy of 187.85 eV, while the C1s, O1s and N1s individual high-resolution spectra were taken at a pass energy of 29.35 eV and a 0.1-eV energy step. All spectra were referenced to the main C1s peak of the carbon atoms which was assigned a value of 284.8 eV. The XPS spectra were measured on pristine coir fibers and on fibers treated with oxygen plasma at 50 Pa and 75 Pa for 10 s (the samples were analysed immediately after plasma treatment) in the case of when small chamber is used for plasma treatment. The concentration of the different chemical states of carbon in the C1s peak was determined by fitting the curves with symmetrical Gauss–Lorentz functions. The spectra were fitted using MultiPak v7.3.1 software from physical electronics, which was supplied with the spectrometer. A Shirley-type background subtraction was used.

2.1.2.3 Fluoroalkyl functional siloxane (FAS) Sol-Gel coating on coir fibers

The surface modification of lignocellulosic coir fibers was done with the use of low-pressure oxygen plasma, followed by the application of a spray-dry-cure sol–gel coating with the water and oil repellent organic–inorganic hybrid precursor fluoroalkyl-functional siloxane (FAS), with the aim of creating the extremely hydrophobic coir fiber surface. The plasma pre-treatment increased the effective concentration of the FAS network on the lignocellulosic coir fibers.

The sol-gel is an organic-inorganic nanocomposite coating, with a thickness of about 50 nm. The spray-dry-cure method was used to coat FAS on the surface of lignocellulosic natural coir fibers. The schematic illustration is shown in figure Fig.2.4. Prior to the spraying of FAS on the coir fiber surface, the fibers were treated with O_2 plasma. The plasma-treated fibers were sprayed with 10% sol-gel coating (FAS, Protectosil, Chemcolor Slovenia). The sprayed

fibers were dried at a temperature of 100⁰C for 15 minutes and cured at a temperature of 150⁰C for 5 minutes. After the sol-gel application, the coated coir fiber samples were left for 14 days under standard atmospheric conditions (65 ± 2 % relative humidity and 20 ± 1 C) to allow the complete network formation of the applied finishes.

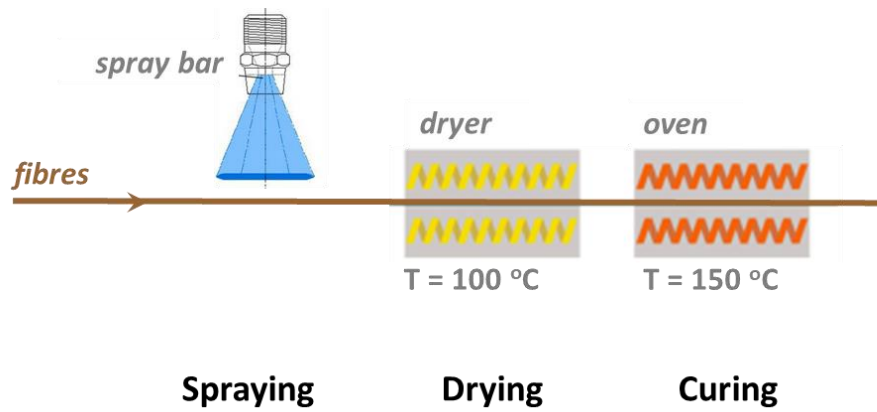


Fig.2.4 Scheme of the spray-dry-cure sol-gel-coating process

2.1.2.3.1 Wettability analysis

Contact angle measurements were performed using a Digidrop (GBX, France) contact angle instrument. Measurements were taken at 20°C and 48% RH. An air sprayer system is used to deposit micro- and nanoscale liquid droplets on coir fiber surfaces. It generates ultra-small droplets by mixing macro scale droplets with a jet of compressed air. Commercially available atomizers are able to spray ultrafine droplets with a wide range of sizes. The contact angle is measured using the image of a sessile drop at the points of intersection (three-phase contact points) between the drop contour and the projection of the surface (baseline). For precision, contact angle was measured for at least five specimens of both control as well as coated fibers, and the measurements were repeated 5–10 times on different places of the same sample. The measurements of contact angles were carried out using several different liquids for which at least one is non-polar and two must be polar, and then the dispersive and polar components of the surface can be determined.

By using water (polar), ethylene glycol (polar) and tricresylphosphate (TCP-nonpolar) as the test liquid medium, the measurement of contact angle, the dispersive and polar components of the surface are determined. In a simple system where a liquid (L) adheres to a solid (S), the work of adhesion is defined as

$$W_A = \gamma_S + \gamma_L - \gamma_{SL} \dots \dots \dots (2.2)$$

Where γ_s , γ_L and γ_{SL} are the total surface free energy of the sample to test (solid surface), total surface free energy of the test liquid and total surface free energy of the solid-liquid interface respectively.

A very useful expression for adhesion work is (Young–Dupre’ equation)

$$W_A = (1+\cos\theta)\gamma_L \dots\dots\dots(2.3)$$

Where ‘ θ ’ is the contact angle measured on the examined true surface (the contact angle of the liquid on the solid surface in air). We can express the total surface free energy of any sample as a sum of components due to dispersion forces (γ_d) and polar (e.g. dipolar and hydrogen bonding) forces, γ_p .

$$\text{I.e. } \gamma = \gamma^d + \gamma^p \dots\dots\dots (2.4)$$

Similarly the work of adhesion can be expressed as

$$W_A = W_A^d + W_A^p \dots\dots\dots (2.5)$$

Firstly, the surface energy values were calculated by using Owens-Wendt formula (based on geometric mean approach) as shown in Equation (2.2) [2].

$$W_A = (1+\cos\theta)\gamma_L = 2[(\gamma_L^d \gamma_s^d)^{0.5} + (\gamma_L^p \gamma_s^p)^{0.5}] \dots\dots\dots(2.6)$$

Where θ is the contact angle measured on the examined true surface (the contact angle of the liquid on the solid surface in air), γ_L^d , γ_L^p and γ_L are dispersive and polar components and total surface free energy of the test liquid, respectively, and γ_s^d and γ_s^p are dispersive and polar components of surface free energy of samples, respectively.

To compare the calculated values more closely to the chemical nature of the phases, Van Oss et al. [3] expressed the polar component in terms of acid–base interactions.

According to Van Oss et al. an interfacial tension can be expressed as

$$\gamma = \gamma^{LW} + \gamma^{AB} \dots\dots\dots (2.7)$$

Where γ^{LW} is a nonpolar London/van der Waals component and γ^{AB} is the polar(acid–base component). The acid–base component, γ^{AB} comprises of two non-additive parameters. These acid–base interactions are complementary in nature and are the electron-acceptor

surface tension parameter (γ^+) and the electron-donor surface tension parameter (γ^-). Thus the total acid–base contribution to the surface free energy is given by

$$\gamma^{AB} = 2(\gamma^+ \gamma^-)^{1/2} \dots\dots\dots(2.8)$$

Therefore the work of adhesion is defined as,

$$W_A = 2[(\gamma_L^{LW} \gamma_S^{LW})^{0.5} + (\gamma_L^+ \gamma_S^-)^{0.5} + (\gamma_L^- \gamma_S^+)^{0.5}] \dots\dots\dots (2.9)$$

2.1.2.3.2 Water absorption studies

The water absorption capacity of the untreated and FAS coated coir fibers were performed according to the standard ISO9073-6:2003 with measuring the water absorbency time and water absorptive capacity. The detailed procedure is given in section 2.1.2.2.2.

2.1.2.3.3 Scanning Electron Microscope (SEM) Analysis

Surface features of the pristine and FAS coated coir fibers were analysed by scanning electron microscopy technique using Jeol JSM-6031 scanning electron microscope. Initially untreated as well as coated coir fibers were sputter-coated with a thin gold layer using Edwards Sputter Coater. The samples were examined at 100×, 1000x and 2000× magnification, and the changes of morphology were examined for control as well as FAS coated samples.

2.1.2.3.4 Atomic Force Microscope (AFM) Analysis

Initially the lignocellulosic natural coir fibers were glued onto a metallic disk for imaging under atomic force microscopy (AFM). The obtained samples were imaged by atomic force microscopy (AFM) with a multimode equipped with the nanoscope III-a (Bruckernano, Santa Barbara, USA). The AFM was used in contact mode imaging. The tips 240 (DNP–10, Bruckernano) were made of Si3N4 and had a 0.24 N/m nominal spring constant. The deflection set point was chosen at the limit of the tip retraction. Surface scans of 5µm² and 10 µm² square areas were performed at 22⁰C in atmosphere for different sample positions. The imaging speed was between 1 and 2 Hz depending on the surface. The pictures obtained were processed with NanoScope(R) Analysis v1.5 software.

2.1.2.3.5 X-ray photoelectron spectroscopy (XPS) Analysis

Surface of fibers were analysed with an XPS instrument TFA XPS Physical Electronics. The base pressure in the XPS analysis chamber was about 6×10^{-8} Pa. The samples were excited with X-rays over a 400 μ m spot area with a monochromatic Al $K_{\alpha 1, 2}$ radiation at 1486.6 eV. The photoelectrons were detected with a hemispherical analyser positioned at an angle of 45° with respect to the normal of the sample surface. The energy resolution was about 0.5 eV. Survey scan spectra were obtained at a pass energy of 187.85 eV, while the C1s, O1s, N1s, Si1s and F1s individual high-resolution spectra were taken at a pass energy of 29.35 eV and a 0.1-eV energy step. All spectra were referenced to the main C1s peak of the carbon atoms which was assigned a value of 284.8 eV. The XPS spectra were measured on pristine coir fibers and on fibers coated with fluoroalkyl-functional siloxane (FAS). The concentration of the different chemical states of carbon in the C1s peak was determined by fitting the curves with symmetrical Gauss–Lorentz functions. The spectra were fitted using MultiPak v7.3.1 software from physical electronics, which was supplied with the spectrometer. A Shirley-type background subtraction was used.

2.1.2.4 Melt blending

Ethylene-propylene-diene rubber (EPDM) and polypropylene was first dried under vacuum at 80°C for 4h to remove moisture and, therefore, to minimize the hydrolytic degradation during processing. Binary blends of polypropylene (PP)/ ethylene-propylene-diene rubber (EPDM) at varying concentrations of EPDM of 2.5, 5, 7.5, 10, 20 and 30 parts per hundred (volume fraction, $\phi_d = 0.02, 0.04, 0.06, 0.08, 0.15$ and 0.2) were prepared first by dry blending followed by melt compounding using a Brabender Plasticorder mixer (model W 50 EHT). The volume fraction, ϕ_d , of the blending polymer was calculated using equation 2.3.

$$\phi_d = \frac{\left(\frac{W_1}{\rho_1}\right)}{\left(\frac{W_1}{\rho_1}\right) + \left(\frac{W_2}{\rho_2}\right)} \dots \dots \dots (2.3)$$

Where W is the weight and ρ is the density of the constituents, subscripts 1 and 2 describing the discrete and continuous phases respectively. For fabricating the composites, firstly the coir fibers were first dried in an oven under vacuum, at 100°C for 24h in order to reduce the humidity content to less than 3 wt%. The blend composition of 100pph polypropylene (PP) and 7.5pph ethylene-propylene-diene rubber (EPDM) was selected for composite fabrication

because it registered highest impact strength as well as pull out strength with pristine as well as FAS coated fibers. Composites of PP/EPDM/Coir were prepared by varying the concentration of coir fiber of 10, 20, 30 and 40 pph (volume fraction $\phi_f = 0.07, 0.13, 0.19$ and 0.24). The ϕ_f values of composites were calculated using equation 2.4.

$$\phi_f = \frac{\left(\frac{W_{coir}}{\rho_{coir}}\right)}{\left(\frac{W_{coir}}{\rho_{coir}}\right) + \left(\frac{W_{PP}}{\rho_{PP}}\right) + \left(\frac{W_{EPDM}}{\rho_{EPDM}}\right)} \dots \dots \dots (2.4)$$

The formulations of PP/EPDM blends as well as PP/EPDM/Coir composites are shown in Table 2.4 and Table 2.5.

Table 2.4 PP/EPDM blend formulations

Polypropylene(in phr)	EPDM (in phr)	Volume fraction of EPDM, ϕ_a
100	0	0.00
100	2.5	0.02
100	5	0.04
100	7.5	0.06
100	10	0.08
100	20	0.15
100	30	0.21

Table 2.5 PP/EPDM/Coir composite formulations

Polypropylene(in phr)	EPDM (in phr)	Coir (in phr)	Volume fraction, ϕ_f
100	7.5	10	0.07
100	7.5	20	0.13
100	7.5	30	0.19
100	7.5	40	0.24

2.1.2.5 Preparation of test specimens

The melt compounded PP/EPDM blends and PP/EPDM/Coir composites were moulded into sheets using hot pressing (compression moulding) technique. The prepared sheets then cut using a numerically controlled cutting machine viz Fraiseuse as shown in figure Fig.2.5 into dumb-bell shaped specimens for tensile testing and rectangular specimens for Izod impact testing and flexural testing.



Fig. 2.5 Numerically controlled cutting machine “Fraiseuse”

2.1.2.6 Breaking strength analysis and Pull-out stress of coir fibers

The tensile tests and pull out tests were conducted at a controlled temperature (23°C) and relative humidity (48%). The longitudinal mechanical properties such as young's modulus, ultimate strength and failure strain of elementary coir fibers, fluoroalkyl-functional siloxane (FAS) coated coir fibers and pull stress of these fibers with different compositions of PP/EPDM blends were determined. To carry out tensile tests for elementary as well as coated fibers, due to the short fiber length (about 20–30 mm), a gauge length of 10 mm was chosen. The fiber was clamped on a universal MTS type tensile testing machine fitted with a 50 N capacity load cell and loaded at a constant crosshead displacement rate of 1 mm/min up to rupture. The determination of the mechanical properties was made in accordance with the NFT 25-704 standard which takes into account the compliance of the loading frame. For each kind of fiber, at least 50 fibers were tested. Before tensile test, the diameter of every fiber is

measured with an optical microscope. The diameter taken into account is an average value from five points obtained along the fiber.

2.1.2.6.1 Pull-out test of coir fibers

Fibers having an average length of 125 mm and average diameter $300 \pm 30 \mu\text{m}$ were used for preparing pull out test samples by sandwiching individual coir fibers between two PP/EPDM blend sheets ($80 \cdot 80 \cdot 2 \text{ mm}$) and hot pressing at a temperature of 150°C . The fiber was kept straight and oriented by fixing it's both ends, extending outside the PP/EPDM blend sheets, on the mold using glue. Samples were removed from the mould after allowing it to cool to room temperature. The desired fiber length embedded in the PP/EPDM matrix was obtained by cutting the fiber by punching a hole through the sample [4]. The schematic of the pull-out specimen is shown in figure **Fig. 2.6**.

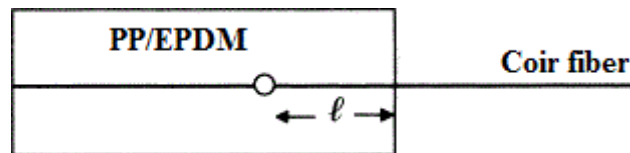


Fig.2.6. Schematic of the pull-out specimen (Reproduced with permission from Elsevier) [4]

The pull-out tests were conducted in MTS Synergy RT1000 testing apparatus at 23°C , relative humidity of 48% and crosshead speed of 1 mm/min up to rupture. At least six samples were tested for fiber embedded length of 40mm in PP/EPDM matrix and the average values are reported. To find out the critical length of coir fiber in PP/EPDM 7.5 matrix, different embedded fiber lengths of 40mm, 30mm, 20mm, 10mm, 5mm and 2.5mm in PP/EPDM 7.5 matrix were tried.

2.1.2.7 Mechanical property analysis

2.1.2.7.1 Impact analysis

Notched Izod impact tests were performed using a Tinius-Olsen machine at ambient temperature (23°C). Specimens for Izod tests were cut from the compression moulded specimens according to ISO 180 A. Results were obtained from the average of at least 10 samples for each set.

2.1.2.7.2 Tensile analysis

Tensile values of neat polypropylene, PP/EPDM blends and the composite samples were measured by MTS Synergy RT1000 testing apparatus at 23°C and a relative humidity of 48% according to ISO 527. The tensile sample was clamped on a universal MTS type tensile testing machine fitted with a 10kN capacity load cell and loaded at a constant crosshead displacement rate of 1 mm/min up to rupture. An MTS extensometer was used with a nominal gauge length of 25 mm. The tests were carried out at least 6 times for each sample and the results were averaged arithmetically.

2.1.2.7.3 Flexural analysis

Flexural tests of neat polypropylene, PP/EPDM blends and the composite samples were performed by MTS Synergy RT1000 testing apparatus at 23°C and a relative humidity of 48% according to ISO 178. The sample was clamped on a universal MTS type tensile testing machine fitted with a 200N capacity load cell and loaded at a constant crosshead displacement rate of 1 mm/min up to rupture. An MTS extensometer was used with a nominal gauge length of 25 mm. The tests were carried out at least 6 times for each sample and the results were averaged arithmetically.

2.1.2.8 Morphological Analysis

2.1.2.8.1 High resolution transmission electron microscopy (HRTEM)

The morphology structure of PP/EPDM blend was observed by means of Transmission electron microscopy (TEM) (JEM-2100 HRTEM). The micrographs were obtained in point to point resolution 0.194 nm, operating at an accelerating voltage of 200 kV. Ultrathin sections of bulk specimens (Cryocut specimens ~ 100nm thickness) prepared using an ultra-microtome (Leica, Ultracut UCT) were placed on a 300 mesh Cu grids (35mm diameter) and were analysed without staining.

2.1.2.8.2 Scanning Electron Microscopy (SEM)

The morphology of cryo-fractured and impact fractured blend as well as impact fractured composite surfaces were analysed using a Jeol JSM-6031 scanning electron microscope. To see the morphology of cryo-fractured surfaces, the sample cut from the compression moulded specimen is fractured in liquid nitrogen parallel to the thickness direction in order to reveal the internal morphology and to find out the failure mechanism in blends. Initially, both the

cryo fractured as well as impact fractured surface of the specimens was sputter-coated with a thin gold layer (Edwards Sputter Coater) before viewing it under scanning electron microscope..

2.1.2.9 Differential Scanning Calorimetry

2.1.2.9.1 Non-isothermal Crystallization Kinetics

The crystallisation study of polypropylene in blends and composites are performed on a differential scanning calorimeter Model Mettler-Toledo DSC-882 .The sample weight was about 10 mg. Samples are cut from the compression moulded specimens from three different places and vacuum dried at 80⁰C for 4h. The samples were subjected to two heating and cooling ramps starting from 25⁰C up to 190⁰C and down to 25⁰C at a scanning rate of 10⁰C.min⁻¹ under nitrogen atmosphere. The samples are first heated from 25⁰C to 190⁰C at a heating rate of 10⁰C/min, held at 190⁰C for 2 minutes to remove previous shear, processing, mechanical, thermal and crystallisation history. The melt is then cooled to 25⁰C/min at 10⁰C/min and the resulting exotherms in the cooling curves were recorded. Heats of melting values obtained during the second heating runs (heating rate 10⁰C/min) were employed to determine the crystallinity of PP in blends and composites. The crystallinity was calculated according to Eq. (2.5)

$$\text{Crystallinity (\%)} = \left[\frac{\Delta H}{\Delta H_{100} * w} \right] * 100 \dots \dots \dots (2.5)$$

Where ΔH is the enthalpy of fusion of PP in the blends/composites, ΔH₁₀₀ is the parameter for 100% crystalline PP (209Jg⁻¹) and w is the weight fraction of PP in blends/composites.The DSC exotherms of neat PP, PP/EPDM blends and PP/EPDM/Coir composites at 5 different cooling rates (10, 15, 20, 25 and 30⁰C min⁻¹) were studied.

2.1.2.9.1 Determination of glass transition temperature (T_g)

Thermograms were obtained from a Perkin-Elmer Pyris 1 differential scanning calorimeter (DSC) using the Pyris V 3.0 software under Windows NT 4.0 for data collection and treatment. Calibration was done with indium and tin in the temperature range (+ 15 to +350⁰C). The base line was checked every day. Aluminum pans with holes were used and the sample mass was approximately 10 mg. All samples were first heated to 210⁰C for 5 minutes to get rid of thermal history. All the temperatures measured from a peak extreme (T_c, T_m) were determined at less than ± 0.5⁰C. The samples were subjected to two heating and cooling ramps starting from -90⁰C up to 190⁰C and down to -90⁰C at a scanning rate of

10°C.min⁻¹ under nitrogen atmosphere. The samples are first heated from -90°C to 190°C at a heating rate of 10°C/min, held at 190°C for 5 minutes to remove previous shear, processing, mechanical, thermal and crystallisation history. The melt is then cooled to -90°C/min at 10°C/min and the resulting exotherms in the cooling curves were recorded.

2.1.2.10 Thermo gravimetric analysis

TGA measurements were carried out using a Perkin-Elmer thermal analyzer at a heating rate of 10°C/min under a dynamic nitrogen atmosphere with a flow rate of 80 mL/min from 20 to 700°C.

2.1.2.11 Rheological Analysis

The low shear rate rheology (for shear rates from 0.001 to 100 sec⁻¹) and dynamic viscoelastic properties of polypropylene, PP/EPDM blends and PP/EPDM/Coir composites were studied using an Anton Paar, CTD 450, Physica MCR 301 rheometer. The viscosity versus shear rate and shear stress versus shear rate were determined. The oscillatory frequency analysis was performed at a fixed strain (0.1%) and the frequency was varied in the range from 0.01-100 Hz. The viscoelastic properties such as storage modulus (G'), loss modulus (G''), complex viscosity (η^*) and loss Factor ($\tan \delta$) were measured as a function of angular velocity (ω). Before experiments, the samples were dried at 60°C for 12 h and compression moulded to a circular shape having diameter 25mm and the thickness about 2 mm. The limit of the linear viscoelastic regime was determined by performing a strain sweep at 1 Hz. The rheometer was operated in the dynamic oscillatory mode with parallel plate geometry of 25 mm diameter at 190°C. A strain of 1 %, corresponding to the linear viscoelastic domain, was chosen to perform dynamic measurements over a frequency range of 0.001–100 Hz.

2.2 REFERENCES

1. HIGH-MOLECULAR EPDM GRADE FOR DYNAMIC APPLICATIONS, <http://keltan.com/en/the-power-of-keltan/sustainable-innovation/high-molecular-epdm/>
2. Owens, D. K., & Wendt, R. C. (1969). Estimation of the surface free energy of polymers. *Journal of applied polymer science*, 13(8), 1741-1747.
3. Van Oss, C. J., Omenyi, S. N., & Neumann, A. W. (1979). Negative Hamaker coefficients. *Colloid & Polymer Science*, 257(7), 737-744.

4. Brahmakumar, M., Pavithran, C., & Pillai, R. M. (2005). Coconut fiber reinforced polyethylene composites: effect of natural waxy surface layer of the fiber on fiber/matrix interfacial bonding and strength of composites. *Composites Science and technology*, 65(3), 563-569.

CHAPTER 3

**PLASMA SURFACE MODIFICATION OF
LIGNOCELLULOSIC NATURAL COIR FIBERS**

ABSTRACT

The present chapter describes the plasma induced effects on the surface properties of natural coir fibers. Weakly ionized oxygen plasma was created in two different discharge chambers by an inductively coupled radiofrequency (RF) discharge. The water absorption studies showed an increase of water sorption from 39% to 100%. The morphological study using scanning electron microscopy (SEM) analysis also confirmed the surface changes which were observed after the plasma treatment. The topographic measurements and phase imaging done using atomic force microscopy (AFM) indicated difference in topographic features and etching of coir wall, which points to the removal of the first layer of coir fiber. X-ray photoelectron spectroscopy (XPS) analysis revealed that the oxygen content measured for samples treated at 50 Pa increased from initial 18% to about 32%.

3.1 Plasma surface treatment

During the exposure of fibers to oxygen plasma, which is typically red in colour, also white and green colour of plasma was observed just in-between fibers. This could be due to etching of coir fibers and release of carbon oxide and some other, probably nitrogen based substances. Thermal effect during plasma treatment of fibers is important as we observed heating of samples close to the glass chamber. Longer treatment times (more than 15 s) were no longer appropriate due to temperature effects on the fibers, in the case when small chamber was used for plasma treatment. In the case of large chamber, time of coir fiber treatment was limited to 30s.

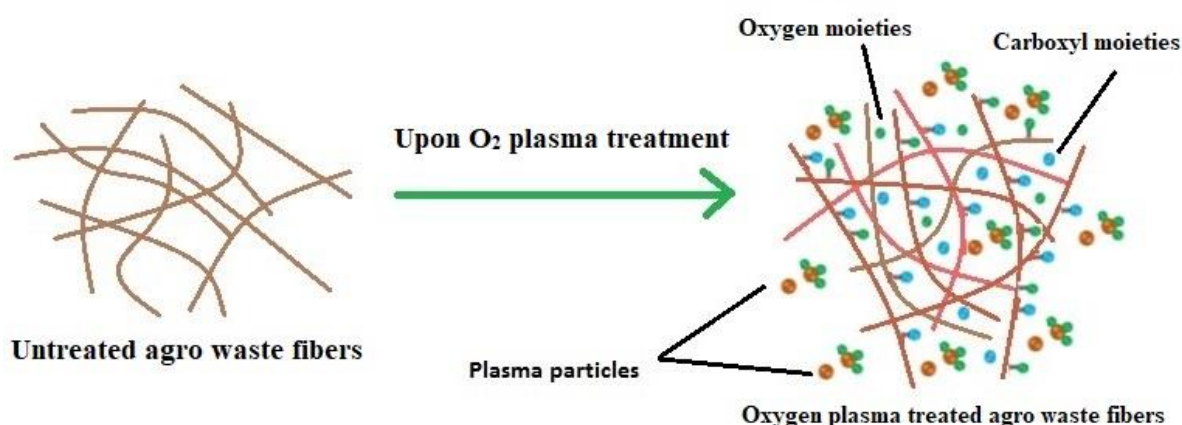


Fig.3.1. Schematic representation of Oxygen plasma treatment of coir fibers

3.2 Optical Emission Spectroscopy

The optical spectrum of oxygen plasma in an empty chamber presented in Figure 2.1 is plotted in Figure 3.2. A couple of lines at the wavelength 777 and 845 prevail. These lines arise from relaxation of highly excited oxygen atoms at the excitation energy of about 11 eV. The radiation appears spontaneously as soon as an atom is excited to these energy levels. The intensive radiation indicates high chemical reactivity of oxygen plasma created in the glass chamber. There is also a band between roughly 500 and 600 nm and it corresponds to

radiative transition of CO molecules (the Angstrom band). The appearance of this band is explained by pollution of the discharge chamber with organic impurities because this chamber is frequently uses for modification of various organic materials.

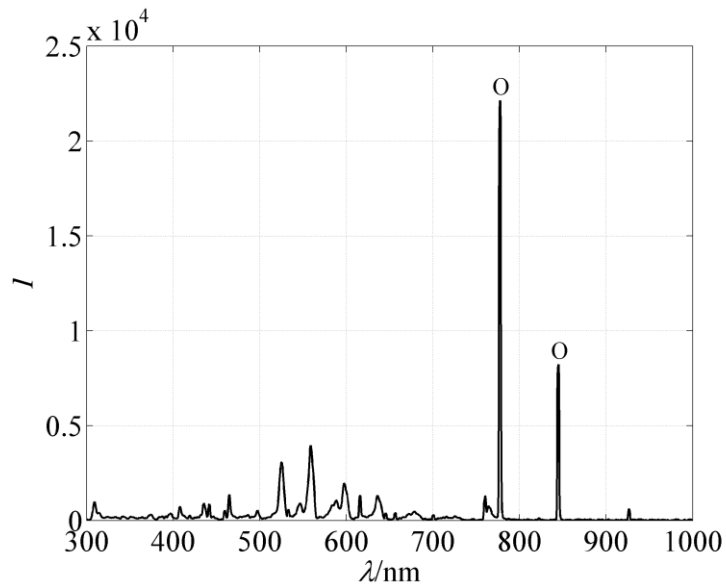


Fig.3.2 An optical spectrum acquired in the small discharge system at the absence of coir.

The spectrum of plasma in the same chamber but loaded with coir fibers is shown in Figure 3.3. This spectrum was acquired 14 seconds after turning on the discharge. It is completely different from the spectrum measured in an empty chamber. The atomic oxygen lines are barely visible and the molecular band predominates. Furthermore, another band is observed in the UV region and that band also corresponds to the relaxation of excited CO molecules (the third positive transition). The huge difference between the spectra presented in Fig.3 and Fig.4 is explained by extensive etching of coir fibers during plasma treatment.

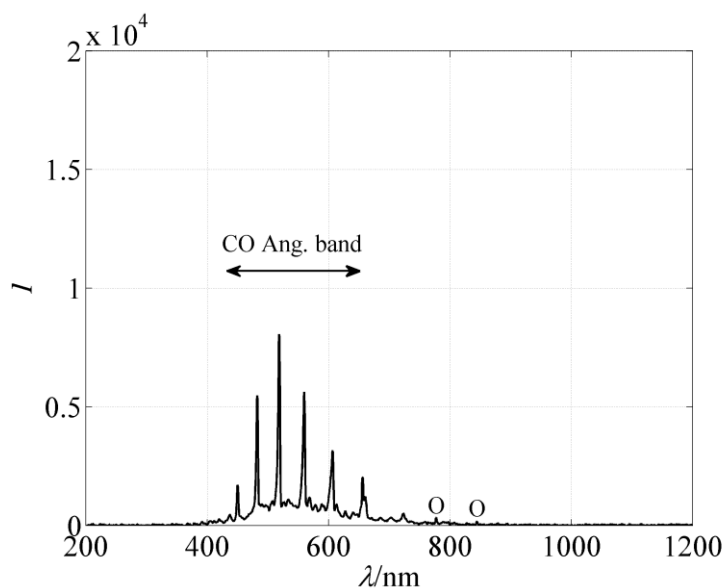


Fig.3.3 An optical spectrum acquired in the small system loaded with coir after 14 s of plasma treatment.

The time evolution of selected spectral features is presented in Figure 3.4. The intensity of oxygen atomic lines rapidly decreases with treatment time and the intensity of CO lines increases. The etching is therefore time-dependent. Just after ignition of the discharge it is rather weak and rapidly increases. Such behaviour is explained by thermal effects. As the discharge is turned on the oxidation of coir fibers starts. The chemical reactions on the surface of the fibers are exothermic causing increase of the fibers' temperature. The higher temperature facilitates more intensive oxidation and therefore more intensive heating and so on.

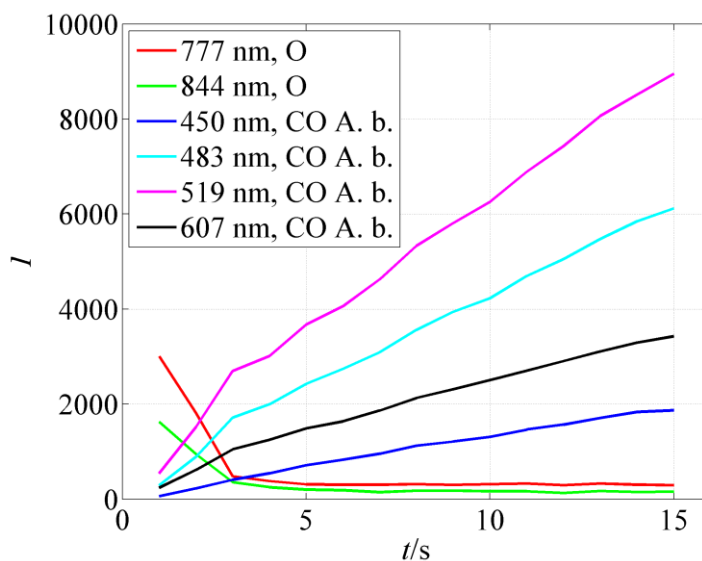


Fig.3.4 Time evolution of the O-atom lines at 777 and 845 nm and selected lines of CO Angstrom band.

3.3 Water Absorption Studies

Samples were tested for water absorption, about 2 h after treatment. The results of water absorbency time and water absorptive capacity of untreated and plasma treated samples are shown in Table 3.1.

Table 3.1 Average water absorbency time and water absorptive capacity of coir fibers according to plasma treatment

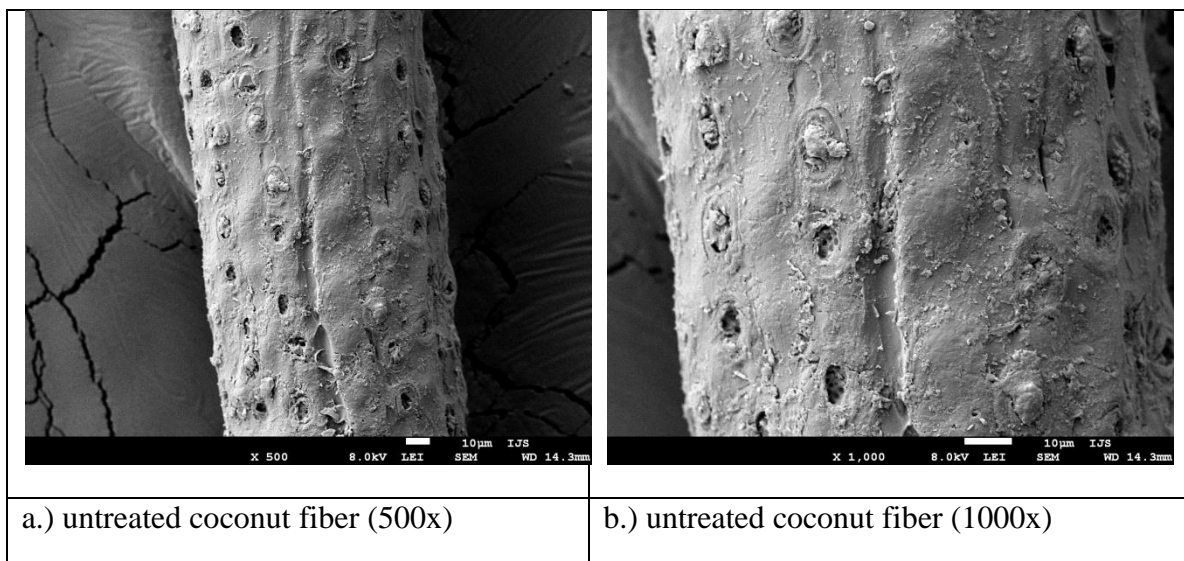
Size of plasma chamber	Pressure (Pa)	Treatment time (s)	Water absorbency time (s)	Water absorptive capacity (%)
-	0	0	122	39
Small	50	1	2	68
		3	2	78
		5	2	78
		10	2	83
		15	1	85
Small	75	1	1	76
		3	1	83

		5	1	86
		10	1	94
		15	1	94
Large	50	20	2	99
		30	1	100

The untreated fibers are very hydrophobic as it is evident from the very long time needed for sample to submerge into water, with water absorbency time nearly 2 minutes. The untreated fibers are relatively hydrophobic as it is evident from the very long time needed for sample to submerge into water, with water absorbency time nearly 2 min. The hydrophobic nature of coir fibers is due to its high lignin content (lignin 40–45% by weight, cellulose 32–43% by weight, hemicellulose 0.15–0.25% by weight and pectin 3–4% by weight) compared with other natural fibers [26]. For the same sample low water absorption capacity (39%) was calculated. Regardless of the plasma chamber size, pressure or treatment time, coir fibers become immediately hydrophilic upon plasma treatment. Time needed for sample to descend is only one or two seconds. The differences between samples treated at different plasma process parameters are in water absorptive capacity. Coir fibers treated in small plasma chamber for 1 s at 50 Pa have absorption capacity of 68%, while at 75 Pa the absorption capacity is 76%. With the increased time of plasma treatment, the absorption capacity of coir fibers towards water also increased. No significant differences were noticed between samples treated for 3 and 5 s or between samples treated for 10 and 15 s. The water absorption capacity of coir fibers treated at 75 Pa for 15 sec were 94%. Even higher absorption capacity was found for fibers treated in large plasma chamber (100%). The reason for increased hydrophilicity of plasma treated fibers is in chemical and physical changes induced by plasma, and can be explained with XPS, SEM and AFM results.

3.4 Scanning Electron Microscope (SEM) Analysis

The SEM analysis of plasma treated samples, when both small chamber and large chamber are used separately for plasma generation, is discussed here. In the case of small chamber used for plasma generation, as the most differences according to water absorption studies were noticed on samples treated for 10 s, further analysis of these samples were done with SEM. SEM analysis gave us better insight on changes in surface morphology, as we could observe that already pristine natural fibers have non uniform morphology with long cracks and small voids which are in some cases closed with small bundles (Figure 3.5a and Figure 3.5b). The size of these structures is about 10 μ m. After 10 s exposure to oxygen plasma at 50 Pa and 75 Pa we observe changes in morphology, as the surface seems to be etched by reactive oxygen species and becomes smoother. Morphological features of holes become more pronounced as can be seen in Figure 3.5c and Figure 3.5d. The bundles in the holes seem to be etched and in some cases, especially those treated at 75 Pa, seem to be removed from the holes and the surface around the holes seems to be more etched (Figure 3.5e and Figure 3.5f).



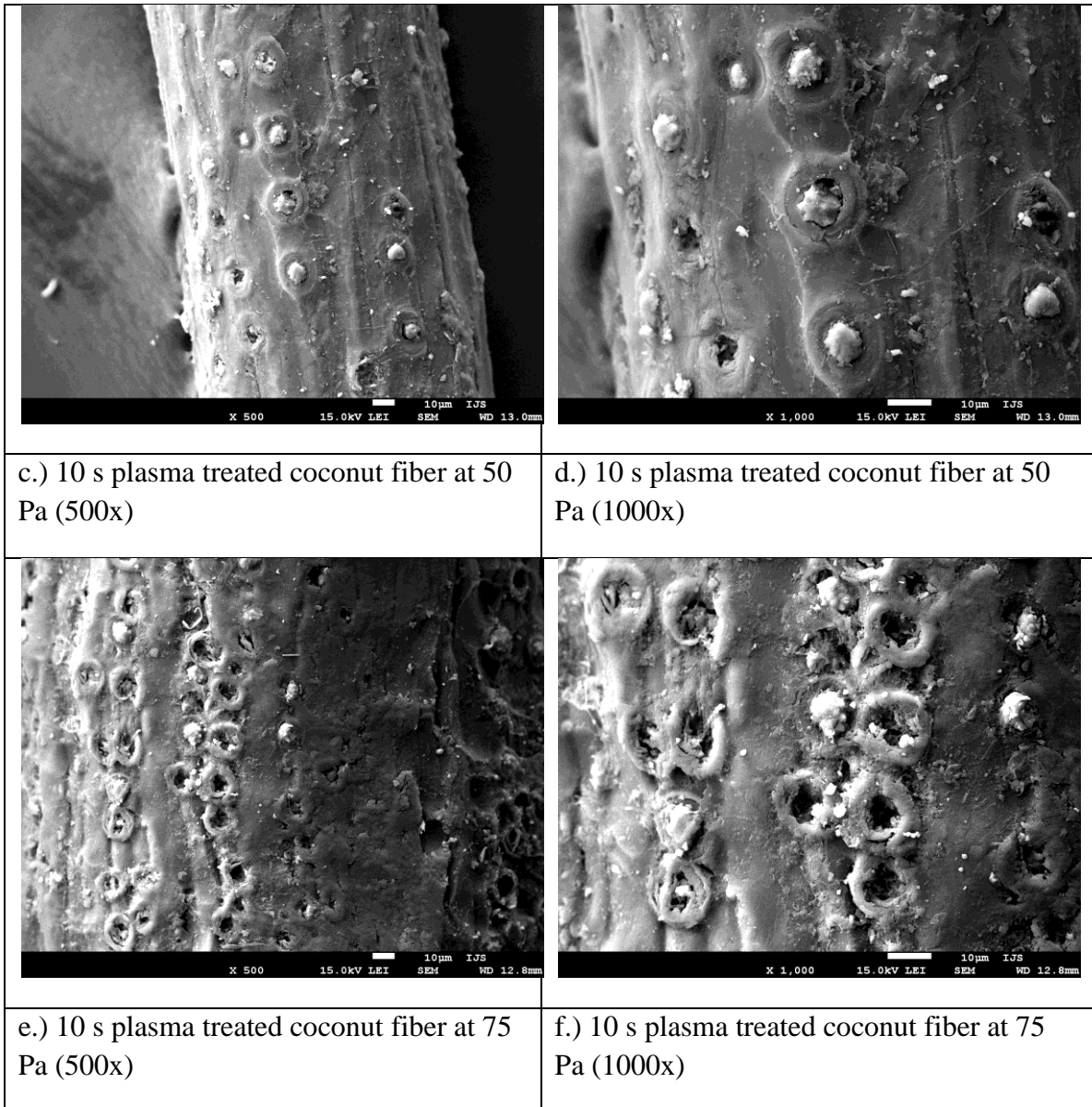
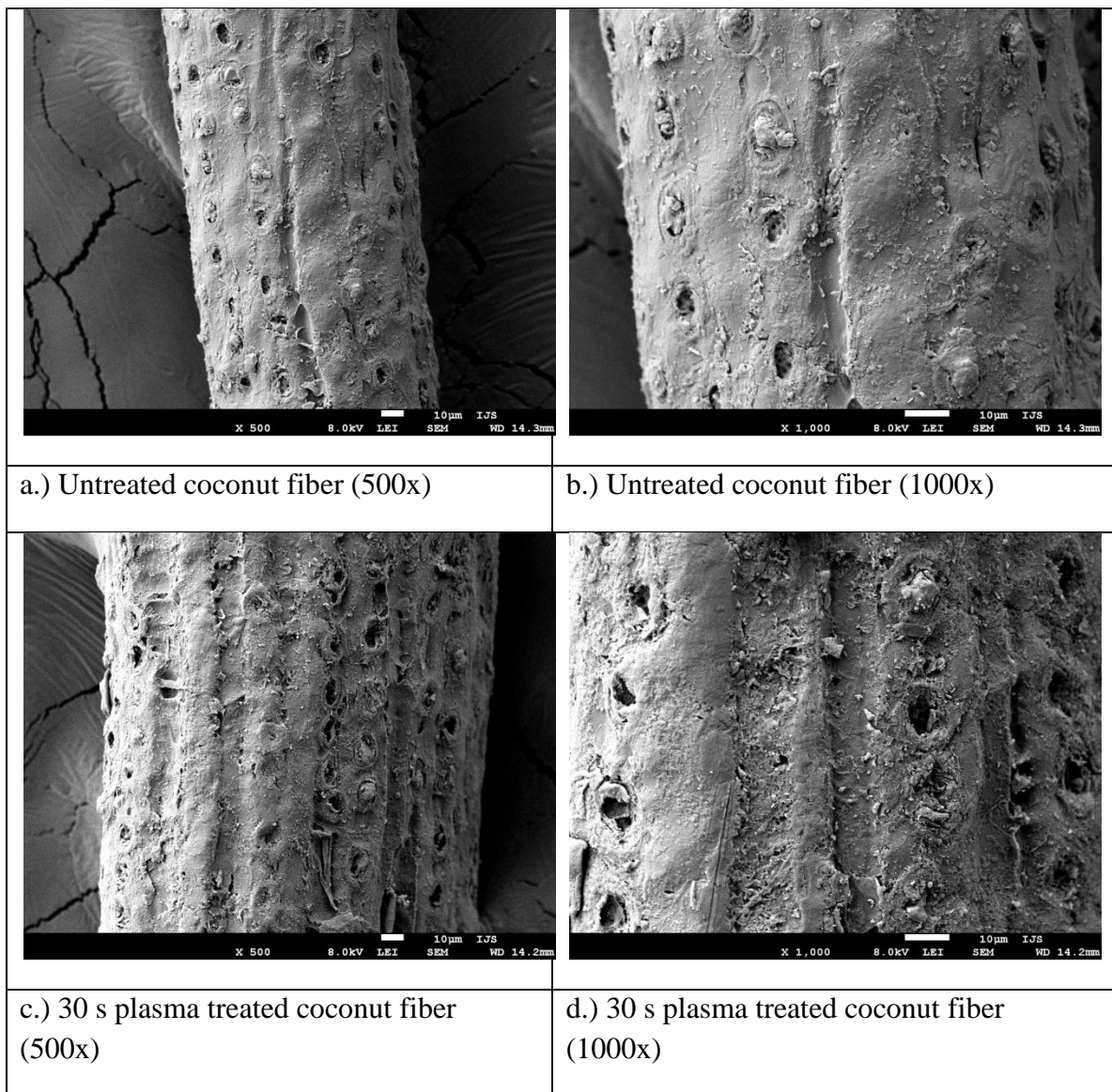
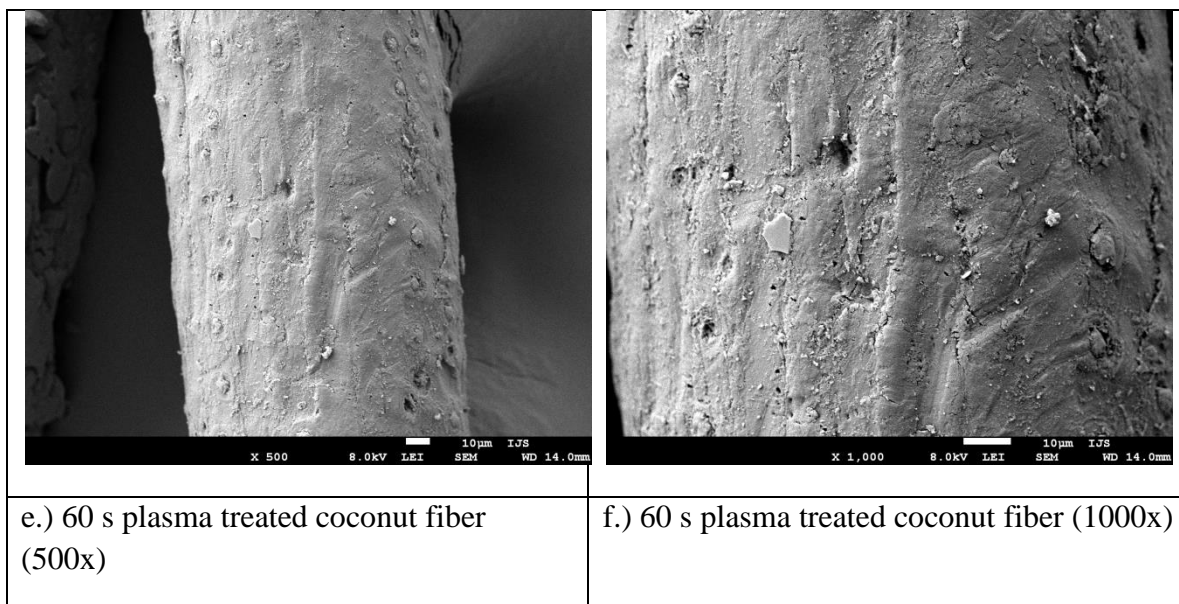


Fig.3.5 SEM analysis of untreated-pristine coconut fibers (**a, b**), 10 s plasma treated at 50 Pa (**c, d**) and 10s plasma treated at 75 Pa (**e, f**) coconut fibers.

In the case of large chamber used for plasma generation, after 30 s exposure to oxygen plasma we observe changes in morphology, as the surface seems to be etched by reactive oxygen species and becomes rougher. Morphological features become more pronounced as can be seen in Figure 3.5c and Figure 3.5d. The holes are more prominent and the bundles are in most cases lost from the surfaces. Those bundles which remain on the surface seem not to be as closely packed as in pristine coconut surface (**Figure 3.6a** and

Figure 3.6b). In order to study the effects of longer treatment time on morphology we exposed fibers to plasma for 60 s. In this case we indeed observed more pronounced morphological changes as in this case surface features (**Figure 3.6e** and **Figure 3.6f**) were not as prominent and the roughness seemed to be lower. The surface in this case seemed to be more uniformly ached, which could be explained also by temperature effects, which were observed during plasma treatment- some parts of the surface became dark brown due to overheating.





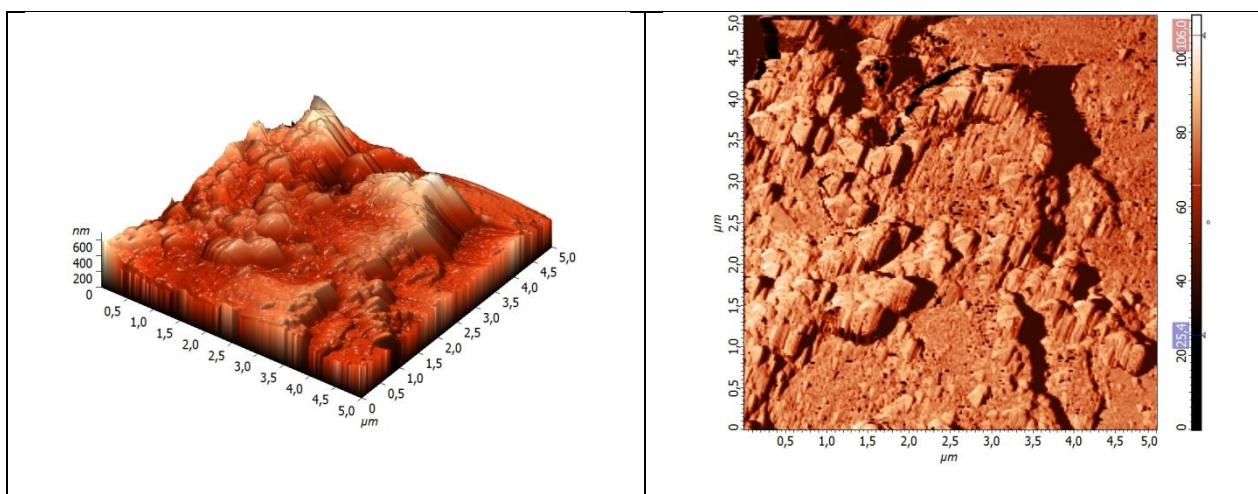
e.) 60 s plasma treated coconut fiber (500x)

f.) 60 s plasma treated coconut fiber (1000x)

Fig.3.6 SEM analysis of untreated-pristine coconut fibers (a,b), 30 s plasma treated (c,d) and 60s plasma treated (e,f) coconut fibers.

3.5 Atomic Force Microscope (AFM) Analysis

The AFM analysis of plasma treated samples, when both small chamber and large chamber are used separately for plasma generation, is discussed here. In the case of large chamber used for plasma generation, AFM analysis was done on untreated and 30 s treated sample in the case of large chamber when used. The changes in topography are presented in Figure 3.7. The height image presents the 3D topographical features of the surface, while the phase image shows also different viscoelastic properties of the surface.



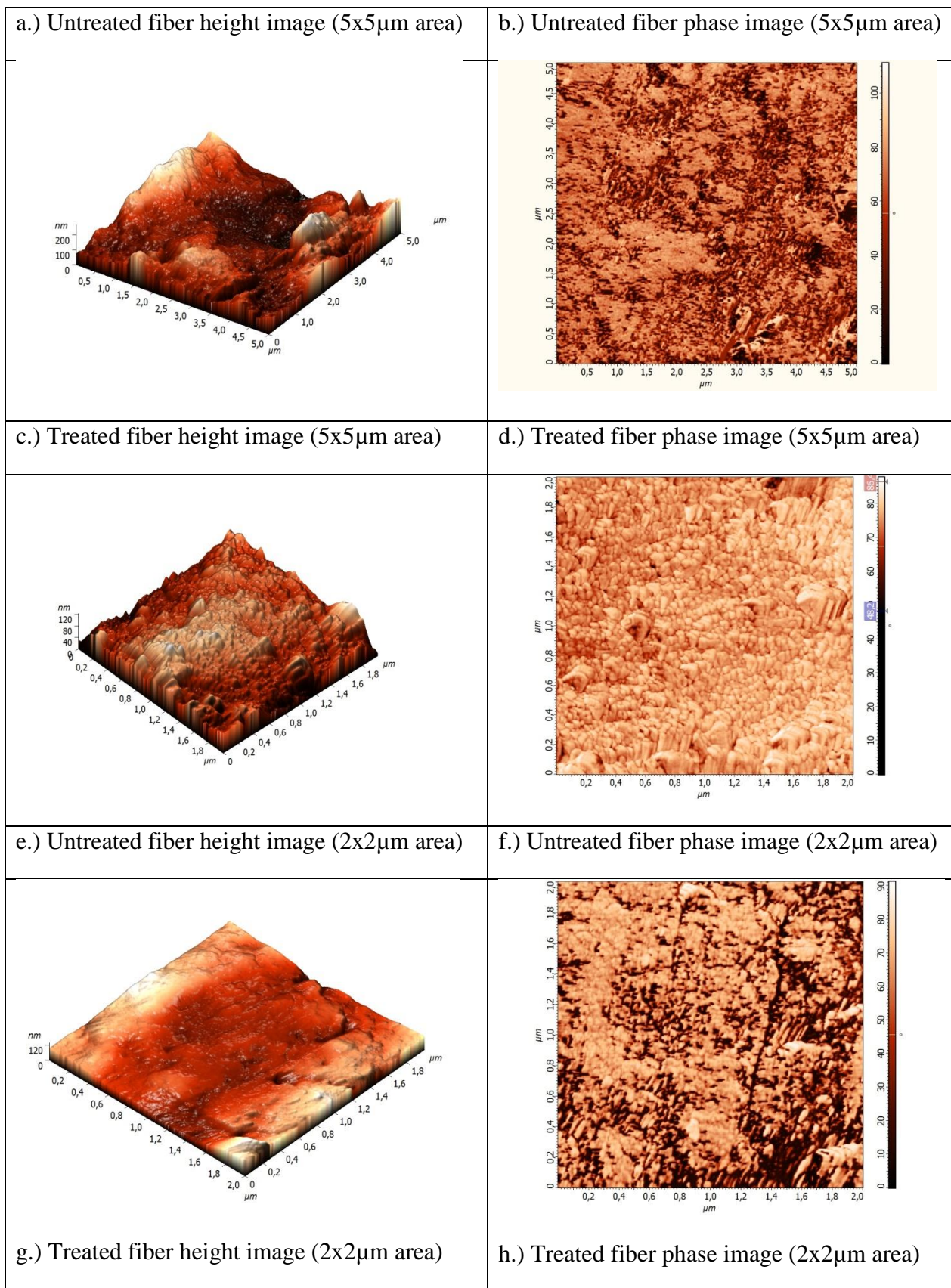


Fig. 3.7 AFM height and phase images done on 5x5 and 2x2 μm area of untreated and 30 s treated coconut fibers.

AFM analysis of fibers enabled us to observe differences in surface topography and viscoelastic properties on the nanoscale. Although natural coconut fibers are not uniform and statistical analysis is not possible with AFM technique, we could observe difference between untreated and plasma treated fibers. It seems that untreated fibers have rougher surface as can be seen from height images in **Figure 3.7 a, c, e and g**. This could be explained by etching of the surface of coconut wall. Difference in viscoelastic properties of the surface can be seen from phase image, especially at higher magnification (**Figure 3.7 f and h**). Here we can see uniform grain structure on the untreated surface; while on the treated surface black patches observed and are correlated with different surface properties.

3.6 X-ray photoelectron spectroscopy (XPS) Analysis

XPS analysis was done on coconut fibers before plasma treatment and immediately after 10s of plasma treatment at 50 Pa and at 75 Pa, when small chamber is used for plasma generation. The oxygen content increased on all plasma treated surfaces. A bit higher oxygen content was measured for samples treated at 50 Pa (oxygen increased from initial 18 at% to about 32 at %). Increase in oxygen content is the result of incorporation of novel oxygen functional groups [27]. Reduced oxygen content due to etching effects could be to some point appointed to removal of lignin, which has less oxygen. The O/C ratio for lignin is about 0.35, while cellulose, hemicellulose and pectin have higher ratio about 0.83. Some lignocellulosic materials can have also silicon in their composition (Rosas et al Hemp-derived activated carbon fibers by chemical activation with phosphoric acid. *Fuel*, 88 (2008) 19–26.), which was noticed also on untreated fibers and was slightly reduced after oxygen plasma treatment (from 3.4 at% to about 1.3 at %). Slight increase in nitrogen functional groups was also observed on the surface after plasma treatment, especially for the case when fibers were treated at 50 Pa for 10s, for this case nitrogen content increased from initial about 1.1 at% to about 4.1 at%.

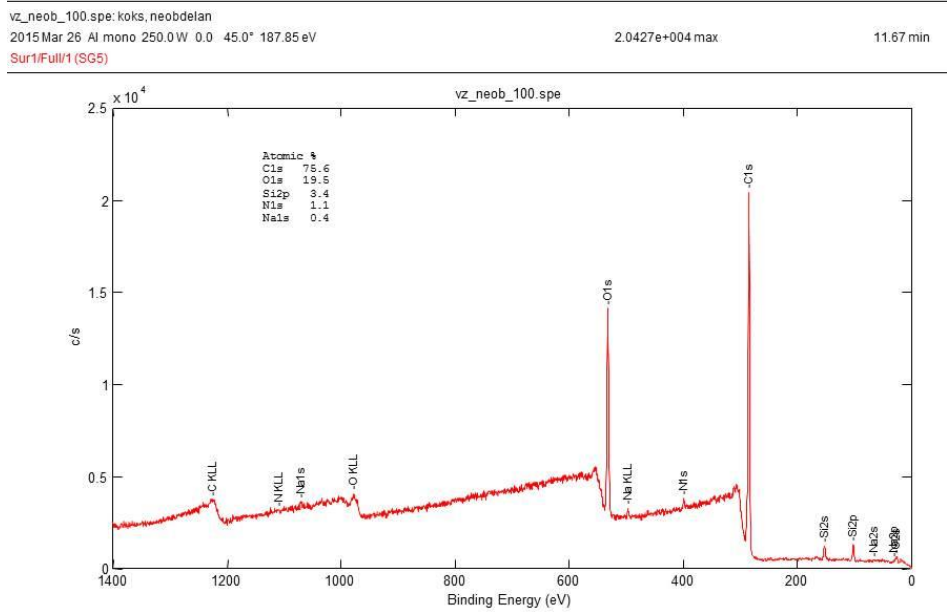


Fig.3.8a XPS Spectrum for Untreated coir fiber when small chamber is used for plasma generation

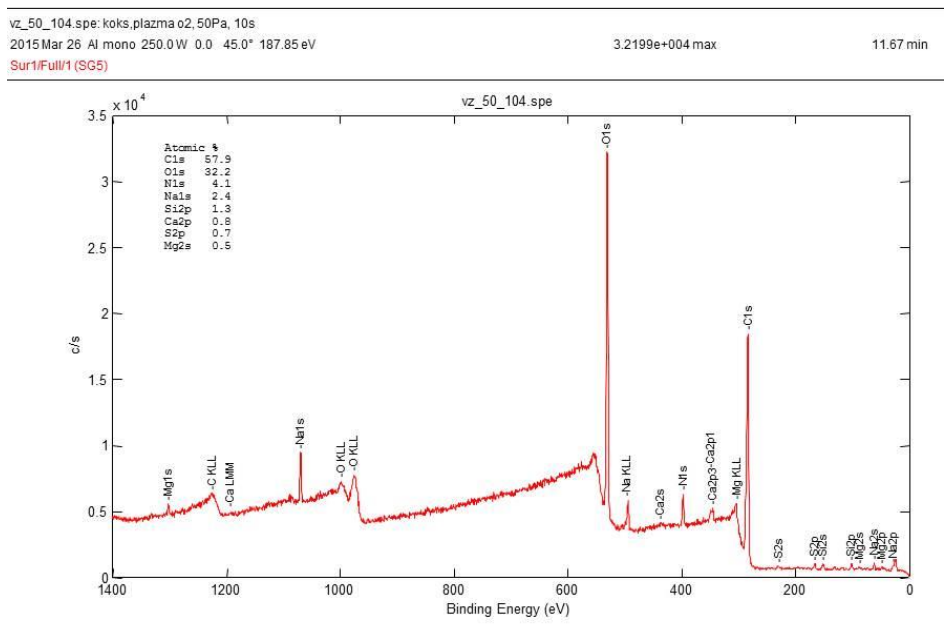


Fig. 3.8b XPS Spectrum coir fiber after 10s of plasma treatment at 50 Pa

Case 2

In the case of small chamber used for plasma generation, preliminary results on the effects of plasma treatment on water absorption and topography of coir fibers clearly indicates the enhancement of surface properties of fibers. Water absorption has increased already after 1 s of treatment from initial 39 to 68% and 76% for 50 Pa and 75 Pa treatment conditions, respectively. It was observed that water absorption was higher for fibers treated at 75 Pa. The most prominent increase in water absorption was noticed after 10s of treatment for both treatment conditions (50 Pa and 75 Pa). These fibers were analysed in detail by SEM and XPS. SEM analysis showed changes in morphology as etching of the surface seems to take place and probably removes waxes, pectin and lignin from the surface. The surface becomes smoother and holes on fibers become more pronounced. Difference between etching of fibers treated at 50 Pa and 75 Pa was not observed with SEM. However XPS results showed that fibers treated at 50 Pa had more pronounced chemical changes. Increase in oxygen functional groups was noticed on both plasma treated samples, but a slightly higher increase was noticed for fibers treated at 50 Pa. Interestingly less silicon was observed on all plasma treated surfaces. It is hard to determine which material was removed by plasma treatment, as removal of lignin could be connected to higher oxygen content which can in the present case be also due to functionalization with novel oxygen functional groups from plasma.

3.8 CONCLUSIONS

In the present study, an attempt has been made to investigate the effect of oxygen plasma treatment on the surface modification of coir fibers. Weakly ionized oxygen plasma was created in discharge chamber by an inductively coupled radiofrequency (RF) discharge. The plasma experiments were conducted in two different discharge chambers having

chamber volumes, 17 L and 3.1 L, respectively. The pressure was set to 75 Pa and the treatment time was 20 s and 30 s, when 17 L chamber was used for plasma generation. For the 3.1 L chamber used for plasma generation, the plasma treatment was done at 2 different pressures (75 Pa and 50 Pa) and at 5 different treatment times (1, 3, 5, 10 and 15 s). The water absorption studies showed an increase in water absorption from 39% to about 100%. The morphological study using SEM analysis also confirmed changes in the surface topography after plasma treatment. The topographic measurements done using atomic force microscopy showed etching of fiber wall which influences the higher water absorption. XPS analysis reveals that oxygen content measured for samples treated at 50 Pa increased from initial 18 at% to about 32 at%. This study explores the possibilities of plasma treatment as a viable technique for surface modification of natural fibers. By controlling the plasma parameters and by understanding the plasma chemistry, it is possible to effectively modify surfaces of natural fibers. From the engineering point of view, the modified fibers' surfaces are very important as they serve as interfaces of composites which are used for high-performance applications.

3.9 REFERENCES

1. Holbery, James, and Dan Houston. "Natural-fiber-reinforced polymer composites in automotive applications." *Jom* 58.11 (2006): 80-86.
2. Jahan, A., Rahman, M. M., Kabir, H., Kabir, M. A., Ahmed, F., Hossain, M. A., & Gafur, M. A. (2012). Comparative study of physical and elastic properties of jute and glass fiber reinforced LDPE composites. *International Journal of Scientific and Technology Research*, 1(10), 68-72.
3. Lee, S., Shi, S. Q., Groom, L. H., & Xue, Y. (2010). Properties of unidirectional kenaf fiber-polyolefin laminates. *Polymer Composites*, 31(6), 1067.

4. Yan, T. H. (2012, November). Experimental Research on the Flax/PP Thermoplastic Composite Material Hot Pressing Process. In *Advanced Materials Research* (Vol. 573, pp. 1216-1219).
5. Zhao, X., Li, R. K., & Bai, S. L. (2014). Mechanical properties of sisal fiber reinforced high density polyethylene composites: Effect of fiber content, interfacial compatibilization, and manufacturing process. *Composites Part A: Applied Science and Manufacturing*, 65, 169-174.
6. Hussain, S. A., Pandurangadu, V., & Palanikuamr, K. (2011). Mechanical properties of green coconut fiber reinforced HDPE polymer composite. *International Journal of Engineering Science and Technology*, 3(11), 7942-7952.
7. Dong, Y., Ghataura, A., Takagi, H., Haroosh, H. J., Nakagaito, A. N., & Lau, K. T. (2014). Polylactic acid (PLA) biocomposites reinforced with coir fibers: Evaluation of mechanical performance and multifunctional properties. *Composites Part A: Applied Science and Manufacturing*, 63, 76-84.
8. Arib, R. M. N., Sapuan, S. M., Ahmad, M. M. H. M., Paridah, M. T., & Zaman, H. K. (2006). Mechanical properties of pineapple leaf fiber reinforced polypropylene composites. *Materials & Design*, 27(5), 391-396.
9. Shinoj, S., Visvanathan, R., Panigrahi, S., & Varadharaju, N. (2011). Dynamic mechanical properties of oil palm fiber (OPF)-linear low density polyethylene (LLDPE) biocomposites and study of fiber–matrix interactions. *Biosystems engineering*, 109(2), 99-107.
10. Akil, H. M., Cheng, L. W., Ishak, Z. M., Bakar, A. A., & Rahman, M. A. (2009). Water absorption study on pultruded jute fiber reinforced unsaturated polyester composites. *Composites Science and Technology*, 69(11), 1942-1948.

11. Abdullah, A. H., Khalina, A., & Ali, A. (2011). Effects of fiber volume fraction on unidirectional kenaf/epoxy composites: the transition region. *Polymer-Plastics Technology and Engineering*, 50(13), 1362-1366.
12. Harish, S., Michael, D. P., Bensely, A., Lal, D. M., & Rajadurai, A. (2009). Mechanical property evaluation of natural fiber coir composite. *Materials characterization*, 60(1), 44-49.
13. George, J., Sreekala, M. S., & Thomas, S. (2001). A Review on Interface Modification and Characterization. *Polymer engineering and science*, 41(9).
14. Mohanty, A. K., Misra, M., & Drzal, L. T. (Eds.). (2005). *Natural fibers, biopolymers, and biocomposites*. CRC Press.
15. Panaitescu, D. M., Vuluga, Z., Ghiurea, M., Iorga, M., Nicolae, C., & Gabor, R. (2015). Influence of compatibilizing system on morphology, thermal and mechanical properties of high flow polypropylene reinforced with short hemp fibers. *Composites Part B: Engineering*, 69, 286-295.
16. Sofiah, M. K., Lin, O. H., Akil, H. M., & Ishak, Z. A. M. (2015, January). Effect of Polypropylene-Methyl Polyhedral Oligomeric Silsesquioxane Compatibilizer in Polypropylene/Silica Nanocomposites: Mechanical, Morphological and Thermal Studies. In *Materials Science Forum* (Vol. 803, pp. 265-268).
17. Baykus, O., Mutlu, A., & Doğan, M. (2015). The effect of pre-impregnation with maleated coupling agents on mechanical and water absorption properties of jute fabric reinforced polypropylene and polyethylene biocomposites. *Journal of Composite Materials*, 0021998315573288.
18. Suzuki, K., Sato, A., Okumura, H., Hashimoto, T., Nakagaito, A. N., & Yano, H. (2014). Novel high-strength, micro fibrillated cellulose-reinforced polypropylene composites using a cationic polymer as compatibilizer. *Cellulose*, 21(1), 507-518.

19. Sojoudiasli, H., Heuzey, M. C., & Carreau, P. J. (2014). Rheological, morphological and mechanical properties of flax fiber polypropylene composites: influence of compatibilizers. *Cellulose*, 21(5), 3797-3812.
20. Zhao, X., Li, R. K., & Bai, S. L. (2014). Mechanical properties of sisal fiber reinforced high density polyethylene composites: Effect of fiber content, interfacial compatibilization, and manufacturing process. *Composites Part A: Applied Science and Manufacturing*, 65, 169-174.
21. Srubar, W. V., Pilla, S., Wright, Z. C., Ryan, C. A., Greene, J. P., Frank, C. W., & Billington, S. L. (2012). Mechanisms and impact of fiber–matrix compatibilization techniques on the material characterization of PHBV/oak wood flour engineered biobased composites. *Composites Science and Technology*, 72(6), 708-715.
22. Pracella, M., Haque, M. M. U., & Alvarez, V. (2010). Functionalization, compatibilization and properties of polyolefin composites with natural fibers. *Polymers*, 2(4), 554-574.
23. Haque, M. M., Hasan, M., Islam, M. S., & Ali, M. E. (2009). Physico-mechanical properties of chemically treated palm and coir fiber reinforced polypropylene composites. *Bioresource Technology*, 100(20), 4903-4906.
24. Karmarkar, A., Chauhan, S. S., Modak, J. M., & Chanda, M. (2007). Mechanical properties of wood–fiber reinforced polypropylene composites: Effect of a novel compatibilizer with isocyanate functional group. *Composites Part A: Applied Science and Manufacturing*, 38(2), 227-233.
25. Yang, H. S., Kim, H. J., Park, H. J., Lee, B. J., & Hwang, T. S. (2007). Effect of compatibilizing agents on rice-husk flour reinforced polypropylene composites. *Composite Structures*, 77(1), 45-55.

26. N. Ayrilmis, S. Jarusombuti, V. Fueangvivat, P. Bauchongkol, R.H. White, Coirfiber reinforced polypropylene composite panel for automotive interior applications, *Fibers Polym.* 12 (7) (2011) 919–926.
27. Jazbec, K., Šala, M., Mozetič, M., Vesel, A., & Gorjanc, M. (2015). Functionalization of Cellulose Fibers with Oxygen Plasma and ZnO Nanoparticles for Achieving UV Protective Properties. *Journal of Nanomaterials*, 2015.

CHAPTER 4

**DEVELOPMENT AND CHARACTERISATION OF
FLUOROALKYL FUNCTIONAL SILOXANE (FAS) BASED
HYDROPHOBIC COATING ON LIGNOCELLULOSIC
NATURAL COIR FIBERS**

ABSTRACT

This chapter describes a novel technique based on spray-dry-cure method to establish a hydrophobic sol-gel coating on the coir fiber surface. The hydrophobic surface was characterized by water contact angle analysis, scanning electron microscopy (SEM), atomic force microscopy (AFM) and X-ray photoelectron spectroscopy (XPS). The contact angle measurements shows the hydrophobic behavior of coir fiber surface. AFM analysis shows that the surface architecture of the FAS coated coir samples was significantly changed as a result of the sol-gel coating. The smooth surface morphology of FAS coated coir fibers obtained using SEM confirms the uniform spraying of fluoroalkyl functional siloxane (FAS) on the surface. Surface survey spectra from XPS analysis reported a fluorine (F 1s) content of 52.1% for FAS coated coir fiber which contributes to the hydrophobic nature of coir fibers. The tensile analysis were performed on the elementary as well as FAS coated fibers to determine the average breaking force, breaking strength, modulus and elongation at break of both uncoated and FAS coated fibers.

4.1 FAS Sol–gel coating

A sol of 10 % FAS was prepared in distilled water and applied to the plasma pre-treated coir fiber samples by the spray-dry-cure method, including full immersion at 20⁰C, followed by a wet pick-up adjustment to 85 %, drying at 100⁰C and curing at 150⁰C for 5 min. After the sol application, the samples were left for 14 days under standard atmospheric conditions (65 ± 2 % relative humidity and 20 ± 1⁰C) to allow the complete network formation of the applied finishes. The effectiveness of FAS coating was analyzed by studying water contact angle analysis, scanning electron microscopy (SEM), atomic force microscopy (AFM) and X-ray photoelectron spectroscopy (XPS).

4.2 Wettability analysis

The contact angle measurements were carried out on different conditions of coir fibers (untreated and FAS coated) using three different liquids (of which at least one is non-polar and two must be polar, and then the dispersive and polar components of the surface can be determined) to study the effect of the treatments on the hydrophobic nature of coir fibers. Table 4.1 shows the average values of contact angle measured on the different conditions of coir fibers using three different liquids.

Table 4.1 Average values (n=30) of the contact angle of the different conditions of coir fibers (untreated, and FAS coated).

Liquid used	Name of the sample	Work of adhesion	Number of measurements	Average value of contact angle	Standard deviation
Water	Untreated Coir	121.7	30	48	3.91
	FAS coated Coir	46	30	112	3.86
Ethylene glycol	Untreated Coir	83.7	30	43	3.63
	FAS coated Coir	43.5	30	96	3.41
Tricresylphosphate (TCP)	Untreated Coir	65	30	29	2.41
	FAS coated Coir	77	30	54	3.58

From the table 4.1, it is clearly see that the FAS coated Coir shows a tremendous improvement in hydrophobicity compare with pristine coir fibers. The water repellent properties (hydrophobic behaviour) of coir fibers are due to the extremely low surface free energy of the FAS polymer network formed on the coir fibers. Similar results were obtained in previous studies [1, 2, 3, 4]. The plasma pre-treatment increased the effective concentration of the FAS network on the lignocellulosic coir fibers, which resulted in enhanced repellency before and after repetitive washing, compared with that of the FAS-coated fiber sample without the plasma pre-treatment. Barbara et al. also reported that the plasma pre-treatment enables the formation of the hydrophobic and self-cleaning properties of the FAS coated samples, which manifested as the simultaneous increase in the water contact angle and decrease in the water sliding angle. The same group also proved the oleophobicity of the FAS coated surface by measuring the contact angle of the formed surface by using n-hexadecane as the liquid. They obtained an oil contact angle of n-hexadecane droplet equal to 140⁰C. The higher water contact angle and lower sliding angles undoubtedly underlines that the plasma pre-treatment contributed to the creation of the “lotus effect” (water to roll off the fabric surfaces very easily) on the FAS coated sample surface. In Table 4.2, the surface energies of the untreated as well as FAS coated coir samples were calculated by using Owens-Wendt formula (based on geometric mean approach)

Table 4.2 Surface energy components (mJ/m^2) γ_s , γ_s^d and γ_s^p of untreated as well as sol-gel coated coir fibers were calculated by using Owens-Wendt formula (based on geometric mean approach)-All dimensions are in “mN/m”

Sample	γ_s	γ_s^d	γ_s^p
Untreated Coir	48.2	20.2	28
FAS Coated coir	22.4	22.4	0

From the Table 4.2, it can be inferred that, the untreated coir fibers shows a dispersive surface free energy component of 20.4mN/m and a polar surface free energy component of 28mN/m. It is due to the fact that the uncoated coir fibers surfaces are rich in hydroxyl groups which contribute to the hydrogen bonding. But in the case of FAS coated fiber surfaces, it can be seen that surface energy/tension is purely dispersive. It is an indication of hydrophobic nature of the FAS coated coir fiber surfaces. The total surface free energy dropped from 48mN/m for uncoated coir fibers to 22.4mN/m for FAS coated fiber also confirms the transformation to hydrophobic behavior of coated fibers.

In Table 4.3, the surface energies of the untreated as well as FAS coated coir samples were calculated by using Van Oss et al. approach.

Table 4.3 Surface energy components (mJ/m^2) of untreated as well as sol-gel coated coir fibers were calculated by the acid–base method using three probe liquids [water (polar), ethylene glycol (polar) and tricresylphosphate (TCP-nonpolar)] -All dimensions are in “ mN/m ”

Sample	Υ_s	Υ_s^{LW}	Υ_s^-	Υ_s^+	Υ_{AB}
Untreated Coir	36.9	36.1	41.3	0.0	0.8
FAS Coated coir	27.5	25.7	0.8	1	1.8

Table 4.3 shows another approach of the surface energy based on Lewis acid–base concept applied to surfaces by Van Oss et.al. method. The Lifshitz–van der Waals (Υ^{LW}), acid–base components (Υ_{AB}), and total surface free energies of uncoated and FAS coated coir fibers were calculated from contact angle measurements. The total free energy is the sum of the Lifshitz–Van der Waals and the combined acid (Υ_s^+) and base (Υ_s^-) components. According to Lewis, the acidity can be calculated based on the probability of chemical groups to accept electrons whereas the basicity is the probability of chemical groups to donate electrons. The acid–base interactions include hydrogen bonds. Table 4.3 presents the surface energy of coir fibers measured experimentally using Acid–base approach. The FAS coating provide surface energy values significantly different than for uncoated fibers.

It can be inferred that, the hydrophobic coating decreases the concentrations of water on the coir fiber surface which in turn leads to the slight decrease of Lifshitz–van der Waals components and the total surface tension. The most pronounced effect was observed for the acid–base parameters.i.e. in the case of untreated fibers, the presence of water causes a very high decrease in acid component and increases the base parameters of the coir fiber surface. But in the case of FAS coated fibers, the inverse trend is observed, i.e. basic component of the free surface energy decreases to $0.8\text{mJ}/\text{m}^2$ from $41.3\text{mJ}/\text{m}^2$ and acid component of the free surface energy slightly increases to $1\text{mJ}/\text{m}^2$ from $0\text{mJ}/\text{m}^2$. The thermodynamic work of adhesion, W_A , calculated from contact angle measurements also indicates that the FAS coated fibers shows lower value of work of adhesion compare with uncoated fibers which in turn shows the hydrophobic behavior exhibited by FAS coated fibers. Similar trend of results obtained by Baley et al. when they used flax fibers in polyester resins [5].

4.3 Water absorption studies

Samples were tested for water absorption, about 2 h after treatment. The results of water absorbency time and water absorptive capacity of untreated and plasma treated samples are shown in Table 4.4.

Table 4.4 Average water absorbency time and water absorptive capacity of uncoated and FAS coated coir fibers

Type of coir fibers	Water absorbency time (s)	Water absorptive capacity (%)
UNCOATED	122	39
FAS COATED	Infinite	Infinite

The sample of uncoated as well as FAS coated coir fibers (5 g) was inserted into wire basket of defined dimensions as shown in figure Fig.4.1. It can be clearly seen from pictures that in the case of FAS coated coir fibers, the time for fibers spent in water is infinite and because there is no water uptake.

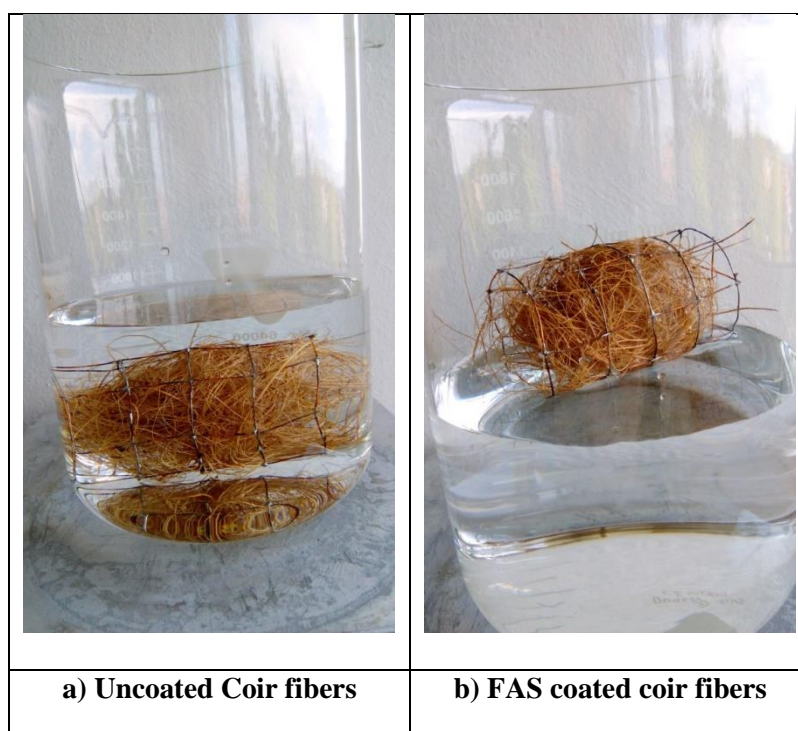
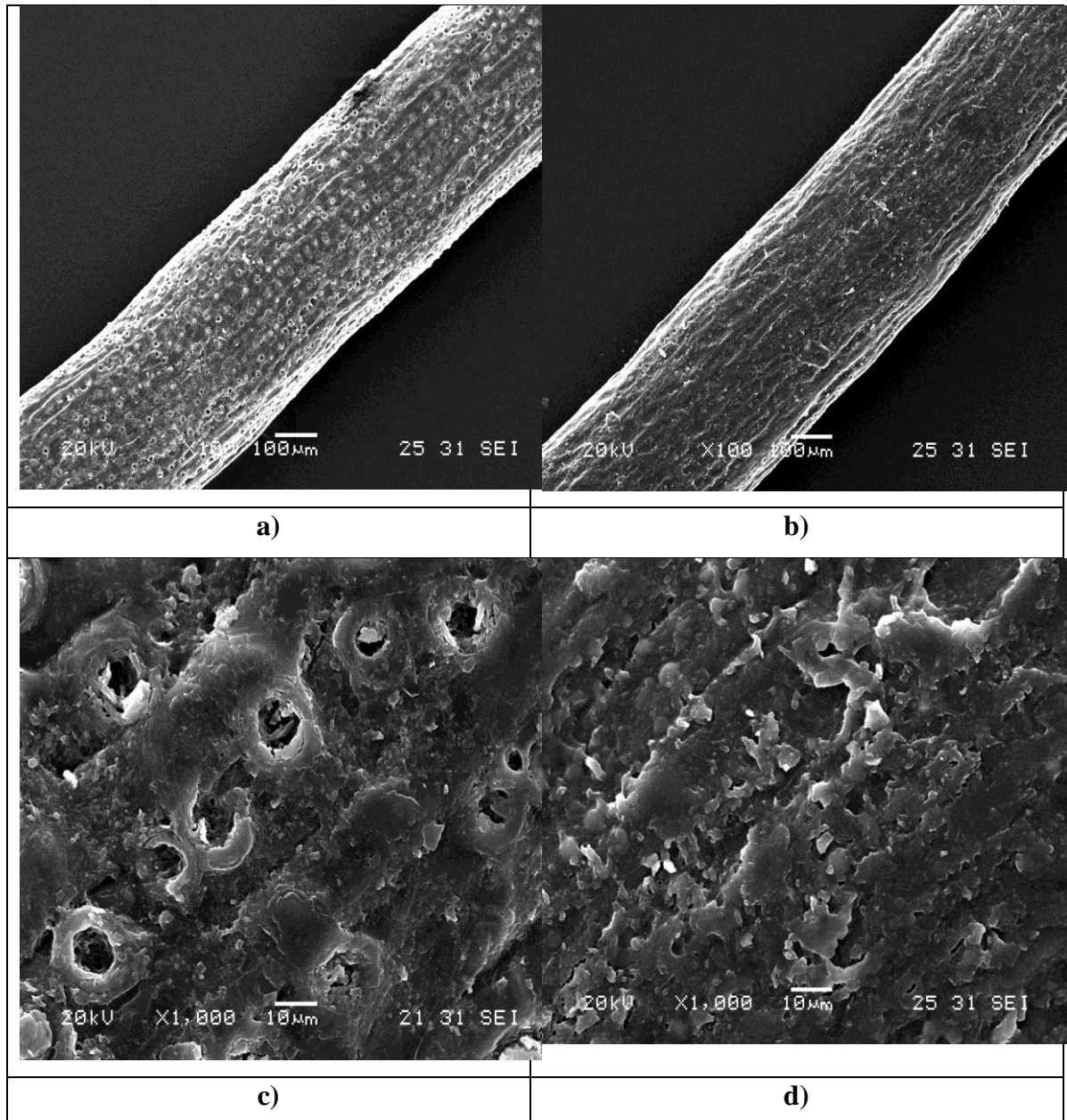


Fig.4.1 Water absorption test for uncoated and FAS coated coir fibers

4.4 Scanning Electron Microscope (SEM) Analysis

Scanning Electron Microscope (SEM) images of untreated and FAS coated coir fibers are shown in Figure 4.2. Figure 4.2a, Figure 4.2c and Figure 4.2e shows uncoated coir fibers whereas Figure 4.2b, Figure 4.2d and Figure 4.2f show FAS coated coir fibers. Figures shows 100x, 1000x and 2000x resolution micrographs which explains the morphological differences between the uncoated and FAS coated coir fibers.



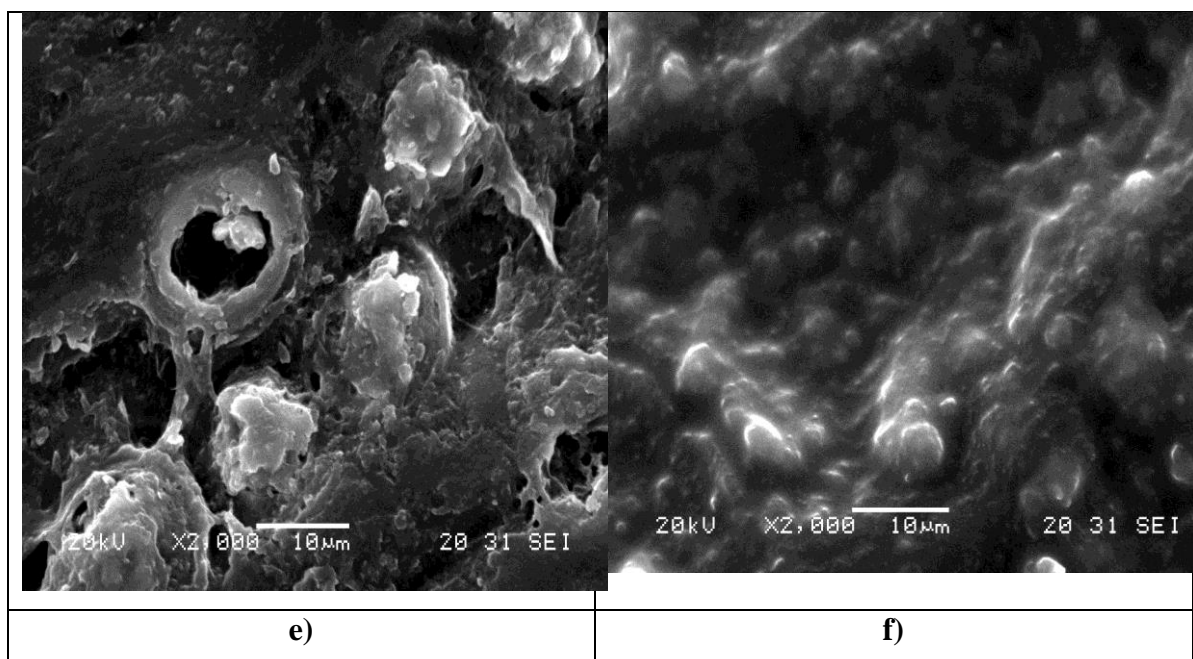


Fig.4.2 Scanning Electron Microscope (SEM) images of untreated and FAS coated coir fibers

It can be inferred that the uncoated coir fibers have non-uniform morphology with long cracks and small voids which are in some cases closed with small bundles (**Figure 4.2 a, c & e**). The size of these structures is about 10µm. These structures are very clear at high resolutions of SEM images. The wettability (hydrophilic) behaviour of uncoated coir fibers can be validated using these results. Chapter 3 also explains the water absorptive capacity of these fibers with the aid of SEM. It can be seen that, long cracks and small voids which are present in uncoated fibers, are absent in FAS coated fibers. From the SEM images, it is evident that the FAS coating is sprayed uniformly all over the coir fiber surface. The hydrophobic behaviour of the FAS coated coir fibers, confirmed with water contact angle analysis results, can be validated with these SEM micrographs.

4.5 Atomic Force Microscope (AFM) Analysis

AFM images showing the surface morphology of uncoated and FAS coated fibers are presented in Figure 4.3 . Imaging was done in the tapping mode. In tapping mode, the tip is not in constant contact with the sample's surface. Instead, the cantilever oscillates at its resonant frequency, which makes the tip lightly tap on the surface during scanning. A constant tip sample interaction is maintained by monitoring the oscillation amplitude and an image is obtained.

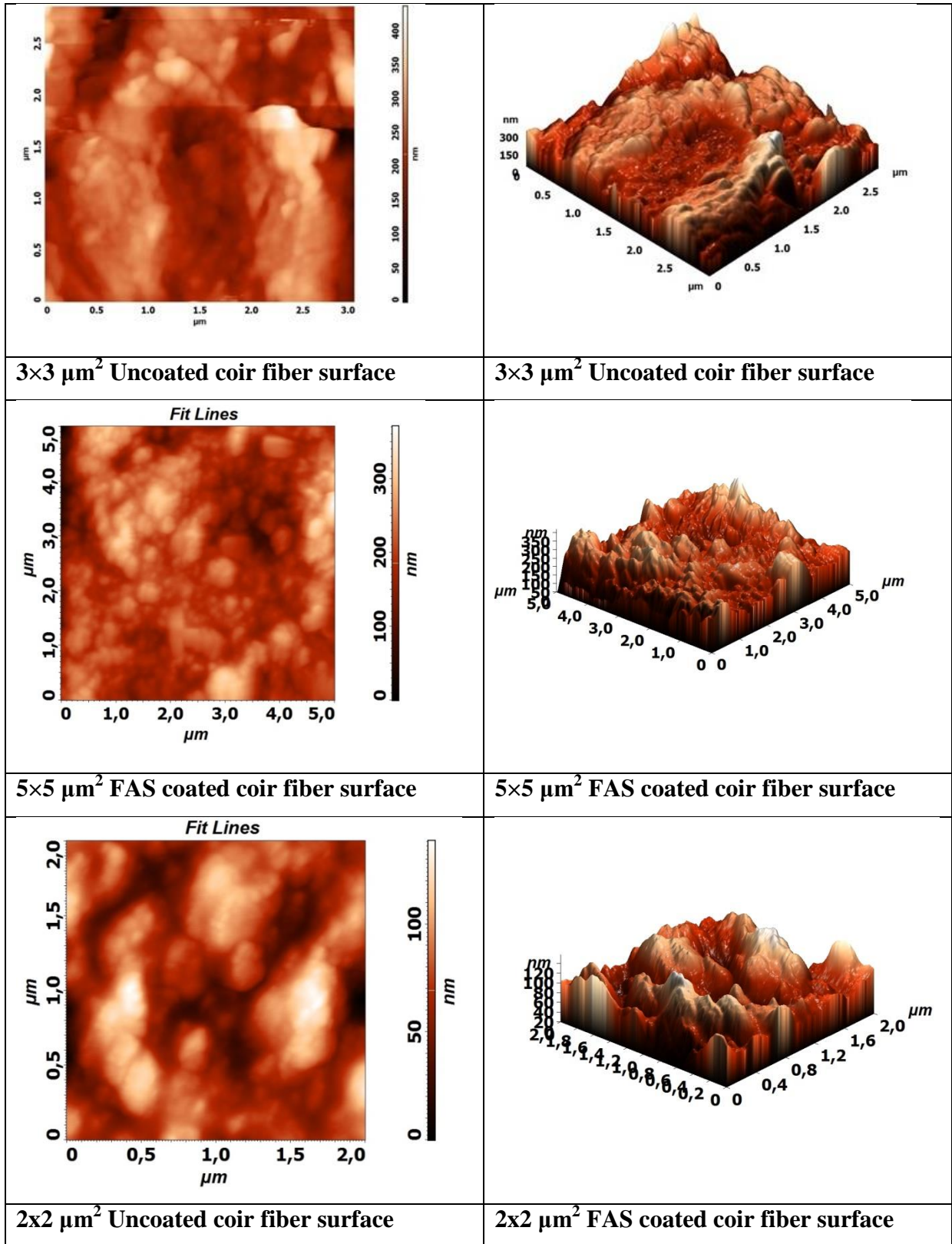


Fig.4.3 AFM topography of uncoated and FAS coated coir fiber surfaces

AFM analysis clearly shows (Figs. 4.3) that the surface architecture of the FAS coated coir samples was significantly changed as a result of the sol–gel coating. In the case uncoated coir surfaces no distinct morphological features are observed whereas in the case of FAS coated

coir surfaces spherical shaped nano sized small particles are observed which are imparted by the polymerization of fluoroalkyl functional siloxane sol gel coating. The application of the FAS coating after plasma pre-treatment turn the fiber surface smooth and decreased the surface roughness indicating that the architecture of the surface was significantly changed. In addition to the average surface roughness, the surface pattern also affects the surface properties of fibers. This observation can be correlated to our finding that the plasma pre-treatment helps in imparting the nanoscopic topography which leads to the formation of a dual micro to nano-structured composite fiber surface with a high content of air pockets (shown figure Fig.4.4), which significantly decreased the interfacial area between the water and the fibers after the sol-gel coating was applied and imparted the “hydrophobic effect” to the sample. Simončić et.al observed the same phenomena during introduction of FAS coating to cellulose fibers. As mentioned in previous sections, it can also be inferred that the plasma pre-treatment increased the effective concentration of the FAS network on the lignocellulosic coir fibers which are also in line with the findings of Simončić et.al [1].

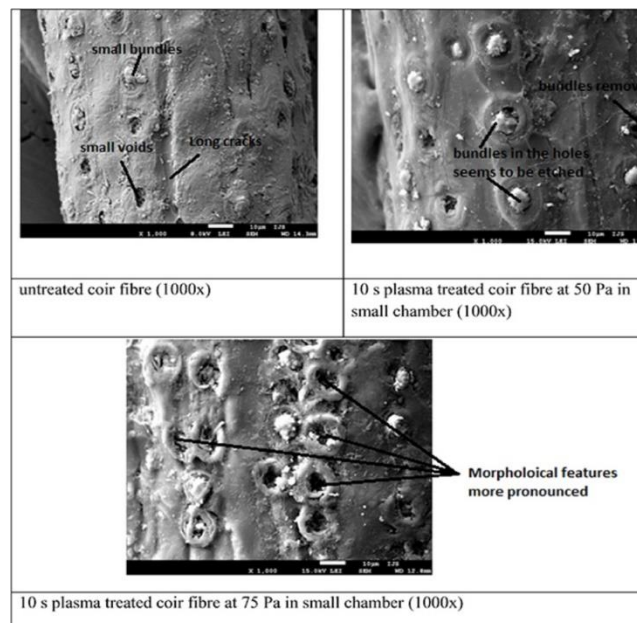


Fig.4.4 Micro to nano-structured composite fiber surface with a high content of air pockets

4.6 X-ray photoelectron spectroscopy (XPS) Analysis

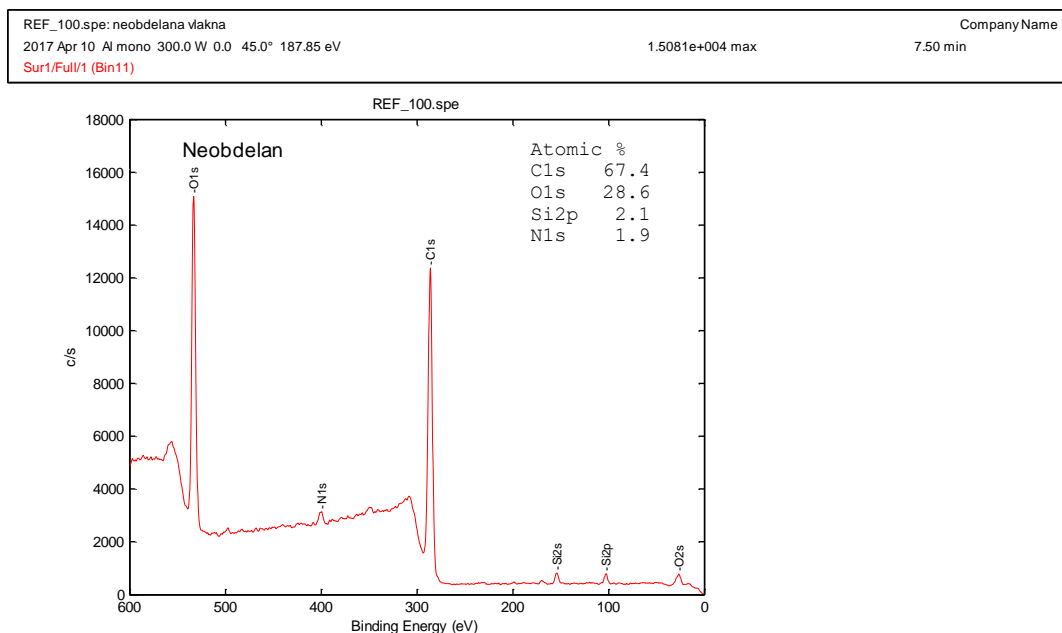
The chemical composition of the FAS network on coir fiber surface was evaluated by XPS analysis. The atomic concentrations of carbon,(C 1s), oxygen (O 1s), fluorine (F 1s) and silicon (Si 2p), as well as the O/C atomic ratio, were calculated are shown in Table 4.4. The

surface survey spectra for untreated fibers, only plasma treated fibers, and plasma treated and FAS coated fibers are shown in figure Fig.4.5

Table 4.5 Sample's surface composition in at. % (average of two measurements)

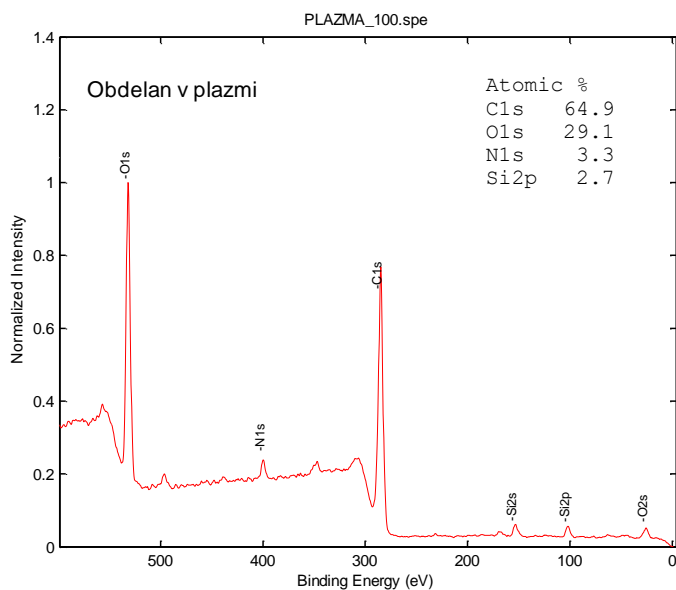
	C	N	O	F	Si	O/C ratio
Untreated	68.1	2.2	28.3		1.5	0.42
Plasma	63.8	3.2	30.1		2.9	0.47
Plasma + sol-gel	35.5	-	8.2	52.1	4.3	0.23

It can be inferred from the results that the oxygen plasma pre-treatment simultaneously induced a decrease in the atomic concentration of carbon and an increase in the atomic concentration of oxygen, which resulted in an increase in the O/C atomic ratio of the plasma treated sample compared with the untreated sample.



PLAZMA_100.spe: neobdelana vlakna
 2017 Apr 10 Al mono 300.0 W 0.0 45.0° 187.85 eV
 Sur1/Full/1 (Bin11 Sht)

Company Name
 1.0000e+000 max
 5.00 min



SolGel_101.spe: sol gel obdelava
 2017 Apr 10 Al mono 300.0 W 0.0 45.0° 187.85 eV
 Sur1/Full/1 (Bin11 Sht Sht)

Company Name
 1.0000e+000 max
 4.59 min

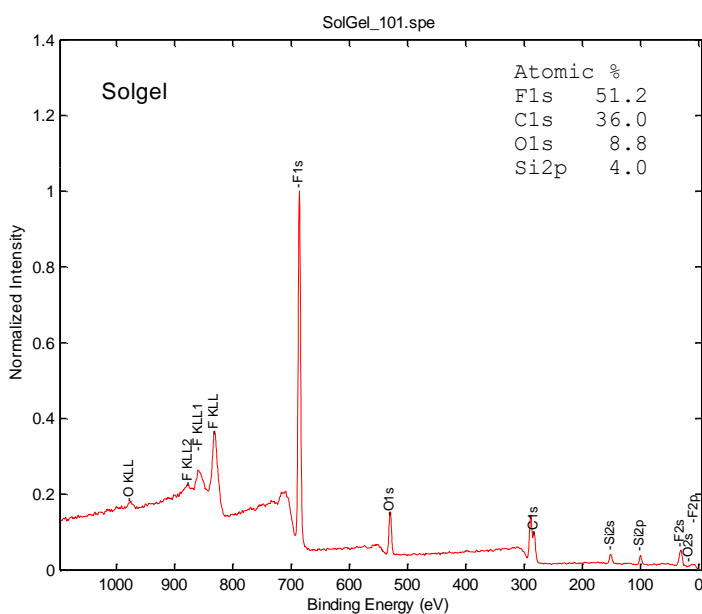
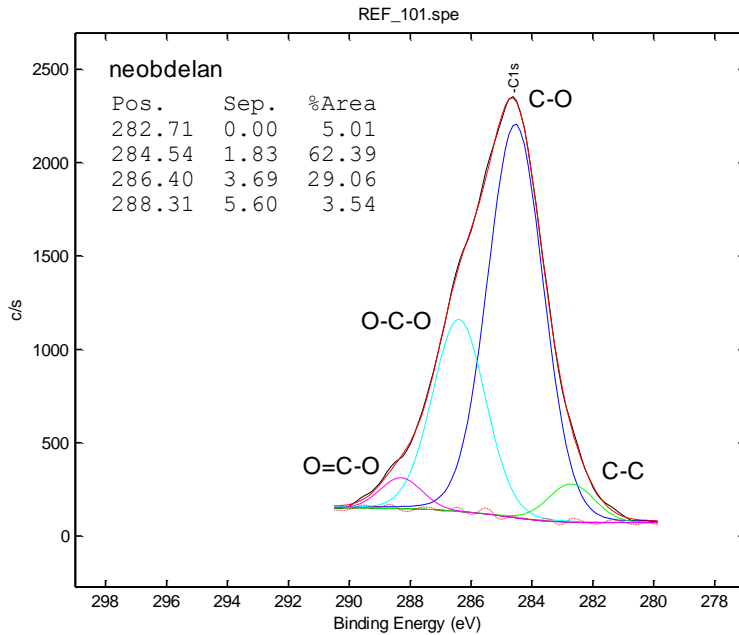


Fig.4.5 Examples of surface survey spectra for untreated fibers (top), only plasma treated fibers (middle), and plasma treated and sol-gel coated fibers (bottom)

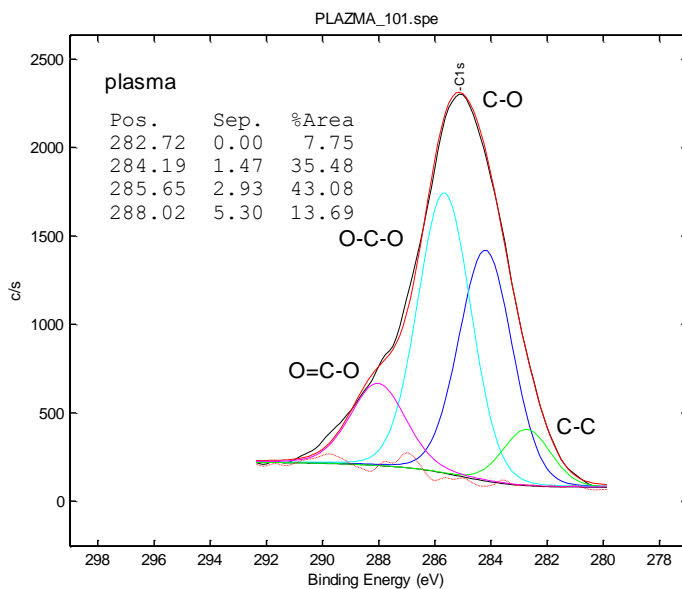
This result points to fact that the plasma pre-treatment increased the concentration of the oxygen-containing functional groups on the surface of the plasma treated sample and the surface becomes hydrophilic. After applying the sol-gel FAS coating to coir fiber surface, two additional characteristic bands such as F 1s and Si 2p, were detected on the FAS coated coir samples, accompanied by a significant decrease in the carbon and oxygen concentrations,

which confirmed that the FAS coating was covered the lignocellulosic coir fiber surface. The deconvolution spectra of untreated fibers, oxygen plasma treated fibers, and plasma treated and FAS coated fibers are shown in figure Fig.4.6

REF_101.spe: neobdelana vlakna
 2017 Apr 10 Al mono 300.0 W 0.0 45.0° 29.35 eV
 Sur1/Full/1 (Bin11)
 2.3532e+003 max
 Company Name
 1.21 min



PLAZMA_101.spe: obdelana v plazmi
 2017 Apr 10 Al mono 300.0 W 0.0 45.0° 29.35 eV
 Sur1/Full/1 (Bin11)
 2.3013e+003 max
 Company Name
 1.21 min



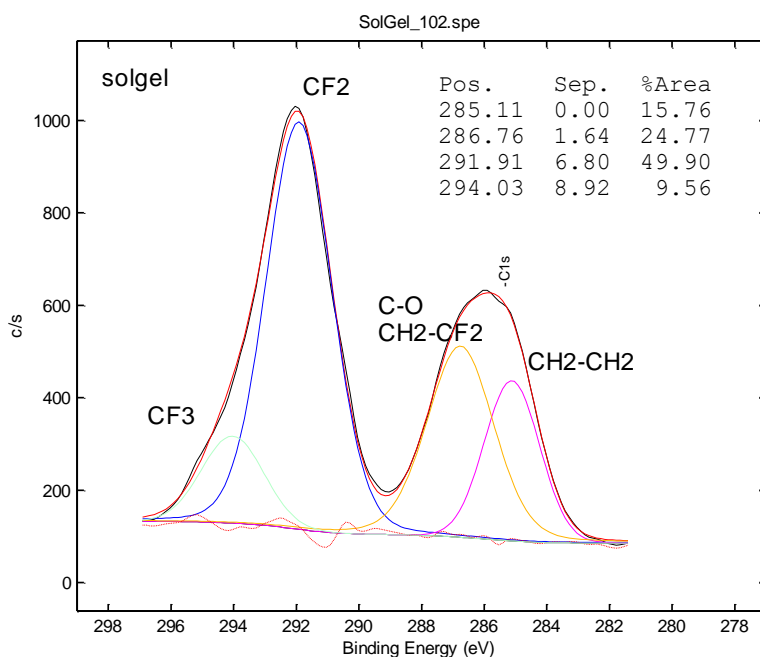


Fig.4.6 Examples of the deconvolution spectra of high-resolution XPS spectra of untreated fibers (top), only plasma treated fibers (middle), and plasma treated and sol-gel coated fibers (bottom).

The plasma treated and sol-gel coated fibers sample spectra clearly shows a new peak at about 292 eV, which corresponds to fluoro functional groups.

4.7 Tensile Analysis of uncoated and FAS coated coir fibers

The determination of the mechanical properties was made in accordance with the NFT 25-704 standard which takes into account the compliance of the loading frame. For each kind of fiber, at least 50 fibers were tested. Before tensile test, the diameter of every fiber is measured with an optical microscope. The diameter taken into account is an average value from five points obtained along the fiber.

The images generated in desktop computer with the help of software and camera of optical microscope for the measurement of diameter of uncoated as well as FAS coated fibers are shown in Fig.4.7. The diameter of 5 points along the fiber is measured and averaged. The average diameter of 50 samples was found to be 329.500µm.

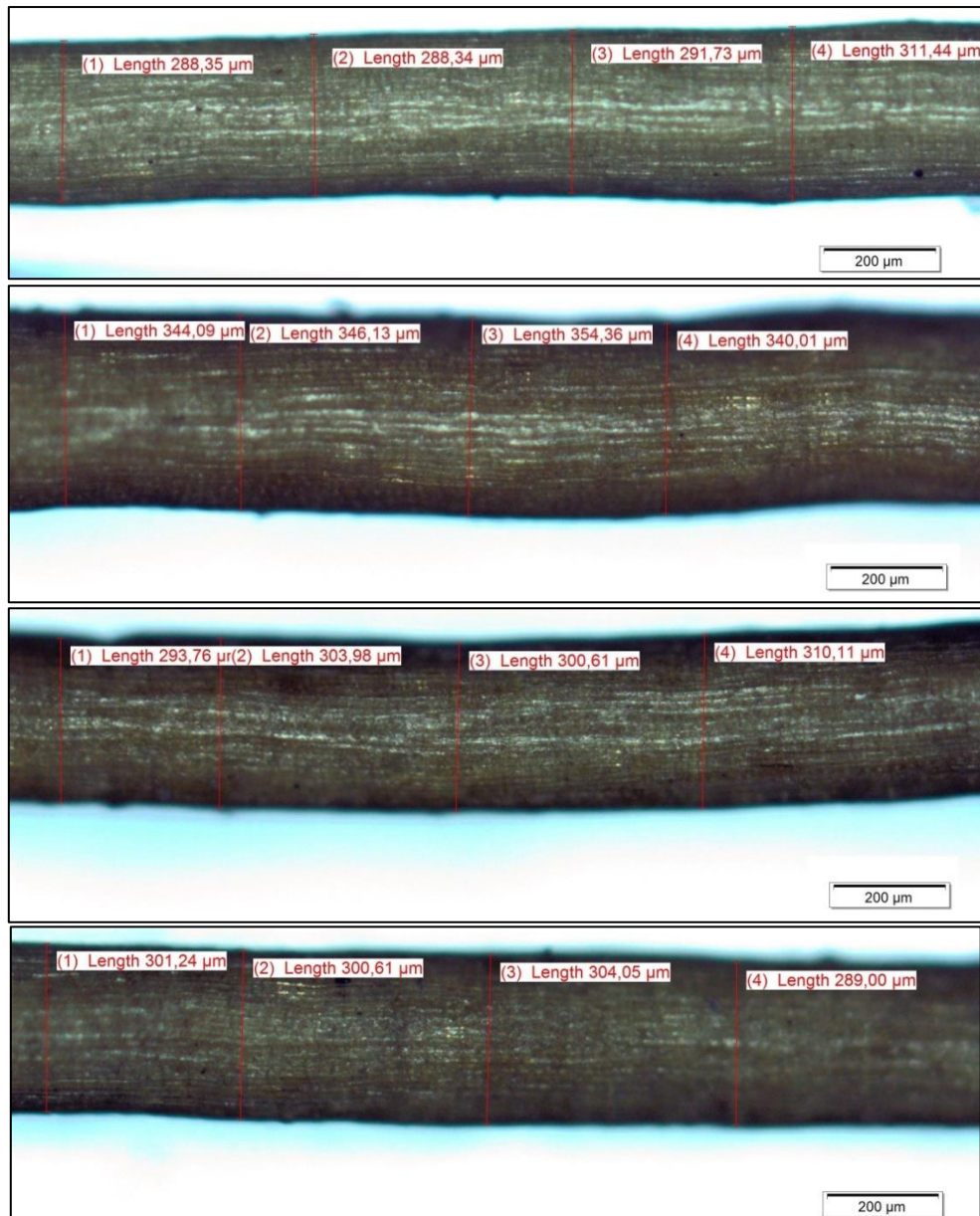


Fig.4.7. Coir fibers images of diameter measurement using optical microscope

To carry out tensile tests for elementary as well as FAS coated fibers, due to the short fiber length (about 20–30 mm), a gauge length of 10 mm was chosen. The fiber was clamped on a universal MTS type tensile testing machine fitted with a 50 N capacity load cell and loaded at a constant crosshead displacement rate of 1 mm/min up to rupture. The coir fibers loaded in MTS machine for tensile testing are shown in figure Fig.4.8.

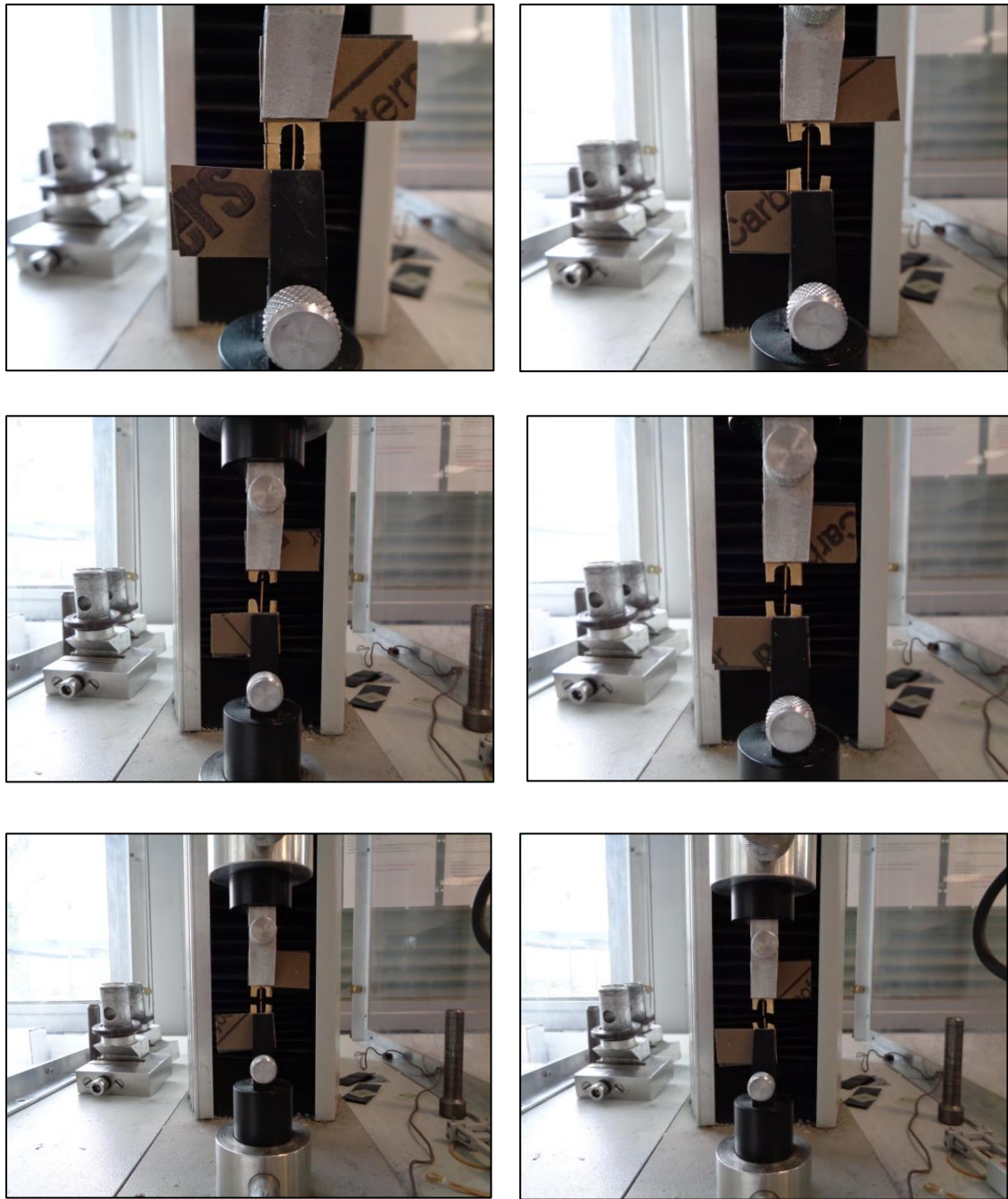


Fig.4.8. Coir fibers loaded in MTS machine for tensile testing

The values obtained via tensile analysis are shown in Table 4.5.

Table 4.6 Tensile measurements of uncoated and coated fibers

Type of coir fibers	Breaking force (N)	σ	Breaking strength (MPa)	σ	Modulus (MPa)	σ	Elongation at break (%)	σ
Uncoated	6.4	0.8	108.1	8.5	1819.1	35.3	45.9	3.3
FAS coated	9.8	1.1	148.3	10.4	2004.6	42.4	60.4	2.5

Where “ σ ” is the standard deviation

The average breaking force, breaking strength, Modulus, elongation at break of untreated fibers was found to be 6.4N, 108.1MPa, 1819.1MPa, and 4.6mm (45.9%) respectively. The average breaking force, breaking strength, Modulus, elongation at break of FAS coated fibers was found to be 9.8N, 148.3MPa, 2004.6MPa, and 6.2mm (60.4%) respectively. It can be very clear seen that the FAS coated coir fibers shows better tensile properties compare with the uncoated ones. The plasma pre-treatment increased the effective concentration of the FAS network on the lignocellulosic coir fibers and also enables good bonding with the fibers after allowing the coating to polymerise. A tight polymeric siloxane network is created on the organic ligocellulosic coir fiber treated with oxygen plasma. The increase in mechanical properties of FAS coated fibers can be correlated with this aspect. Gorjanc et al also observed the increase in the breaking strength of fabric sample after plasma treatment [1]. The stress versus strain graph generated for uncoated and FAS coated coir fibers in the present study are shown in figure Fig.4.9

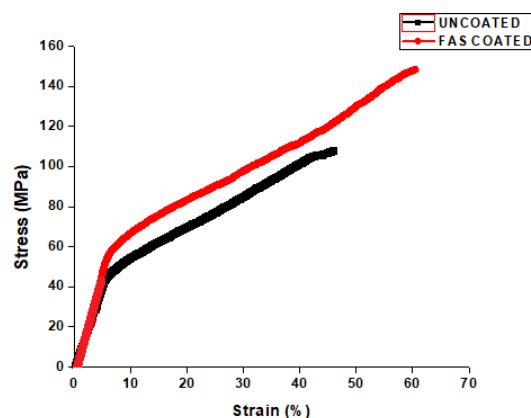


Fig.4.9 Stress versus strain curve for uncoated & FAS coated fibers

It can be seen that the yield point of FAS coated fibers has been shifted to higher value compare with uncoated fibers. Materials with large areas under the stress/strain curve are known to be more effective energy absorbers (having high strain energy absorbing capacity). It is also known that materials containing fibers with a greater strain energy absorbing capacity offering improved Izod energies. From the figure Fig.4.9, it is clearly seen that FAS coated coir fibers gives large areas under the stress/strain curve compare with uncoated ones which points to the scope for improved Izod energy when use with fiber reinforced composite systems.

4.8 Conclusions

The hydrophobic coating based on fluoroalkyl functional siloxane was found to be an effective coating to impart hydrophobicity to lignocellulosic natural coir fibers. The average water contact angle of FAS coated fiber reached to 112° from 48° for uncoated fiber. The total surface free energy dropped from 48mN/m for uncoated coir fibers to 22.4mN/m for FAS coated fiber also confirms the transformation to hydrophobic behavior of coated fibers. The lower thermodynamic work of adhesion for FAS coated fibers is also an indication of improved hydrophobicity of coir fibers. The AFM observation points to the finding that the plasma pre-treatment helps in imparting the nanoscopic topography which leads to the formation of a dual micro to nano-structured composite fiber surface with a high content of air pockets, which significantly decreased the interfacial area between the water and the fibers after the sol-gel coating was applied and imparted the "hydrophobic effect" to the sample. A slight increase in surface roughness value is also reported. SEM micro graphs show the smooth surface morphology obtained for sol-gel coated fibers. XPS analysis shows that the characteristic bands F 1s and Si 2p, were detected on the FAS coated coir samples, accompanied by a significant decrease in the carbon and oxygen concentrations, which confirmed that the FAS coating was covered the lignocellulosic coir fiber surface. The tensile analysis performed on elementary as well as FAS coated fibers shows that the average breaking force, breaking strength, modulus and elongation at break of FAS coated coir fibers was found to be higher than uncoated coir fibers.

4.9 REFERENCES

1. Vasiljević, Jelena, Marija Gorjanc, Brigita Tomšič, Boris Orel, Ivan Jerman, Miran Mozetič, Alenka Vesel, and Barbara Simončič. "The surface modification of cellulose fibers to create super-hydrophobic, oleophobic and self-cleaning properties." *Cellulose* 20, no. 1 (2013): 277-289.
2. Tomšič, Brigita, Barbara Simončič, Boris Orel, Lidija Černe, Petra Forte Tavčer, Mateja Zorko, Ivan Jerman, Aljaž Vilčnik, and Janez Kovač. "Sol-gel coating of cellulose fibers with antimicrobial and repellent properties." *Journal of Sol-Gel Science and Technology* 47, no. 1 (2008): 44-57.
3. Vilcnik, Aljaz, Ivan Jerman, Angela Šurca Vuk, Matjaz Kozelj, Boris Orel, Brigita Tomšič, Barbara Simončič, and Janez Kovac. "Structural properties and antibacterial

effects of hydrophobic and oleophobic sol– gel coatings for cotton fabrics." *Langmuir* 25, no. 10 (2009): 5869-5880.

4. Simončič, Barbara, Brigita Tomšič, Lidija Černe, Boris Orel, Ivan Jerman, Janez Kovač, Metka Žerjav, and Andrej Simončič. "Multifunctional water and oil repellent and antimicrobial properties of finished cotton: influence of sol–gel finishing procedure." *Journal of sol-gel science and technology* 61, no. 2 (2012): 340-354.
5. Baley, C., Busnel, F., Grohens, Y., & Sire, O. (2006). Influence of chemical treatments on surface properties and adhesion of flax fiber–polyester resin. *Composites Part A: Applied Science and Manufacturing*, 37(10), 1626-1637.

CHAPTER 5

**MECHANICAL, MORHOLOGICAL, RHEOLOGICAL AND
THERMAL PROPERTIES OF PP/EPDM BLENDS**

ABSTRACT

Polypropylene (PP) and ethylene-propylene-diene rubber (EPDM) blends were prepared with different constitutive ratios using melt blending followed by compression moulding technique. The tensile, impact and flexural analysis of all blend formulations were carried out. The morphological examinations of cryofractured and impact fractured surfaces were done using SEM and HRTEM to identify mechanisms of toughening in PP/EPDM blends. The low shear rate rheology and dynamic viscoelastic properties of blends were carried out to study rheological behaviour of PP/EPDM blends. Non-isothermal crystallisation kinetics, nucleation activity and glass transition temperature of blends were investigated using DSC analysis. The maximum degradation temperature of blends was obtained by thermo gravimetric (TGA) analysis.

5.1 Polypropylene (PP) and ethylene-propylene-diene rubber (EPDM) blends

Pure polypropylene as well as PP/EPDM2.5, PP/EPDM5, PP/EPDM7.5, PP/EPDM10, PP/EPDM20 and PP/EPDM30 blend formulations were studied in order to find out one which shows highest impact properties and comparable tensile and flexural properties. Here PP denotes 100 parts per hundred polypropylene whereas EPDM2.5, EPDM5, EPDM7.5, EPDM10, EPDM20 & EPDM30 denotes 2.5, 5, 7.5, 10, 20 and 30 parts per hundred ethylene-propylene-diene rubber). The different compositions used for preparing blends are shown in Table 2.4 (Refer Chapter 2, Table 2.4). The PP/EPDM blends were prepared first by dry blending followed by melt compounding using a Brabender Plasticorder mixer (model W 50 EHT). The melt compounded PP/EPDM blends were moulded into sheets using hot pressing (compression moulding) technique. The prepared sheets then cut into appropriate shapes and dimensions for various characterisations.

5.2 Mechanical property (Impact, Tensile and Flexural) analysis of PP/EPDM blends

5.2.1 Impact analysis of PP/EPDM blends

Notched Izod impact tests of PP/EPDM blends were performed using a Tinius-Olsen machine at ambient temperature 23°C according to ISO 180 A. The detailed procedure and conditions were given in section 2.1.2.7.1 (CHAPTER 2). Results were obtained from the average of at least 10 samples for each set. The Impact strength and impact fracture energy plot generated for pure polypropylene and PP/EPDM blends are shown in figure Fig.5.1 and Fig.5.2. respectively. At lower parts of EPDM impact strength & energy values are found to be high for PP/EPDM blends. At higher parts of EPDM, these values show a decreasing trend. Among all the PP/EPDM blend compositions, 7.5 parts of EPDM registered highest impact strength and fracture energy values.

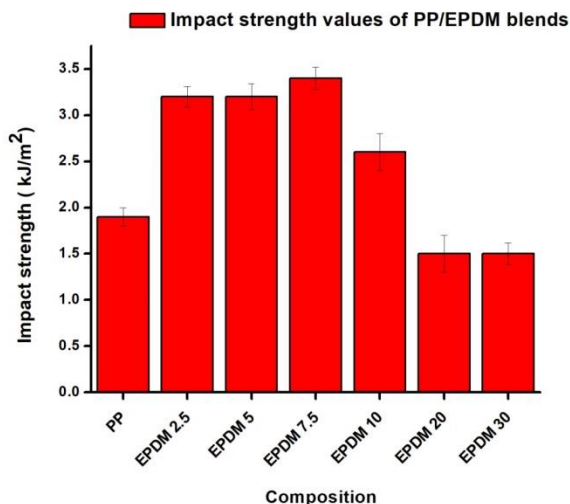


Fig.5.1. Impact strength of pure PP and PP/EPDM blend

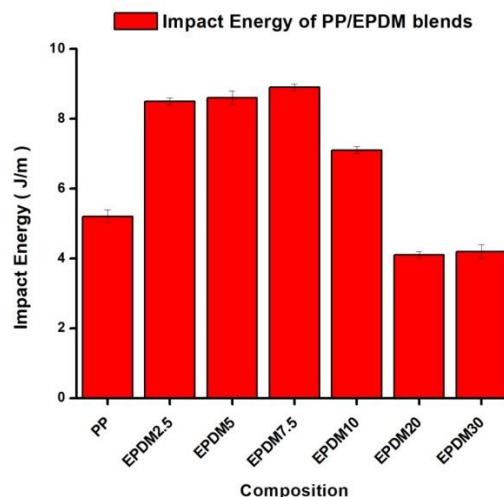


Fig.5.2. Impact energy of pure PP and PP/EPDM blends

One possible reason for increase in impact strength could be the decrease in average diameter of dispersed particles at lower EPDM content leading to better dispersion EPDM in PP matrix. This interpretation can be validated with the help of HRTEM images discussed in section 5.5.1. The ultra-high-molecular grade EPDM used here can also be a reason for high strength and resilience value to the PP/EPDM blends at low concentration of EPDM compare with pure polypropylene. However at higher concentrations of EPDM content, the ductile behaviour of EPDM prevails over the effect of molecular weight and resulted in reduction of impact properties. Matsuoka [1] noted that in the glassy state, the molecular weight affects the toughness and impact strength of the polymer; impact strength increases with molecular weight.

Stricker et al. investigated that impact strength of pure polypropylene is almost independent of molecular weight, whereas impact strength of polypropylene blends increases strongly with increasing polypropylene molecular weight. This information is in line with the present findings. i.e., at lower concentration of EPDM swathe (i.e., at less than or equal to 7.5pph), the combined molecular weight of polypropylene & EPDM may have been contributed to the improvement in impact strength of PP/EPDM blends. The EPDM enhances the impact strength of PP to a significant extend. The enhancement of impact strength may be due to the occurrence of shear yielding at stress concentration points which give rise to local strain inhomogenities [2]. The decrease in impact strength after 7.5pph may be due to the formation of narrower ligaments than critical ligament thickness (interparticle distance). As a result, the crack engulfs the ligaments facilitating its propagation and decreases the impact strength [3].

5.2.2 Tensile analysis of PP/EPDM blends

Tensile testing of neat polypropylene, PP/EPDM blends were performed by MTS Synergy RT1000 testing apparatus at 23°C and a relative humidity of 48% according to ISO 527. The detailed procedure and conditions were given in section 2.1.2.7.2 (CHAPTER 2). The tensile strength, modulus and % deformation plots generated for pure polypropylene and PP/EPDM blends are shown in figure Fig.5.3 a,b and c..At lower concentration of EPDM, tensile strength values are found to be high for PP/EPDM blends. At higher concentrations of EPDM, the values shows a decreasing trend. From plots, it can be seen that at 2.5 parts of EPDM registered highest tensile strength value. The pure polypropylene exhibited highest modulus value and 5 parts of EPDM showed highest strain (% deformation) among all blend formulations. Among all the PP/EPDM blend compositions, tensile measurements such as tensile strength, modulus and % deformation are found to be high at lower concentrations of EPDM (i.e., at parts of EPDM less than equal to 7.5pph). One possible reason could be the lower concentrations of EPDM in PP/EPDM blends which enables better dispersion of EPDM in thermoplastic PP matrix results in an increase of tensile strength values .

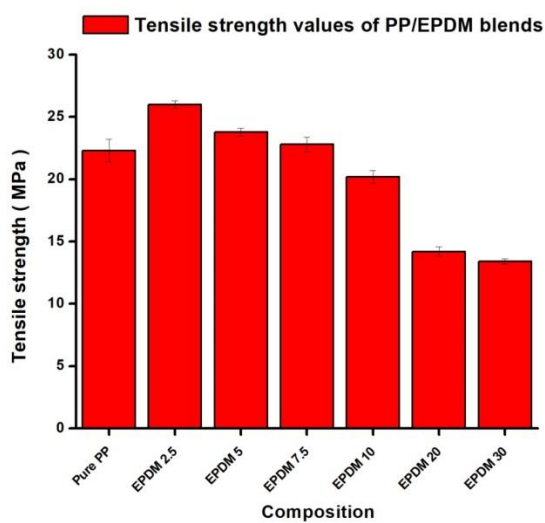


Fig.5.3 a Tensile strength of pure PP and PP/EPDM blends

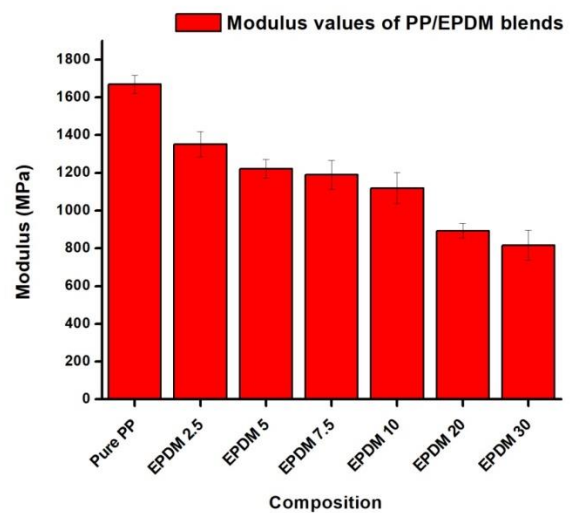


Fig.5.3 b Modulus of pure PP and PP/EPDM blends

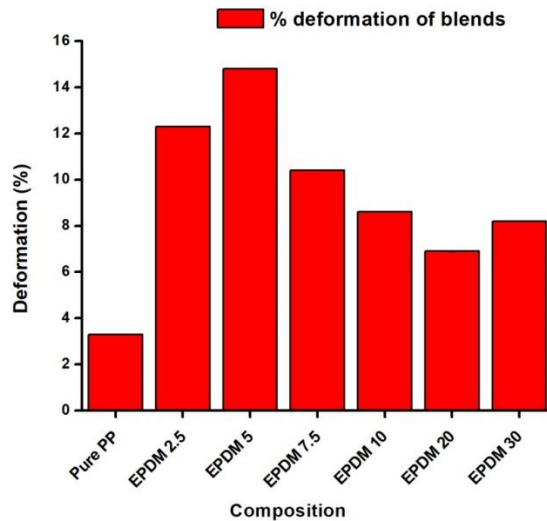


Fig.5.3c % deformation of pure PP and PP/EPDM blends

To be tough, a material should withstand both high stresses and high strains. It can be seen from the above plots that, the high strength and deformation values are obtained at the lower concentration of EPDM swathe (i.e., at less than or equal to 7.5pph). The detailed explanation is given under stress-strain diagram of PP/EPDM blends.

The stress strain diagram of pure polypropylene and PP/EPDM blends are shown in figure Fig.5.4

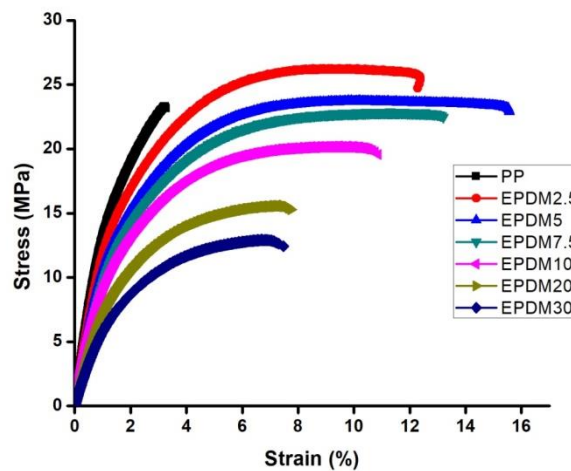


Fig.5.4 % stress strain diagram of pure polypropylene and PP/EPDM blends

It can be clearly seen from the stress-strain plot that, as the EPDM content increases the yield point (the point at which elastic to plastic transformation occurs) shifted to lower value. Pure polypropylene has the highest yield strength value whereas PP/EPDM30 carries

the lowest yield strength value. Among all PP/EPDM blends, at EPDM content swathe less than or equal to 7.5 pph shows the highest fracture energy for the material. The area under the stress-strain curve gives the fracture energy of the material. Toughness is related to the area under the stress–strain curve. In order to be tough, a material must be both strong and ductile. For example, brittle materials that are strong but with limited ductility are not tough; conversely, very ductile materials with low strengths are also not tough. To be tough, a material should withstand both high stresses and high strains. The large area under the stress strain curves of PP/EPDM blends at EPDM content swathe less than or equal to 7.5 pph shows the strain energy capacity of the material.

From the table 5.2 (section 5.5), it can be seen that % crystallinity value of PP/EPDM blend decreases with increase in EPDM content. PP has the highest % crystallinity value. Among all PP/EPDM blend formulations, at the lower concentration of EPDM swathe (i.e., at less than or equal to 7.5pph) shows higher % crystallinity values. This information also points to the ability of the material to withstand high stresses. Similar effects were reported also in other toughened polymer systems where the discrete phase was elastomeric [4].

5.2.3 Flexural analysis of PP/EPDM blends

Flexural testing of neat polypropylene, PP/EPDM blends were performed by MTS Synergy RT1000 testing apparatus at 23°C and a relative humidity of 48% according to ISO 178. The detailed procedure and conditions were given in section 2.1.2.6.3. The plots of flexural strength, flexural modulus and % deformation due to flexural loading generated for pure polypropylene and PP/EPDM blends are shown in figure Fig.5.4 a,b and c. At lower concentration of EPDM, flexural strength values shows an increasing trend for PP/EPDM blends whereas at higher concentrations of EPDM, the values shows a decreasing trend. From plots, it can be seen that at pure PP registered highest flexural strength value and 2.5 parts of EPDM shows a nearby value. Among all blend formulations, the pure polypropylene exhibited highest modulus value and 7.5 parts of EPDM showed highest strain (% deformation) upon subjected to flexural loading. Among all the PP/EPDM blend compositions, flexural measurements such as flexural strength, flexural modulus and % deformation are found to be high especially at lower concentrations of EPDM (i.e., at parts of EPDM around 7.5pph). The lower concentrations of EPDM in PP/EPDM blends enables better dispersion of EPDM in thermoplastic PP matrix results in an increase of flexural strength values (Refer 5.3.1 & 5.3.2).

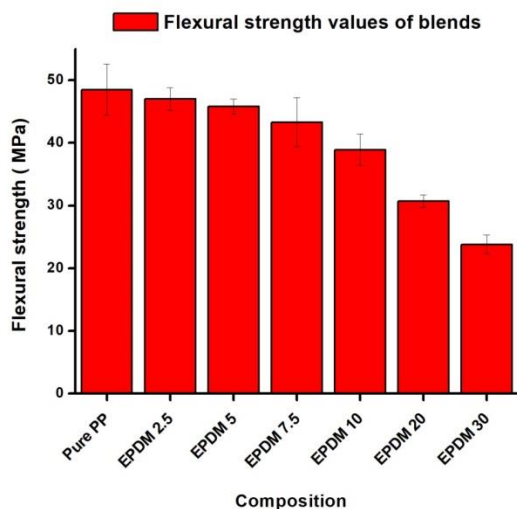


Fig.5.4 a Flexural strength of pure PP and PP/EPDM blends

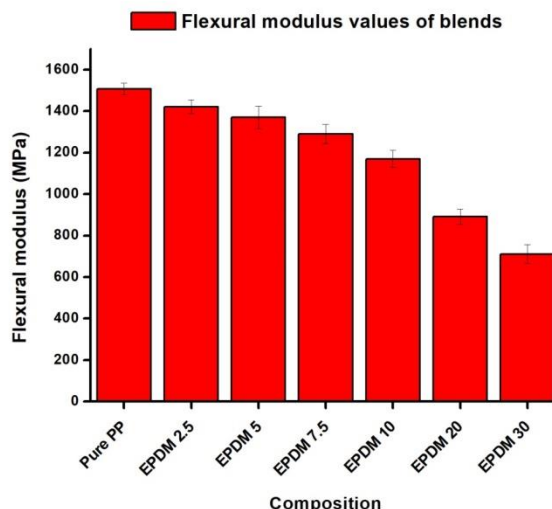


Fig.5.4 b Flexural modulus of pure PP and PP/EPDM blends

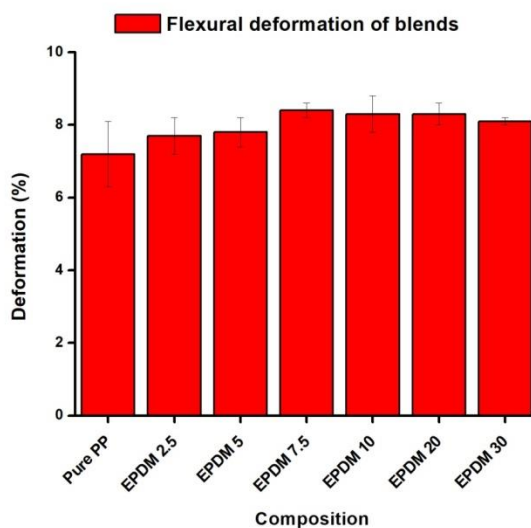


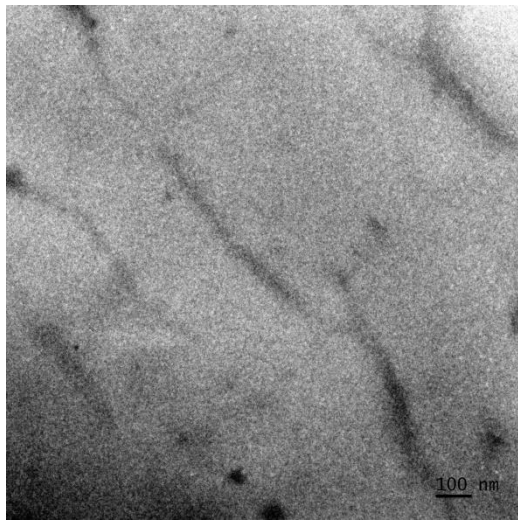
Fig.5.4 c % deformation of pure PP and PP/EPDM blends under flexural loading

5.3 Morphological analysis of PP/EPDM blends

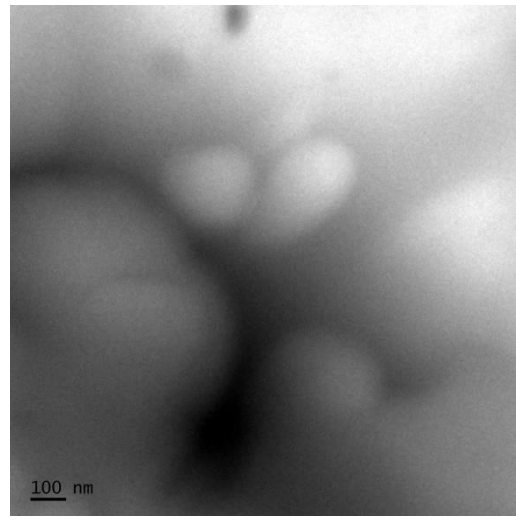
5.3.1 High-resolution transmission electron microscopy (HRTEM)

TEM micrographs of the PP/EPDM blends are shown in figure Fig.5.5. Two-phase morphology was clearly visible in the blend fractured surfaces examined using TEM. It involves a dispersed domain (white part) and one continuous domain (gray part). Gray parts

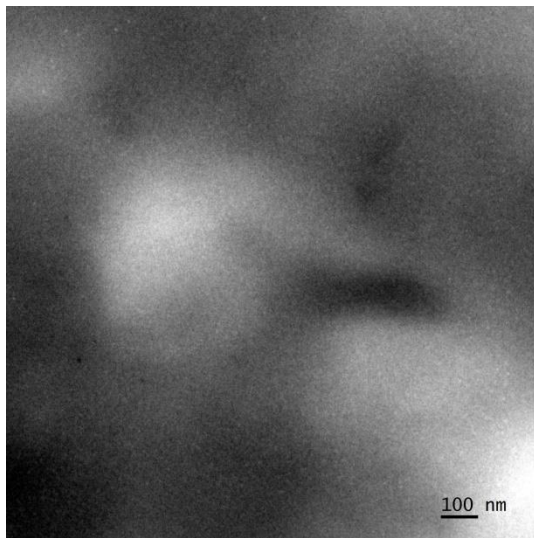
indicated PP as a continuous domain. The white spherical particles with less than 500 nm are designated as EPDM dispersion phase.



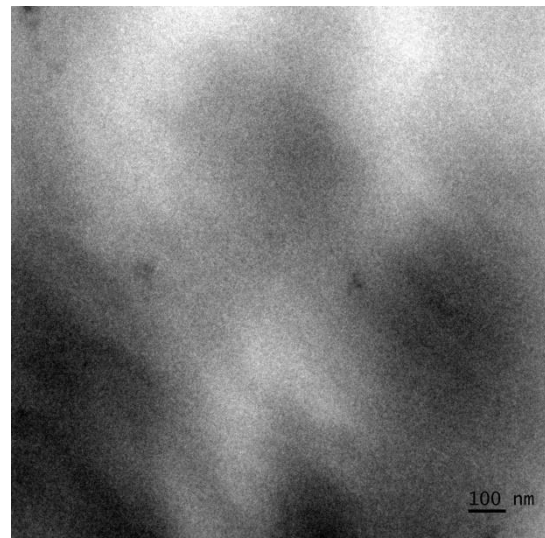
a) PP



b) EPDM2.5



c) EPDM7.5



d) EPDM10

Fig.5.5. TEM micrographs of PP/EPDM blends

It can be seen from the TEM images that the increase of EPDM content increased the average diameter of dispersed particles and causes a decrease in the number of dispersed EPDM particles. The average diameter measured for spherical EPDM particles from the image J analysis (averaged for 50 measurements) are tabulated in Table 5.1

Table 5.1 Average diameter of EPDM spherical particles measures using Image J

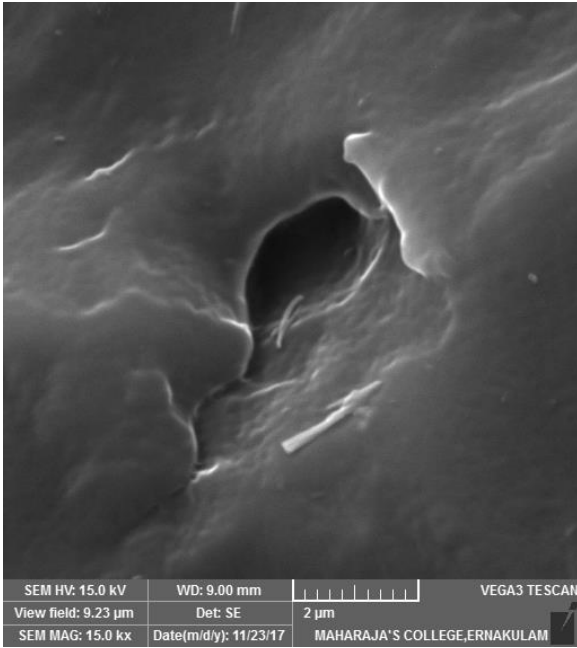
Sample ID	Average diameter (nm)	σ
EPDM2.5	190.5	33.2
EPDM7.5	380.8	41.7
EPDM10	599.6	38.5

Where “ σ ” is the standard deviation

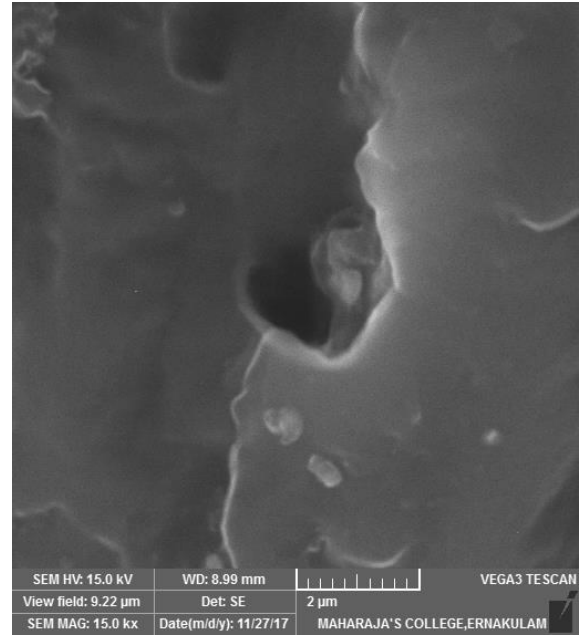
In general, the impact resistance increases with concentration rubber particles (soft disperse phase), however it falls sharply when diameter of the rubber particle is reduced below a critical diameter. Toughness also decreases when the particle size is too large. The average diameter values of spherical EPDM particles in TEM morphology measured using Image J can be correlated with the impact strength values of PP/EPDM blends. One possible reason for increase in impact strength of PP/EPDM blend is , at lower loadings of EPDM could be the decrease in average diameter of dispersed particles at lower EPDM content leading to better dispersion EPDM in PP matrix. At higher loadings, the average diameter of dispersed particles exhibits an increasing trend as we increase the EPDM content resulted in decrease of impact strength values. i.e., the increase of EPDM content increased the average diameter of dispersed particles and causes a decrease in the number of dispersed EPDM particles, leading to the decrease of impact strength values. The obtained results are in line with the results obtained in literatures [5].

5.3.2 Scanning Electron Microscopy (SEM) Analysis

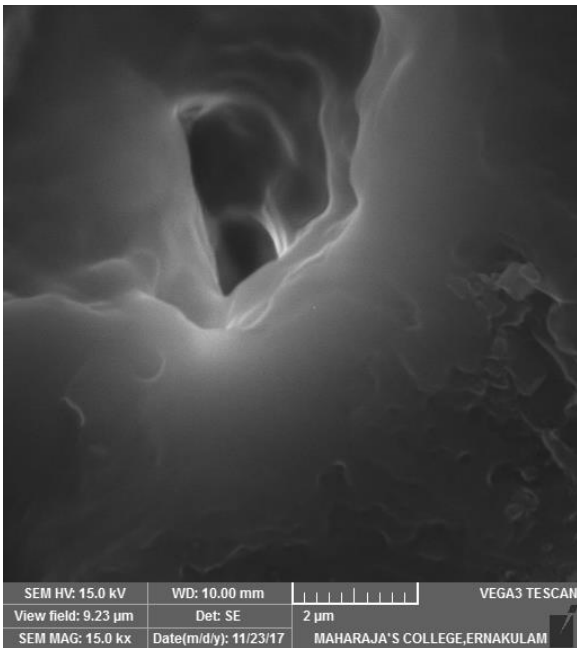
It is well-known that the principal mechanisms of inelastic deformation in rubber-toughened plastics are shear yielding and multiple crazing in the rigid matrix phase, and cavitation in the soft disperse phase. SEM micrographs of the impact fractured PP/EPDM blends are shown in figure Fig.5.6 respectively .The mechanically induced cavitation behaviour is observed in impact fractured PP/EPDM surfaces.



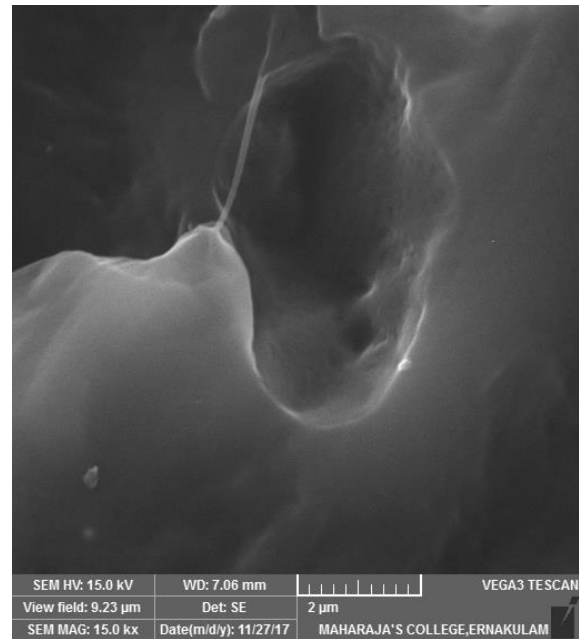
a) PP



b) EPDM2.5



c) EPDM7.5



d) EPDM10

Fig.5.6 SEM micrographs of impact fractured PP/EPDM blends

It is evident from the SEM morphology of impact fractured specimens that, the mechanically induced cavitation behaviour is responsible for the impact resistance of PP/EPDM blends. Cavitation will usually occur preferentially in the soft phase, where the resistance to void expansion is very much lower. In all the SEM pictures of impact fractured surfaces, it can be clearly seen that the growth of the central void is accompanied by expansion of the

surrounding rubber shell and yielding in the adjacent matrix. The obtained results and inferences are matching with the literature reports [6].

5.4 Rheological analysis of PP/EPDM blends

5.4.1 Low shear rate rheology

The low shear rate rheology (for shear rates less than 100 sec^{-1}) of polypropylene and PP/EPDM blends were studied using an Anton Paar, CTD 450, Physica MCR 301 rheometer. Before experiments, the samples were dried at 60°C for 12 h and compression moulded to the thickness about 2 mm. The viscosity versus shear rate of PP/EPDM blends were plotted in figure Fig.5.7. It can be inferred from the plot that, as the EPDM content increases from 2.5 pph to 30pph, the viscosity in the low shear rate region shows a general increasing trend. However as we increases the EPDM content from 5pph to 7.5pph, the viscosity value decreases, and beyond 7.5pph it increases significantly. At 7.5pph EPDM content, the viscosity value found to be the lowest comparing with polypropylene as well as other blend formulations used in this study.

As we increase the shear rate, the viscosity is found to be decreasing exhibiting a shear thinning behaviour. But at the beginning (shear rate from 0.001 to 0.01 $1/\text{s}$), the viscosity shows a small increase with shear rate. This could be due to i.e., at equilibrium and also at extremely low shear rates (less than 0.01 $1/\text{s}$ here), random collisions occur among particles which make it resistant to flow. As the shear rate increases, the particles start to flow forming layers of particles, which causes decrease in viscosity. It follows the same trend of the earlier findings of Metzner et al. [7] and also cited in reviews by Srivastava et.al [8] in their literature.

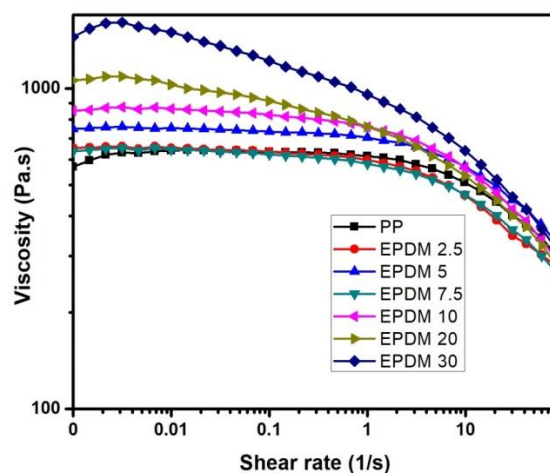


Fig.5.7. Viscosity versus shear rate of PP/EPDM blends

5.4.2 Dynamic viscoelastic property analysis

The principle of parallel plate rheometry was used to find out dynamic viscoelastic properties of blends. The oscillatory frequency analysis was performed at a fixed strain (0.1%) corresponding to the linear viscoelastic domain and the frequency was varied in the range from 0.01-100 Hz. The viscoelastic properties such as storage modulus (G'), loss modulus (G'') and complex viscosity (η^*) were measured as a function of angular velocity (ω) using an Anton Paar, CTD 450, Physica MCR 301 rheometer. Before experiments, the samples were dried at 60⁰C for 12 h and compression moulded to a circular shape having diameter 25mm and the thickness about 2 mm. The complex viscosity versus frequency of polypropylene and PP/EPDM blends are shown in figure Fig.5.8. The complex viscosity found to be decreases with increase in frequency which shows the melt is in pseudo plastic state. Due to the increase in shear flow the chains of EPDM try to open and entangle themselves. However it may be possible that high molecular weight of EPDM is not allowing disentangling them. The same trends of results were reported by sharma et al. when studying the effects of SEBS-g-MA copolymer on non-isothermal crystallization kinetics of polypropylene [9].

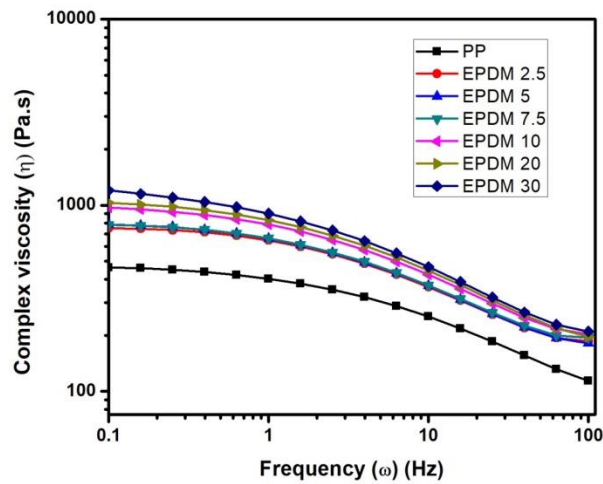


Fig.5.8. Frequency dependence of complex viscosity in PP / EPDM blends

The complex viscosity found to be increases with increase in EPDM content. The effect of the EPDM is noticeable at low frequencies and the relative effect diminishes with increasing frequency due to shear thinning behaviour. This trend is in accordance with previous reports based on experimental observations for EPDM blended polypropylene blends [10]. Among all the blend formulations, EPDM 30 shows the highest value of complex viscosity even at highest value of frequency range chosen. The increase in viscosity may be attributed to hydrodynamic disturbance due to high viscous droplets of EPDM.

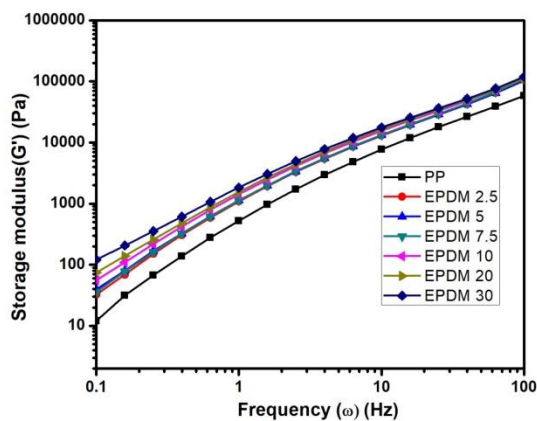


Fig.5.9. Frequency dependence of storage modulus in PP / EPDM blends

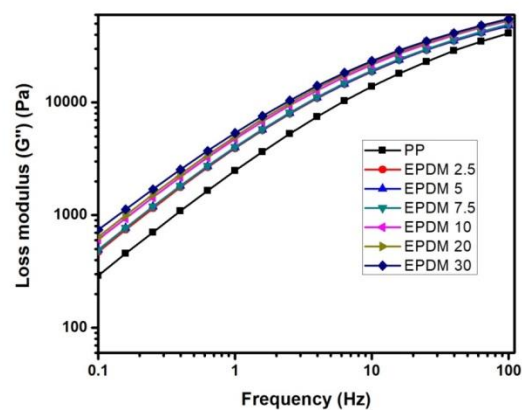


Fig.5.10. Frequency dependence of loss modulus in PP / EPDM blends

The storage modulus (G') and loss modulus (G'') versus frequency is presented in figure Fig.5.9 and Dig.5.10 respectively. It can be observed that the storage modulus (G') and loss

modulus (G'') shows an increasing trend with the frequency. The characteristic relaxation regions of polypropylene were shown at all frequency. A flow region at low frequency, clear plateau region at highest frequency and a clear differentiation between both regions which is characteristic for polydispersity. The plot of PP/EPDM blends showed non terminal behaviour (storage modulus is enhanced with frequency and the value of G' is not proportional to ω^2 as according to Cox-Merz rule) at low frequency.

5.5 Non-isothermal crystallisation kinetics of PP/EPDM blends

It is well known that, the strength properties of semi crystalline polymers can be controlled by engineering the crystallinity value of these polymers. The crystallization in semi crystalline polymers can be achieved by isothermal (temperature constant with respect to time), non-isothermal (temperature constant with respect to time), or by both conditions. Many industrial processes such as extrusion, injection moulding etc are likely to be carried out under non-isothermal conditions. As a result, the investigation of the crystallinity of polymers is very significant under non isothermal conditions. To study the crystallisation kinetics in semi crystalline polymers, the crystallization process is divided into two stages viz. primary and secondary crystallization. The chains of a polymer in molten state stack themselves into two-dimensional lamellar structure when it is crystallised from melt temperature to a lower temperature. The primary crystallisation step involves the growth of the spherulite until they collide with the neighbouring spherulite. The secondary crystallisation step comprises of thickening of lamellae, crystallization of interlamellar chains, and changes of lamellae structure take place. In a phase-separated polymer blend, if the dispersed phase is amorphous, it disturbs the spherulite growth of the polymer matrix and also alters the morphology. As a result, while the polymer crystallises, the amorphous phase is rejected by growing spherulites forcing them to remain in interfibrillar, interlamellar, and interspherulitic regions [11]. Table 5.2 shows important crystallisation parameters such as crystallisation peak (T_c), onset temperature (T_o), Normalised enthalpy (ΔH_c), melting peak (T_m) and under cooling, ΔT_c (where $\Delta T_c = T_m - T_c$) temperatures.

Table 5.2 Non isothermal crystallisation exotherms of PP and PP/EPDM blends

Sample ID	Cooling rate (°C/min)	T _o (°C)	T _c (°C)	ΔH _c (Jg ⁻¹)	T _m (°C)	ΔT _c (°C)
PP	10	120.45	114.17	91.66	164.17	50
	15	118.22	112	90.02	163.5	51.5
	20	116.66	110	88.71	164	54
	25	115.45	108.75	87.97	163.33	54.58
	30	114.54	108	87.27	163.5	55.5
EPDM2.5	10	120.69	113.83	84.14	164.33	50.5
	15	118.65	111.25	83.23	164.25	53
	20	117.16	109.67	81.9	164	54.33
	25	115.92	107.92	80.76	164.17	56.25
	30	114.92	106.5	80.13	164	57.5
EPDM5	10	119.47	113.67	86.49	162.5	48.83
	15	117.09	111.5	84.82	162.25	50.75
	20	115.65	109.67	84.42	162.33	52.66
	25	114.63	108.75	83.08	162.08	53.33
	30	113.82	107.5	81.52	162	54.5
EPDM7.5	10	119.02	111.5	79.57	165.17	53.67
	15	116.42	109	78.24	165.75	56.75
	20	114.63	107	77.46	166.33	59.33
	25	113.3	105.42	77.17	166.25	60.83
	30	112.19	104	75.15	166.5	62.5
EPDM10	10	118.7	111.5	72.89	165.5	54
	15	116.1	108.75	72.11	166	57.25
	20	114.34	107	71.34	166.33	59.33
	25	112.95	105.42	70.75	166.67	61.25
	30	111.8	104	70.26	167	63
EPDM20	10	117.38	112.17	68.43	163.33	51.16
	15	115.63	110.75	67.63	162.5	51.75
	20	114.63	109.67	67.32	162.33	52.66
	25	113.86	108.75	65.91	162.08	53.33
	30	113.21	107.5	65.22	162	54.5
EPDM30	10	116.96	111.33	60.52	164.17	52.84
	15	114.75	109.25	59.56	164.25	55
	20	113.46	107.67	59.44	164.33	56.66
	25	112.48	106.25	59.12	164.58	58.33
	30	111.65	105	58.53	164	59

It is well known that, in the case of semi crystalline polymers, the crystallinity value decreases upon addition of compounding ingredients. The decrease in crystallinity value is a function of volume fraction of additives in the system. In PP/EPDM blends, the percentage

crystallinity value of polypropylene decreases with increase in EPDM content. Table 5.3 shows the average crystallinity values of PP /EPDM blends obtained using DSC analysis.

Table 5.3 % crystallinity of PP and PP/EPDM blends

Sample ID	Crystallinity (%)
PP	43.0
EPDM2.5	40.6
EPDM5	42.6
EPDM7.5	40.3
EPDM10	38.0
EPDM20	38.8
EPDM30	37.3

The effect of crystallinity values on cooling rate of crystallisation is shown in figure Fig.5.11

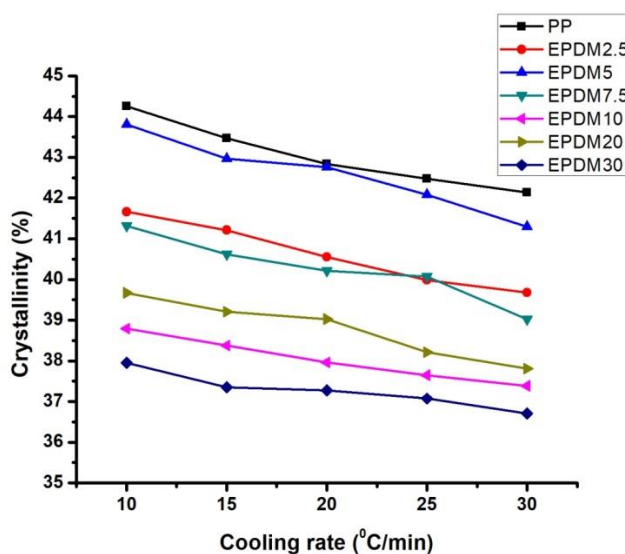
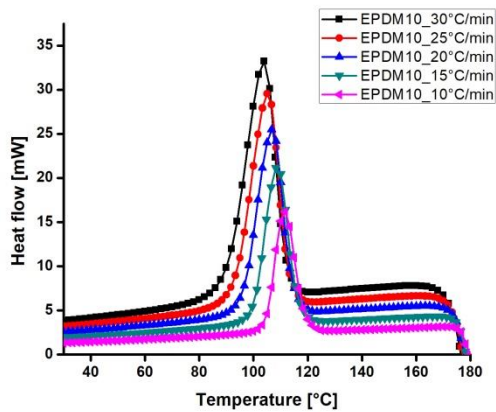
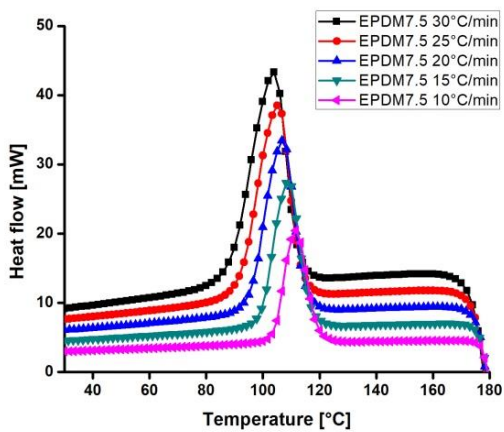
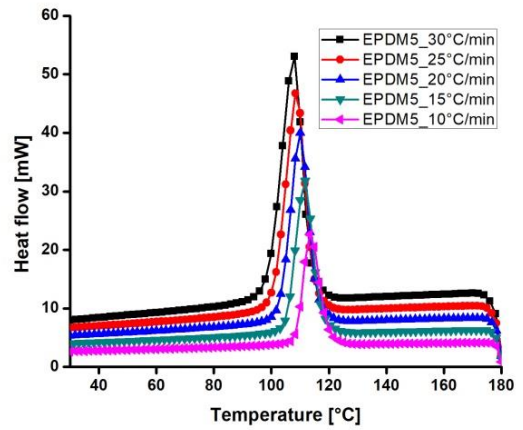
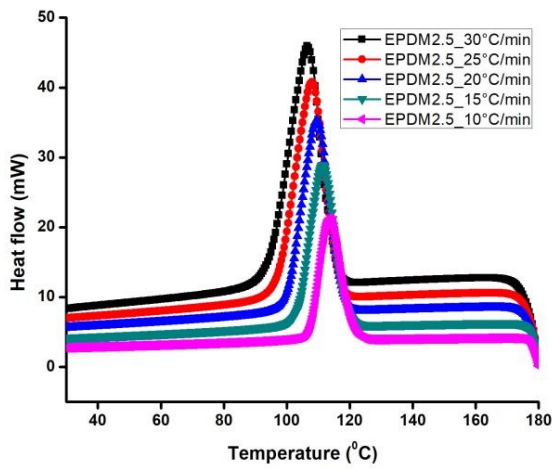
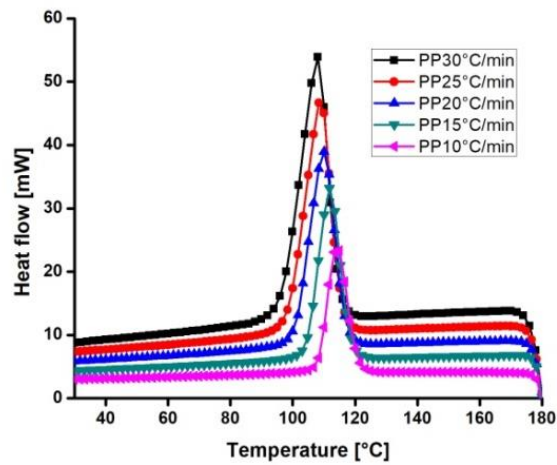


Fig.5.11 % crystallinity versus cooling rate

It is very clearly seen from the plot that, % crystallinity values shows a decreasing trend upon increase in cooling rate of crystallisation. This is due to the fact that, at higher cooling rates, crystallisation time is not sufficient for the PP/EPDM blends to complete crystallisation process which is further explained in relative crystallinity versus temperature/time plots. The DSC exotherms of neat PP and PP/EPDM blends at five different cooling rates (10, 15, 20, 25, 30°C min⁻¹ are presented in figure Fig.5.12.



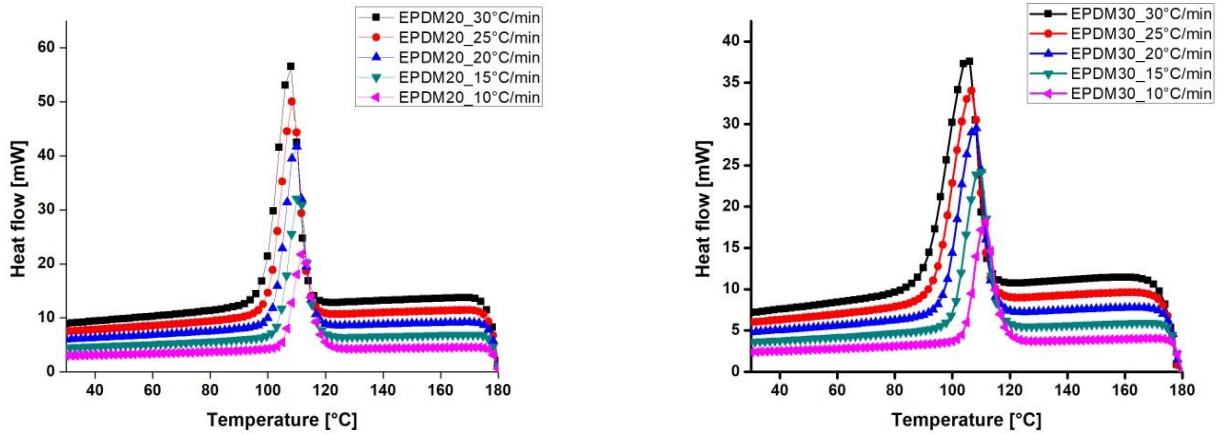
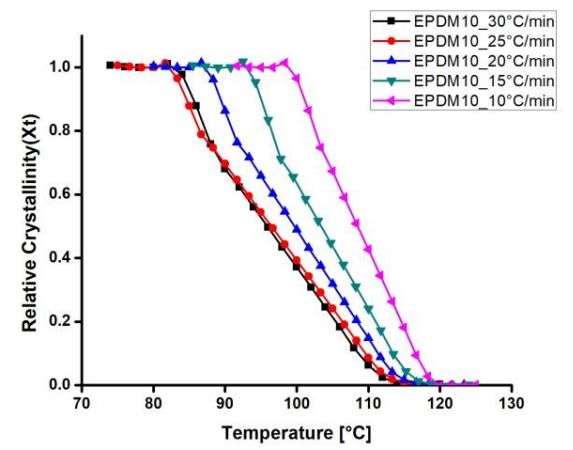
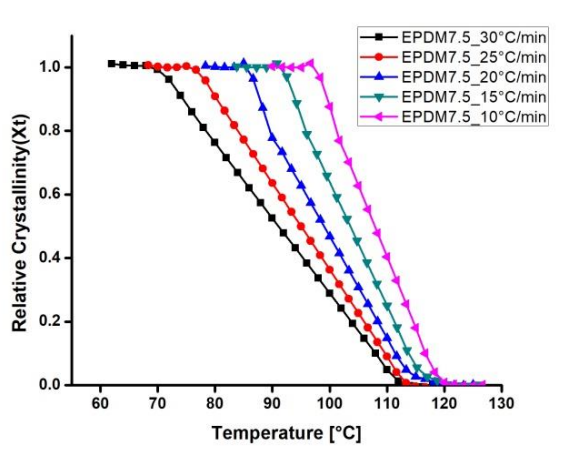
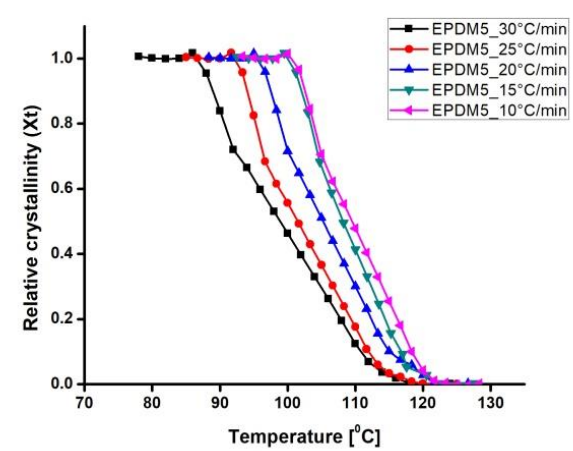
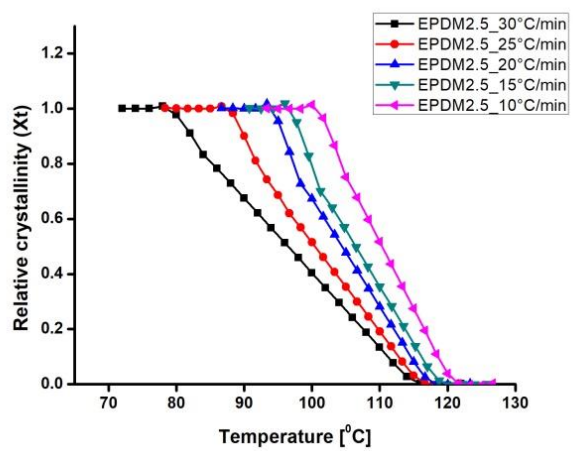
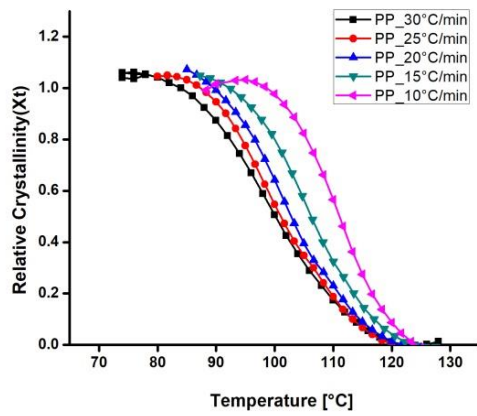


Fig.5.12 Non-isothermal crystallization curves of PP/EPDM blends at different cooling rates and various parts of EPDM: (a) 0 pph, (b) 2.5 pph, (c) 5pph, (d) 7.5pph, (e) 10 pph, (f) 20 pph and (g) 30 pph,

From the DSC crystallisation curves, the values of relative crystallinity, X_t were calculated using equation 5.1

$$X_t = \frac{\int_{T_0}^T \frac{dH_c(T)}{dT} dT}{\int_{T_0}^{T_\infty} \frac{dH_c(T)}{dT} dT} = \frac{A_0}{A_\infty} \dots \dots \dots (5.1)$$

Where T_0 , T_∞ are the temperatures at which crystallisation starts (onset temperature) and ends and T is the temperature at crystallisation time t . A_0 and A_∞ are the areas of DSC exotherms from T_0 to T and T_0 to T_∞ respectively . It can be clearly seen from the figure Fig.5.12 that both polypropylene (PP) and PP/EPDM blends showed single and sharp exotherms in the temperature range from 90^0C to 125^0C which vary with cooling rates. Upon increasing the cooling rates, the exotherms of PP and PP/EPDM blends widen and shifted towards lower temperatures, follows the same trend reported in previous literatures [12]. With increase of cooling rate, we can observe that the heat flow is also increasing (i.e., the polymeric material has to cross that much energy barrier to complete the crystallisation process) The dependence of relative crystallinity (X_t) on temperature (T) at different cooling rates is shown in figure Fig.5.13.



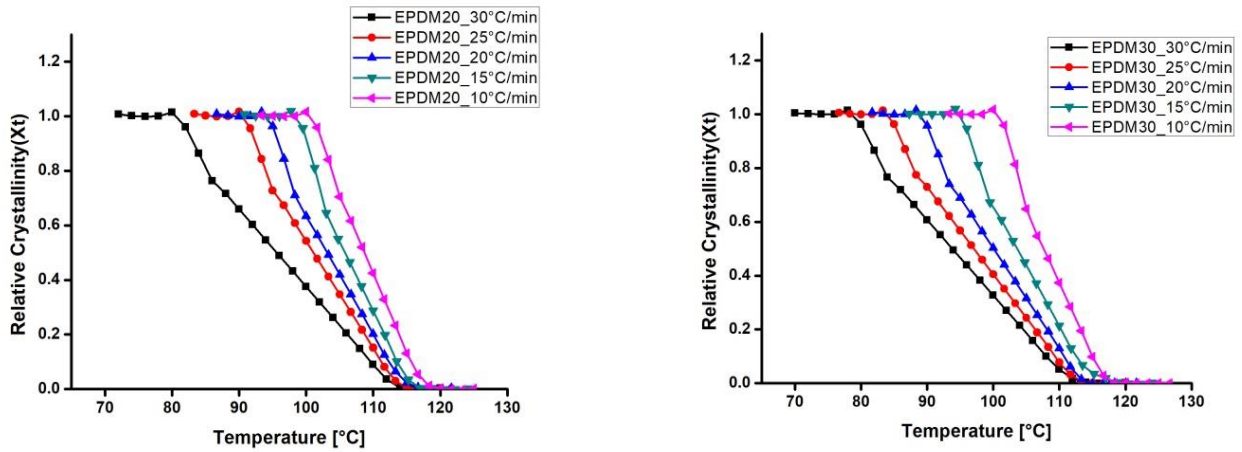


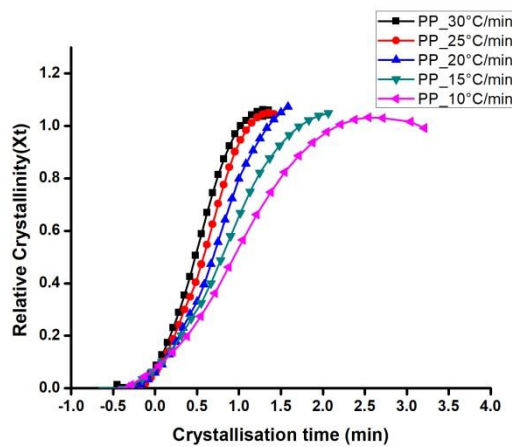
Fig.5.13 Relative crystallinity (Xt) versus Temperature of PP/EPDM blends at different cooling rates and various parts of EPDM: (a) 0 pph, (b) 2.5 pph, (c) 5pph, (d) 7.5pph, (e) 10 pph, (f) 20 pph and (g) 30 pph

The curves exhibits a reverse sigmoidal shape which indicates a lag effect of cooling rate on crystallization in PP and PP/EPDM blends which are identical to similar findings reported [13,14].

The temperature axis in Fig.5.13 can be converted into time scale using equation 5.2 and is re-plotted in figure Fig.5.14.

$$t = \frac{T_0 - T}{R} \dots \dots \dots (5.2)$$

Where R is the cooling rate, T₀ is the temperature at which crystallisation starts (onset temperature) and T is the temperature at crystallisation time t.



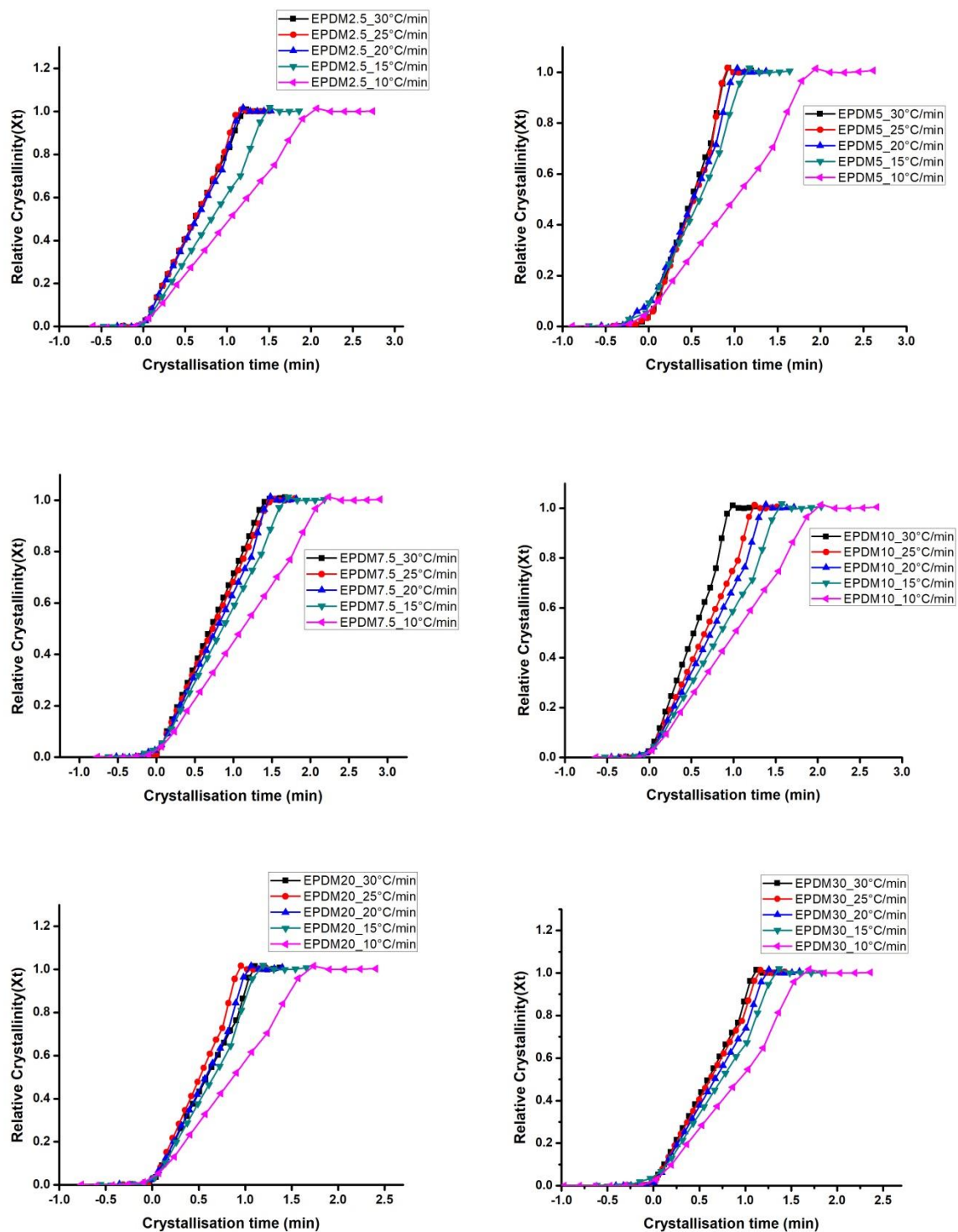


Fig.5.14 Relative crystallinity (X_t) versus Time of PP/EPDM blends at different cooling rates and various parts of EPDM: (a) 0 pph, (b) 2.5 pph, (c) 5pph, (d) 7.5pph, (e) 10 pph, (f) 20 pph and (g) 30 pph,

It can be seen from the plots that, all curves are S shaped and at higher cooling rates, shorter time is required to complete crystallisation process. Crystallisation half time, $t_{1/2}$, the time at

which crystallinity reaches 50 % can be calculated directly from Fig.5.15. It can be inferred from the Table 5.2 and Fig.5.22 that the values of T_o , T_c and $t_{1/2}$ decreases whereas ΔT_c increases as we move from lower to higher cooling rates. It can be due to the fact that, at higher cooling rates, polymer chains do not get sufficient time to crystallise, which in turn results in initiation of crystallisation at higher under cooling (high value of ΔT_c). Also at higher cooling rates, the polymer chain mobility is destroyed and resulting in incomplete crystallisation process. It also follows the same trend reported in other studies in literature [8, 9, 10]. Compare with pure polypropylene, PP/EPDM blends exhibited higher ΔT_c values and lower T_o & T_c values. It can be attributed to the fact that, during crystallisation process, the EPDM rubber hinders the growth of PP crystals during cooling cycle. The hindrance to the mobility of PP chains is due to the dipole induced dipole interactions in PP/EPDM blends analogous to that reported in PP/EPDM-g-MA blend systems [11].

5.5.1 Nucleation Activity

The nucleation activity of EPDM in PP/EPDM blends was determined by Dobrev and Gutzowa method.

$$\text{Log (R)} = A - \frac{B}{2.303\Delta T_c^2} \dots\dots\dots (5.3)$$

$$\text{Log (R)} = A - \frac{B^*}{2.303\Delta T_c^2} \dots\dots\dots (5.4)$$

Table 5.4 Nucleation activity values by Dobrev and Gutzowa method for PP/EPDM blends

Sample ID	Slope (B or B*)	Slope (B or B*)	Nucleation activity
PP	B	4.83	1
EPDM 2.5	B*	4.16	0.86
EPDM 5	B*	4.86	1.01
EPDM 7.5	B*	3.48	0.72
EPDM 10	B*	3.49	0.72
EPDM 20	B*	8.51	1.76
EPDM 30	B*	4.72	0.98

Where A, B and B* are constants and the ratio B*/ B gives the nucleation activity of EPDM in blends. The parameter ΔT_c used in equation 5.3 and 5.4 is given by $T_m - T_c$, where T_m and T_c are the melting and crystallisation peak temperatures respectively. To study the nucleation

activity in the presence of nucleating agent and or substrate, the value of B^*/B is taken into account. If this ratio close to zero indicates nucleating activity and ratio close to one indicates non nucleating activity. The value of B or B^* for the neat polymer and the blends was obtained from the slope of $\text{Log}(R)$ vs. $1/\Delta T_c^2$ shown in figure Fig.5.15. The value of nucleation activity is 1 for PP and close to 1 for other PP/EPDM blend compositions which indicates that EPDM is not acting as a nucleating agent at these compositions. At the 7.5 pph and 10 pph of EPDM, the ratio B^*/B reported the lowest value amounts to 0.72.

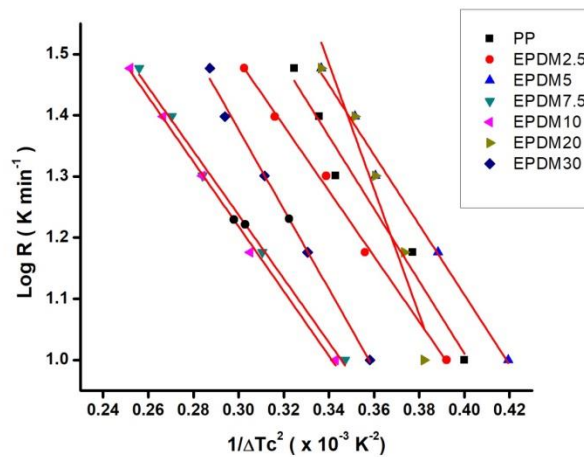


Fig.5.15 Nucleation activity by Dobreva and Gutzowa approach for various PP/EPDM blend compositions

5.5.2 Glass transition temperature

The glass transition temperature obtained using DSC analysis for polypropylene and PP/EPDM blends are shown in Table 5.5.

Table 5.5 Glass transition temperature values of PP/EPDM blends

Sample ID	Glass transition temperature ($^{\circ}\text{C}$)	
PP	-9.77	
EPDM 2.5	-10.06	-48.70
EPDM 5	-10.14	-45.76
EPDM 7.5	-10.10	-53.39
EPDM 10	-10.12	-45.74
EPDM 20	-10.12	-51.40
EPDM 30	-10.19	-49.45

The inflection point located near -10°C for PP/EPDM systems correspond to the glass transition of PP, whereas the point around -45°C to -53°C for all the blends represent the glass transition of EPDM. The two glass transition temperatures obtained for PP/EPDM blends is an indication of immiscible nature of PP/EPDM blends. A slight decrease of the glass transition peak of PP to lower temperature was observed as the result of the presence of EPDM with low glass transition temperature (T_g). It was also noted that the transition peaks of PP in PP/EPDM blend became wider and weaker at the higher loading of EPDM.

5.6 Thermo gravimetric (TGA) analysis

Table 5.6 shows the values of thermo gravimetric analysis (maximum degradation temperature, T_{max} and % weight loss of sample) of PP/EPDM blends.

Table 5.6 Thermo gravimetric analysis (T_{onset} , T_{max} and T_f) of PP/EPDM blends

Sample ID	T_{max} ($^{\circ}\text{C}$)	Weight (loss %) at 700°C
PP	463.29	99.88
EPDM 2.5	464.08	99.87
EPDM 5	465.87	99.86
EPDM 7.5	466.08	99.89
EPDM 10	465.61	99.91
EPDM 20	466.75	99.93
EPDM 30	467.38	99.95

The values of maximum degradation temperature, T_{max} found to be almost constant with all blend formulations; however a slight increase in T_{max} with EPDM content is attributed to the thermal stability of high molecular EPDM grade (Keltan® 9565Q) used. The high value of maximum degradation temperature, T_{max} is an indication of PP/EPDM rubber blends that can withstand high operating temperatures for long periods.

5.7 Conclusions

The average breaking force, breaking strength, modulus and elongation at break of FAS coated coir fibers was found to be higher than uncoated coir fibers. Among pure polypropylene as well as PP/EPDM blends, PP/EPDM 7.5 registers highest impact strength value and also comparable tensile and flexural properties with other blend formulations. The critical diameter of rubber particles were obtained at 7.5 pph of EPDM in PP/EPDM blends and are measured to be 380.8nm. It was found that the mechanically induced cavitation behaviour is responsible for the impact resistance of PP/EPDM blends.

Low shear rate rheology points to the shear thinning behaviour of PP/EPDM blends. The complex viscosity found to be decreases with increase in frequency which shows the melt is in pseudo plastic state. The storage modulus (G') and loss modulus (G'') of blends shows an increasing trend with oscillatory frequency analysis. Non-isothermal crystallisation kinetics studied using DSC analysis shows a lag effect of cooling rate on crystallization in PP and PP/EPDM blends. No specific nucleation activity of EDM was observed in PP/EPDM blends. The high value of maximum degradation temperature obtained using TGA analysis indicates the stability of PP/EPDM blends to withstand high operating temperatures for long periods. By comparing all the above findings, the PP/EPDM 7.5 was chosen as the best blend formulation is chosen for the composite fabrication process.

5.8 REFERENCES

1. Matsuoka, S. (Ed.). (1992). Relaxation phenomena in polymers. Hanser Publishers.
2. Purnima, D., Maiti, S. N., & Gupta, A. K. (2006). Interfacial adhesion through maleic anhydride grafting of EPDM in PP/EPDM blend. *Journal of applied polymer science*, 102(6), 5528-5532.
3. Sharma, R., & Maiti, S. N. (2015). Effects of crystallinity of polypropylene (PP) on the mechanical properties of PP/styrene-ethylene-butylene-styrene-g-maleic anhydride (SEBS-g-MA)/teak wood flour (TWF) composites. *Polymer Bulletin*, 72(3), 627-643.
4. Sharma, R., & Maiti, S. N. (2013). Modification of tensile and impact properties of poly (butylene terephthalate) by incorporation of styrene-ethylene-butylene-styrene and maleic anhydride-grafted-SEBS (SEBS-g-MA) terpolymer. *Polymer Engineering & Science*, 53(10), 2242-2253.

5. Gao, X., Mao, L. X., Jin, R. G., Zhang, L. Q., & Tian, M. (2007). Structure and mechanical properties of PP/EPDM/attapulgite ternary blends. *Polymer journal*, 39(10), 1011.
6. Bucknall, C. B. (2001). Applications of microscopy to the deformation and fracture of rubber-toughened polymers. *Journal of microscopy*, 201(2), 221-229.
7. Metzner, A. B., & Whitlock, M. (1958). Flow behavior of concentrated (dilatant) suspensions. *Transactions of the Society of Rheology*, 2(1), 239-254.
8. Srivastava, A., Majumdar, A., & Butola, B. S. (2012). Improving the impact resistance of textile structures by using shear thickening fluids: a review. *Critical Reviews in Solid State and Materials Sciences*, 37(2), 115-129.
9. Sharma, R., & Maiti, S. N. (2015). Effects of SEBS-g-MA copolymer on non-isothermal crystallization kinetics of polypropylene. *Journal of materials science*, 50(1), 447-456.
10. Prut, E. V., Erina, N. A., Karger-Kocsis, J., & Medintseva, T. I. (2008). Effects of blend composition and dynamic vulcanization on the morphology and dynamic viscoelastic properties of PP/EPDM blends. *Journal of applied polymer science*, 109(2), 1212-1220.
11. Sharma, R., & Maiti, S. N. (2015). Effects of SEBS-g-MA copolymer on non-isothermal crystallization kinetics of polypropylene. *Journal of materials science*, 50(1), 447-456.
12. Wang, B., Hu, G., & Wei, L. (2008). Melting behavior, nonisothermal crystallization kinetics, and morphology of PP/nylon 11/EPDM-g-MAH blends. *Journal of applied polymer science*, 107(5), 3013-3022.
13. Hay, J. N., Fitzgerald, P. A., & Wiles, M. (1976). Use of differential scanning calorimetry to study polymer crystallization kinetics. *Polymer*, 17(11), 1015-1018.
14. Manchanda, B., Vimal, K. K., Kapur, G. S., Kant, S., & Choudhary, V. (2016). Effect of sepiolite on nonisothermal crystallization kinetics of polypropylene. *Journal of materials science*, 51(21), 9535-9550.

**CHAPTER 6 MECHANICAL, MORPHOLOGICAL,
RHEOLOGICAL AND THERMAL PROPERTIES OF
PP/EPDM 7.5/COIR COMPOSITES**

ABSTRACT

The effective length of coir fiber to be used in composites is determined based on critical length of fibers. Based on the optimized PP/EPDM7.5 blend formulation, the uncoated as well as FAS coated coir filled composites were prepared by varying coir fiber content from 10pph to 40pph. The tensile, impact and flexural analysis of all the composite formulations were carried out. The morphological examinations of cryofractured and impact fractured composite surfaces were studied using scanning electron microscopy (SEM). The low shear rate rheology and dynamic viscoelastic properties of composites were carried out to study rheological behaviour of PP/EPDM blends. Non-isothermal crystallisation kinetics, nucleation activity and glass transition temperature of composites were investigated using DSC analysis. The maximum degradation temperature of blends was obtained by thermo gravimetric (TGA) analysis.

6.1 Determination of critical length of coir fibers

The mechanical characteristics of a fiber-reinforced composite depend not only on the properties of the fiber, but also on the degree to which an applied load is transmitted to the fibers by the matrix phase. Some critical fiber length is necessary for effective strengthening and stiffening of the composite material. This critical length is dependent on the fiber diameter d and its ultimate (or tensile) strength (σ) and on the fiber–matrix bond strength (τ).

In single-fiber pull-out test, the pull-out stress in general increases linearly with the fiber length embedded in the matrix. The fiber fails when the pull-out stress reaches the fiber failure stress and the minimum embedded length at which the fiber fails is termed as the critical fiber length, l_c .

To find out the critical length of coir fiber in PP/EPDM 7.5 matrix, different embedded fiber lengths of 25mm,20mm,10mm,5mm,2.5mm,1mm,0.5mm and 0.25mm in PP/EPDM 7.5 matrix were tried. It is found that, the minimum length (critical length) required to hold the coir fiber in PP/EPDM 7.5 matrix will be equal to .25mm. l_c value of FAS coated fibers may be slightly lower compare with uncoated fibers. The melt grafted FAS coated fibers on EPDM enables better bonding between fibers and matrix. i.e., higher the fiber–matrix adhesion, lower the l_c . Brahmakumar et al. also reported the dependence of surface modification on pull out strength of coir fibers in LDPE matrix and they observed that the as-received fiber with waxy surface layer shows higher pull-out stress at all ‘ l/d ’ values resulting in fiber failure at lower embedded length (30 mm) than of the wax-free fiber (40 mm) [1]. To prepare the coir based PP/EPDM composites, the effective length of the fibers is chosen as 30 times the critical length of coir fibers (based on the assumption that, this factor of safety will enable the transfer of stress from matrix to fibers).Therefore the effective length chosen for coir based composite preparation is $0.25\text{mm} * 30=7.5\text{mm}$.

6.2 Polypropylene (PP) / Ethylene-propylene-diene rubber (EPDM) / Coir composites

By selecting PP/EPDM7.5 as the matrix, the coir fiber content was varied from 10pph to 40pph to fabricate the PP/EPDM/Coir composites. The composites were prepared with both uncoated as well as FAS coated coir fibers. The different compositions used for preparing composites are displayed in Table 6.1 and table 6.2. The PP/EPDM/Coir composites were prepared first by dry blending followed by melt compounding using a Brabender Plasticorder

mixer (model W 50 EHT). The melt compounded samples were made into a sheet using compression moulding press.

Table 6.1 PP/EPDM/Uncoated coir composite formulations

Sample codes	Polypropylene(in phr)	EPDM (in phr)	Uncoated Coir (in phr)	Volume fraction, ϕ_f
PP/EPDM 7.5/UC10	100	7.5	10	0.07
PP/EPDM 7.5/UC20	100	7.5	20	0.13
PP/EPDM 7.5/UC30	100	7.5	30	0.19
PP/EPDM 7.5/UC40	100	7.5	40	0.24

Where UC stands for uncoated coir

Table 6.2 PP/EPDM/FAS coated coir composite formulations

Sample codes	Polypropylene(in phr)	EPDM (in phr)	FAS coated coir (in phr)	Volume fraction, ϕ_f
PP/EPDM 7.5/SGC10	100	7.5	10	0.07
PP/EPDM 7.5/SGC20	100	7.5	20	0.13
PP/EPDM 7.5/SGC30	100	7.5	30	0.19
PP/EPDM 7.5/SGC40	100	7.5	40	0.24

Where SGC stands for sol-gel coated coir

The prepared sheets then cut using numerically controlled cutting machine into dumb-bell shaped specimens for tensile testing and notched specimens for izod impact testing and un-notched specimens for flexural test.

6.3 Mechanical property (Impact, Tensile and Flexural) analysis of PP/EPDM/Coir composites

6.3.1 Impact analysis of PP/EPDM/Coir composites

Notched Izod impact tests of composites were performed using a Tinius-Olsen machine at ambient temperature 23°C according to ISO 180 A. Results were obtained from the average of at least 10 samples for each set. The impact strength and impact energy plots generated for uncoted and FAS coated coir fiber filled composites are shown in figure Fig.6.1 and Fig.6.2 respectively.

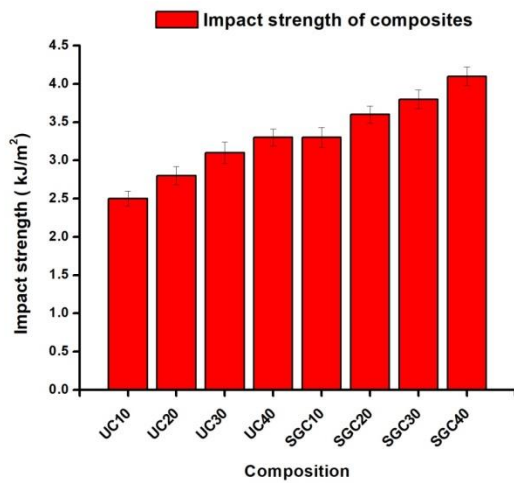


Fig.6.1. Impact strength of PP/EPDM/Coir composites

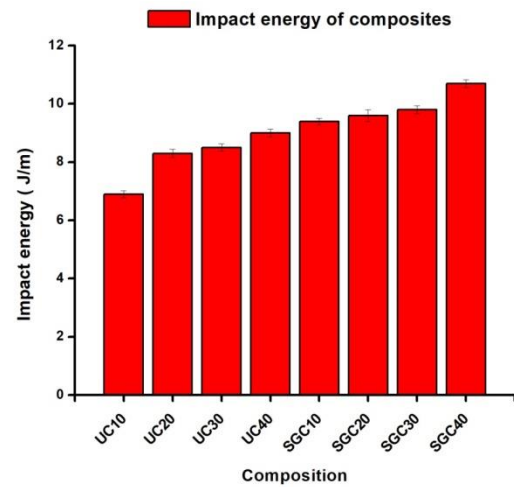


Fig.6.2. Impact energy of PP/EPDM/Coir composites

It can be clearly seen from plots Fig.6.1. and Fig.6.2. that the FAS coated fiber reinforced composites shows significant improvement in impact strength and impact energy values compare with uncoated fiber reinforced composites. As the fiber loading is increased from 10 pph to 40pph, the impact strength is found to be increases. The role of the fibers in a composite structure is extremely important since they are responsible for bearing a significant percentage of the applied load. Hancox et.al. stated that impact response of fiber reinforced composites have proportional relationship with failure strength of fibers. i.e., higher the failure strength of fibers, higher will be the impact resistance [2]. In section 4.7(Chapter 4), it is found that the failure strength of FAS coated coir fibers higher than the uncoated coir fibers which points to the improvement of impact response of composites with FAS coated fibers. Chamis et.al. reported that materials containing fibers with a greater strain energy absorbing capacity offering improved Izod impact energies [3]. Area under the fibers stress/strain diagram represents a useful approach for determining the strain energy of fibers. In chapter 4,from Fig.4.8 a & b, stress versus strain curves for uncoated and FAS coated fibers, the area under the curve for FAS coated coir fibers found to be 75% higher than the uncoated coir fibers which again points to the reason for significant improvement in impact response of FAS coated coir fiber reinforced composites. It can also be inferred from the SEM images that fiber pull-out, fiber fracture and fiber matrix debonding are the primary energy absorbing mechanism in FAS coated fiber filled composites (discussed in section 6.4)

6.3.2 Tensile analysis of PP/EPDM/Coir composites

Tensile testing of composites was performed by MTS Synergy RT1000 testing apparatus at 23°C and a relative humidity of 48% according to ISO 527. The tensile strength, modulus and % deformation plots generated for uncoted and FAS coated coir fiber filled composites are shown in Fig.6.3, Fig.6.4 and Fig.6.5

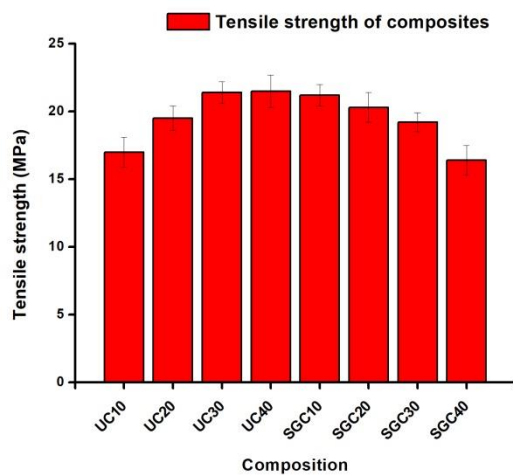


Fig.6.3. Tensile strength of PP/EPDM/Coir composites

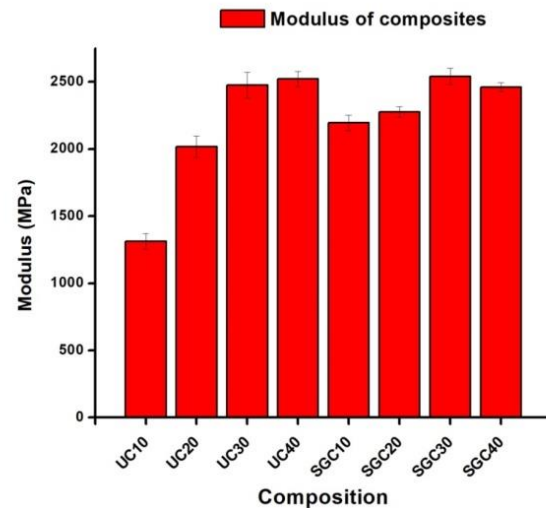


Fig.6.4. Modulus of PP/EPDM/Coir composites

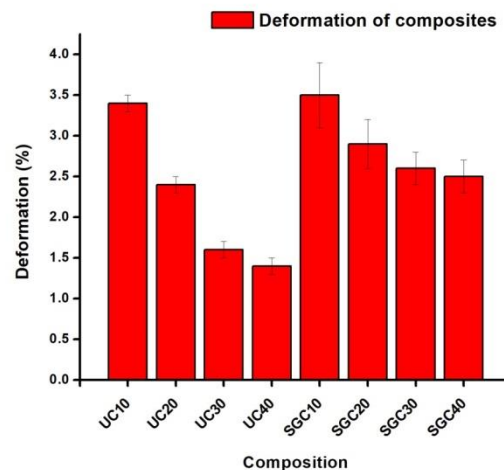


Fig.6.5. % deformation of PP/EPDM/Coir composites

The tensile strength of uncoated and FAS coated coir filled composites is plotted in Fig.6.3. In the case of uncoated coir filled composites, as the fiber loading is increased from 10pph to 40pph, the tensile strength exhibited an increasing trend. In the case of FAS coated coir filled composites, as the fiber loading is increased from 10pph to 40pph, tensile strength shows a

decreasing trend. It is interesting to note that the tensile strength values of uncoated coir filled composites are found to be high at higher parts of filler loading (30pph and 40pph), but the tensile strength values of FAS coated coir filled composites are found to be high at lower parts of filler loading (10pph and 20pph). At 10pph of uncoated fibers, the tensile strength is found to be 19.5 MPa whereas at 10pph of FAS coated coir fibers, the tensile strength is found to be 21.2 MPa. This could be due to at lower filler loading, the extremely hydrophobic FAS coated fibers are grafted effectively on the PP/EPDM7.5 matrix. During internal melt mixing of polypropylene, EPDM and FAS coated coir fibers in Brabender, the fluoro alkyl functional siloxane (FAS) coated coir fibers are melt grafted specifically on EPDM sites. This could be due to the unsaturation in diene monomer exists in EPDM, which creates some additional reactive sites for silane grafting to occur (The grafting can also occur by abstraction of secondary hydrogen from a polypropylene sequence of EPDM). The advent of this new technique involving the grafting of FAS coated coir fibers on to polymer chain in the internal mixer is more attractive due to various industrial advantages. Kozawa et.al reported about silane cross-linkable ethylene-propylene elastomer compositions prepared by reactive extrusion processing [4]. However at higher filler loading of FAS coated fibers (at 30pph and 40pph), the 7.5 pph of EPDM is not sufficient to provide reactive sites for grafting of all fibers.

In the case of uncoated coir filled composites, as the filler loading is increased from 10pph to 40pph, there would be more hydroxyl groups present in the entire volume fraction of fibers and forms better bonding with PP/EPDM7.5 matrix. The reason for increase in tensile strength for uncoated coir filled composites with filler loading is pointing to the better fiber–matrix adhesion. The modulus of uncoated and FAS coated coir filled composites is plotted in Fig.6.4. The modulus values shows an increasing trend with filler loading for uncoated coir filled composites whereas in the case of FAS coated coir filled composites, the modulus shows an increasing trend up to 30pph and decreases at 40pph. The % deformation values of uncoated and FAS coated coir filled composites are plotted in Fig.6.5. It shows a decreasing trend for both uncoated as well as FAS coated coir filled composites. However, the FAS coated fiber filled composites exhibits deformation values higher than that of uncoated coir filled composites. This is due to ductile behaviour of FAS coated coir filled composites imparted by the super hydrophobic nature of fluoroalkyl functional siloxane coated fibers.

6.3.3 Flexural analysis of PP/EPDM/Coir composites

Flexural testing of composites was performed by MTS Synergy RT1000 testing apparatus at 23°C and a relative humidity of 48% according to ISO 178. The flexural strength, modulus and % deformation plots generated for uncoted and FAS coated coir fiber filled composites are shown in Fig.6.6, Fig.6.7 and Fig.6.8

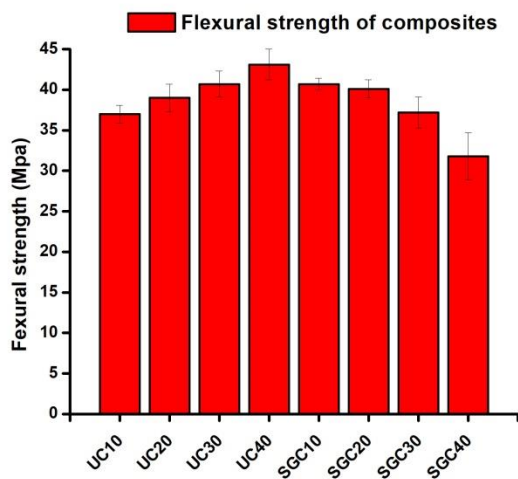


Fig.6.6. Flexural strength of of PP/EPDM/Coir composites

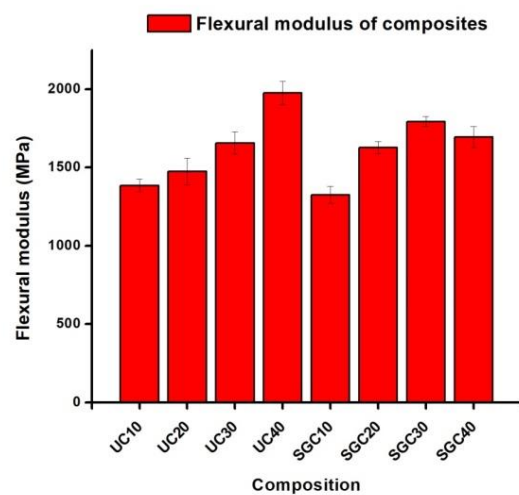


Fig.6.7. Flexural modulus of of PP/EPDM/Coir composites

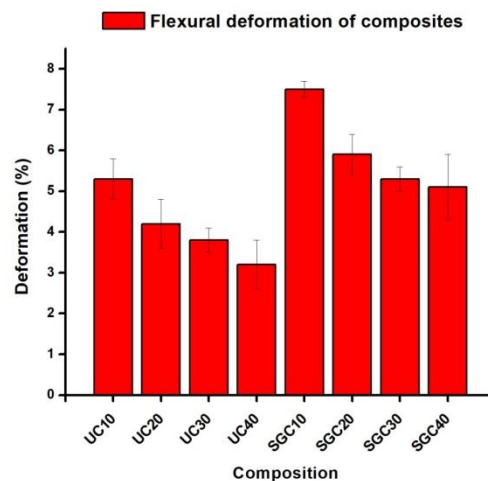


Fig.6.8. Flexural deformation of of PP/EPDM/Coir composites

The flexural strength of uncoated and FAS coated coir filled composites is plotted in Fig.6.6. In the case of uncoated coir filled composites, as the fiber loading is increased from 10pph to 40pph, the flexural strength shows an increasing trend. In the case of FAS coated coir filled composites, as the fiber loading is increased from 10pph to 40pph, flexural strength shows a

decreasing trend from 10pph to 40pph. The flexural strength of composites follows the same trend of tensile strength values. The increase of flexural strength values of composites at lower concentration of FAS coated coir fibers could be due to higher grafting efficiency of coated coir fibers on EPDM during melt blending in internal mixer. The flexural deformation of uncoated and FAS coated coir filled composites is plotted in Fig.6.8. For both uncoated and FAS coated fiber filled composites, it shows a decreasing trend when fiber loading varied from 10pph to 40 pph. However, in the case of FAS coated fiber filled composites, it shows an increase in flexural deformation comparing with uncoated ones. As mentioned before, this can be due to the ductile behaviour of FAS coated coir filled composites imparted by the extreme hydrophobic nature of fluoroalkyl functional siloxane coated fibers. The flexural modulus of uncoated and FAS coated coir filled composites is plotted in Fig.6.7. As expected, it can be clearly seen from the plot that, both uncoated and FAS coated coir filled composites shows an increasing trend in flexural modulus value. Since both set of composites shows a decrease in flexural deformation with filler loadings, it is resulted in an increase of modulus value. As the FAS coated fiber filled composites deforms larger amount compare with uncoated ones, its modulus values are lower compare with uncoated coir composites.

6.4 Determination of pull-out stress

The pull-out tests were conducted in MTS Synergy RT1000 testing apparatus at 23°C , relative humidity of 48% and crosshead speed of 1 mm/min up to rupture. At least six samples were tested for fiber embedded length of 25mm in PP/EPDM matrices and the average values are reported. The pull out experiment is shown in figure Fig.6.9. The experiment is performed based on the detailed procedure discussed under 2.1.2.6.1 The pull out stress of uncoated and FAS coated fibers with PP/EPDM blends were plotted in figure Fig.6.10 a and b.

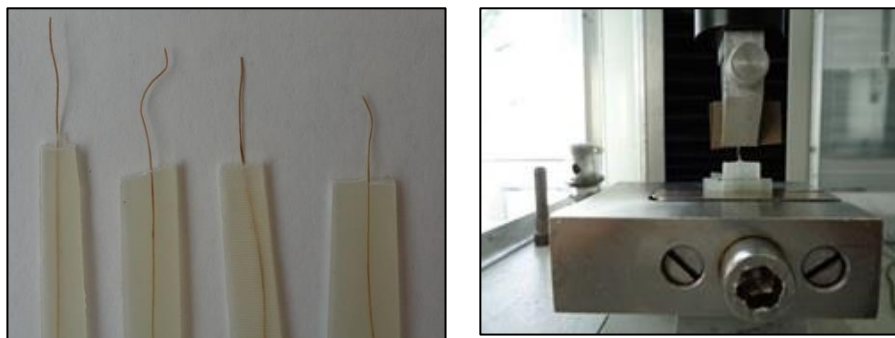


Fig.6.9. Pullout Experiment

From the plots, it can be seen that, there will not be much difference in pull-out strength values of PP/EPDM blend formulations. However at lower concentration of EPDM swathe, pullout strength values are found to be high for coir fibers.

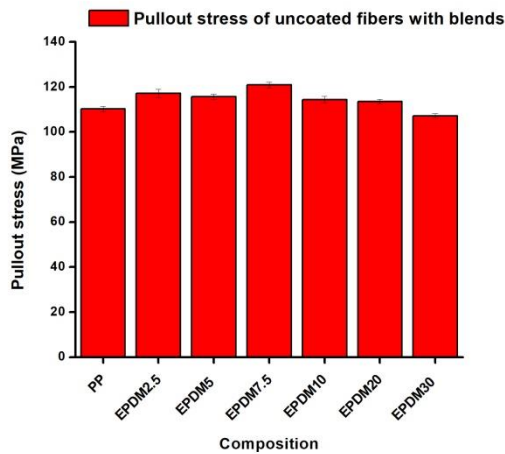


Fig.6.10 a Pull-out stress of uncoated fibers with PP/EPDM blends

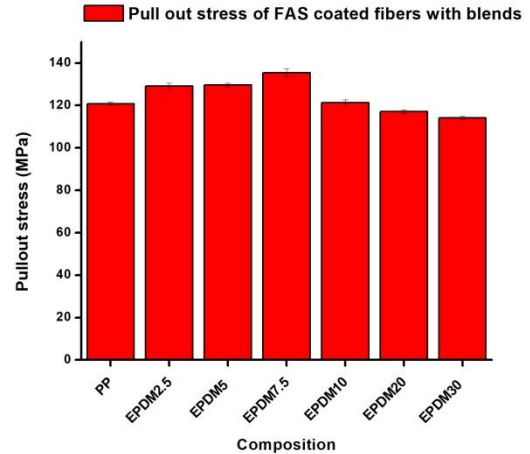


Fig.6.10 b Pull-out stress of FAS coated fibers with PP/EPDM blends

It is well known that the work for debonding and work to pull-out are strong factors for energy dissipation during impact of composites. Therefore it is very important to determine these quantities in order to interpret the results of impact resistance of composites. Beaumont gives expressions for work associated with micro-mechanical fracture processes such as debonding and fiber pull-out [5].

The work to pull-out is given as:

$$W_p = \frac{\pi d \tau l_c^2}{24} \dots \dots \dots (1)$$

Where l_c = critical transfer length ($= \sigma_f * d / 2\tau$) and τ = constant frictional shear stress/ fiber-matrix interfacial shear strength

By using critical length values obtained in section 6.1, the frictional shear stress can be found out. This fiber-matrix interfacial shear strength is one of the most important parameters in controlling the toughness and the strength of a composite material. The frictional shear stress is found to be higher for FAS coated fibers than uncoated ones. The work to pull-out uncoated coir fibers from PP/EPDM matrix was found to be 0.2Nmm. The work to pull-out FAS coated coir from PP/EPDM matrix was found to be 0.3Nmm. It is seen that, compare

with uncoated ones, slightly higher work is required to pull out FAS coated coir fibers from PP/EPDM 7.5 matrix. This could be due to the fact that, the extremely hydrophobic silane based FAS coated fibers melt grafted on EPDM in Brabender melt mixer which in turn improves the pull-out strength values for FAS coated fibers in PP/EPDM matrix.

The work for debonding is given as:

$$W_d = \frac{\pi d^2 \sigma_f^2 l_d}{24 * E_f} \dots\dots\dots (2)$$

Where d = fiber diameter, σ_f = failure strength of the fiber, l_d = length of the debonded zone and

E_f = fiber modulus.

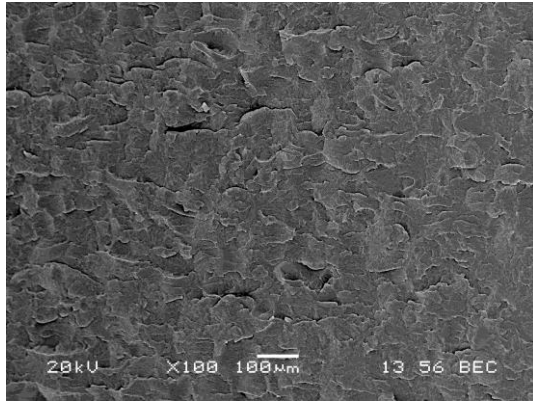
By assuming the unit length of the debonded zone in composites, it is found that the FAS coated coir filled composites requires more work to debond the fibers from PP/EPDM7.5 matrix than uncoated ones. If the length of fiber debonded zone increases upon impact on composites, the work for debonding is found to be higher or in other words, more energy is dissipated if the debonded zone is long. The super hydrophobic behaviour of coir fibers pointing to the fiber matrix debonding in this system. The higher work to pull-out as well as work for debonding values of FAS coated coir fibers with PP/EPDM7.5 matrix than uncoated fibers points to the efficient energy dissipation in these composites upon impact loads.

6.5 Morphological analysis of PP/EPDM/Coir composites

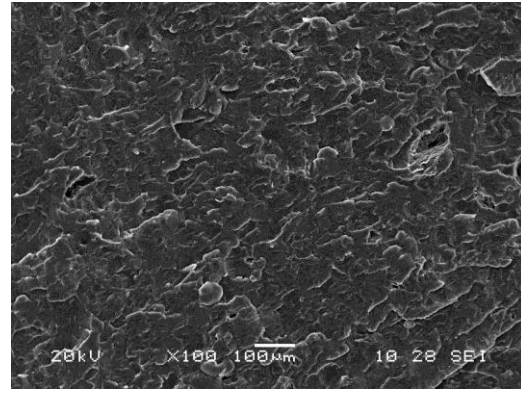
The impact fractured samples of pure polypropylene (PP), PP/EPDM7.5 blend and its uncoated & FAS coated coir filled composite's morphologies were analysed by scanning electron microscopy technique using Jeol JSM-6031 scanning electron microscope. The sample preparation procedure was explained in section 2.1.2.8.2. Initially, the impact fractured surface of the composite samples was sputter-coated with a thin gold layer (Edwards Sputter Coater) before viewing it under scanning electron microscope.

6.5.1 Morphology of impact-fractured samples

Morphology of impact fractured pure PP and PP/EPDM7.5 blend are shown in figure Fig.6.11.



a) I-Pure PP

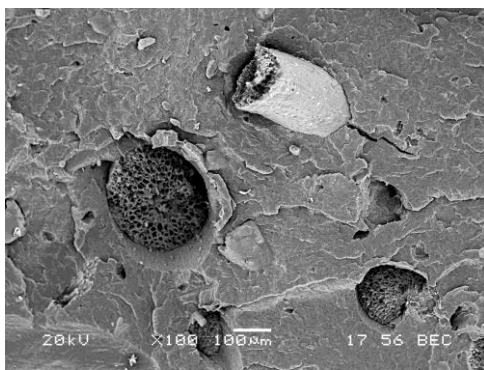


b) I-PP/EPDM7.5 blend

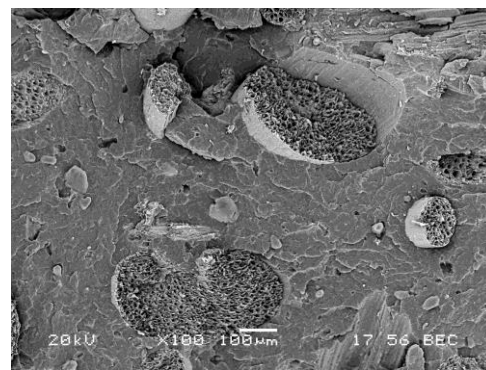
Fig.6.11. Morphology of impact fractured pure PP and PP/EPDM7.5 blend

*The prefix 'I' denotes impact fractured samples

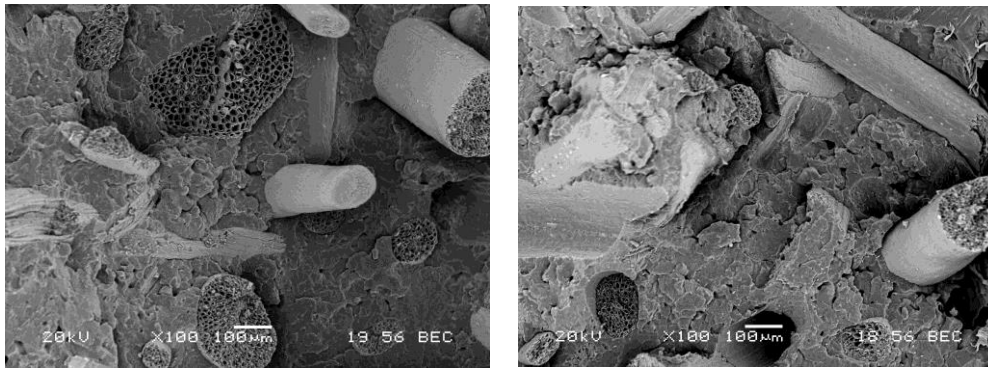
Scanning electron microscope images shows that the impact fractured polypropylene surfaces gives almost uniform morphology with a layer by layer structure on the surface. The impact fractured PP/EPDM blend surfaces exhibits layer by layer structure with white patches and cavities on the surface. It is well known that the principal mechanisms of inelastic deformation in rubber-toughened polymers are shear yielding and multiple crazing in the rigid matrix phase, and cavitation in the soft disperse phase. The white patches on the PP/EPDM surface can be correlated with crazing behaviour and cavities present in these surfaces can be correlated with mechanically induced cavitation behaviour of the blends. [3], Morphology of impact fractured PP/EPDM7.5/Uncoated coir composites are shown in figure Fig.6.12.



a) I-UC10



b) I-UC20



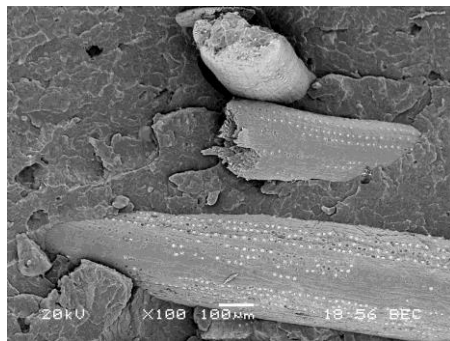
c) I-UC30

d) I-UC40

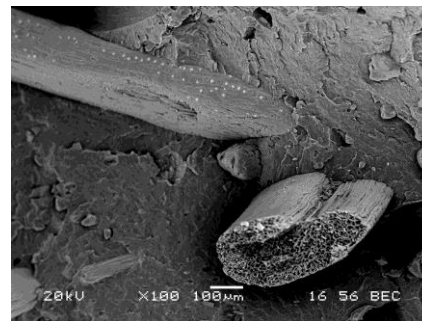
Fig.6.12. Morphology of impact fractured PP/EPDM7.5/Uncoated coir composites

*The prefix 'I' denotes impact fractured samples

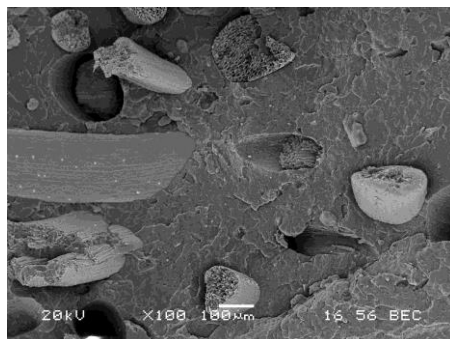
In the case of uncoated coir filled composites, it can be read from the SEM images that, at lower filler loadings (at 10pph and 20pph) the dominant failure mechanism in the composite is the fiber fracture. Upon increasing the filler loading (30pph and 40pph) it can be inferred from the SEM images that the main mechanisms of failure of composites are driven by both fiber pull-out and fiber fracture. The combined effect results in improvement in impact properties upon increasing the fiber volume fraction in composites. Morphology of impact fractured PP/EPDM7.5/FAS coated coir composites are shown in figure Fig.6.13.



a) I-SGC10



b) I-SGC20



c) I-SGC30



d) I-SGC40

Fig.6.13. Morphology of impact fractured PP/EPDM7.5/FAS coated coir composites

*The prefix 'I' denotes impact fractured samples

In the case of FAS coated coir filled composites, it can be read from the SEM images that, the failure mechanisms are fiber fracture, fiber pullout and fiber matrix debonding. It is well known that the failure modes that involve fracture of the matrix or interphase region result in low fracture energies whereas failures involving fiber failure modes such as fiber fracture, pull-out and debonding result in significantly greater energy dissipation. The role of the fibers in a composite structure is extremely important since they are responsible for bearing a significant percentage of the applied load. The effect of work to debonding and work to pull-out are discussed under section 6.4.

6.6 Rheological analysis of PP/EPDM/Coir composites

6.6.1 Low shear rate rheology

The low shear rate rheology (for shear rates less than 100 sec⁻¹) of uncoated and FAS coated coir fiber filled PP/EPDM composites were studied using an Anton Paar, CTD 450, Physica MCR 301 rheometer. Before experiments, the samples were dried at 60⁰C for 12 h and compression moulded to the thickness about 2 mm. The viscosities versus shear rate of PP/EPDM/Coir composites were plotted in figure Fig.6.14.

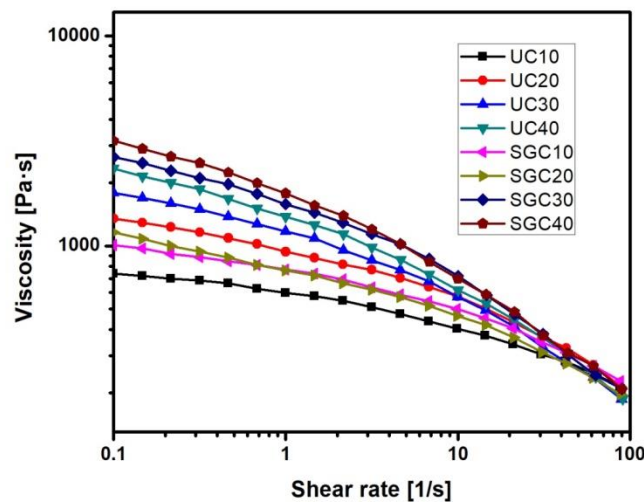


Fig.6.14. Viscosity versus shear rate of PP/EPDM/Coir composites

It can be inferred from the plot that, all the FAS coated coir filled composites exhibit high viscosity values especially in the low shear rate regions (for shear rates less than 5 1/s). The extremely hydrophobic fluoroalkyl functional siloxane coating on coir fibers

contributed to the high viscous nature of composites. The affinity of the coated coir fibers with EPDM (due to grafting of FAS coir on to EPDM in internal melt mixing process) provides higher resistance to shear forces. At lower shear rates the fluoro alkyl functional siloxane coating on the surface of coir fibers shows a tendency to form hydro clusters which causes an increase in viscosity. As the shear rate increases, the viscosity is found to be decreasing exhibiting a shear thinning behaviour. As the shear rate increases, the particles start to flow forming layers of particles, which causes decrease in viscosity. These observations follows the same trend of the earlier findings cited in literatures [5]

6.6.2 Dynamic viscoelastic property analysis

The principle of parallel plate rheometry was used to find out dynamic viscoelastic properties of composites .The oscillatory frequency analysis was performed at a fixed strain (0.1%) corresponding to the linear viscoelastic domain and the frequency was varied in the range from 0.01-100 Hz. The viscoelastic properties such as storage modulus (G'), loss modulus (G'') and complex viscosity (η^*) were measured as a function of angular velocity (ω) using an Anton Paar, CTD 450, Physica MCR 301 rheometer. Before experiments, the samples were dried at 60⁰C for 12 h and compression moulded to a circular shape having diameter 25mm and the thickness about 2 mm. The complex viscosity versus frequency of polypropylene and PP/EPDM composites are shown in figure Fig.6.15.

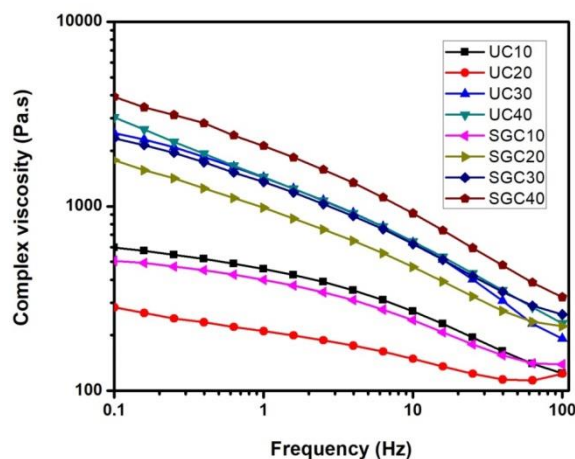


Fig.6.15. Frequency dependence of complex viscosity in PP/EPDM/Coir composites

The complex viscosity found to be decreases with increase in frequency which shows the melt is in pseudo plastic state. It can also observe that the values of viscosity increases continuously with increasing concentration of coir fibers which may be attributed to the

hydrodynamic disturbance due to hard lignocellulosic coir fibers. The FAS coated coir filled composites shows high complex viscosity values compare with uncoated ones.

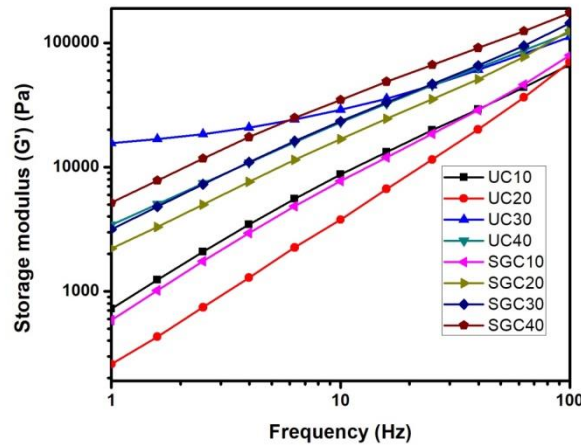


Fig.6.16. Frequency dependence of storage modulus in PP/EPDM/Coir composites

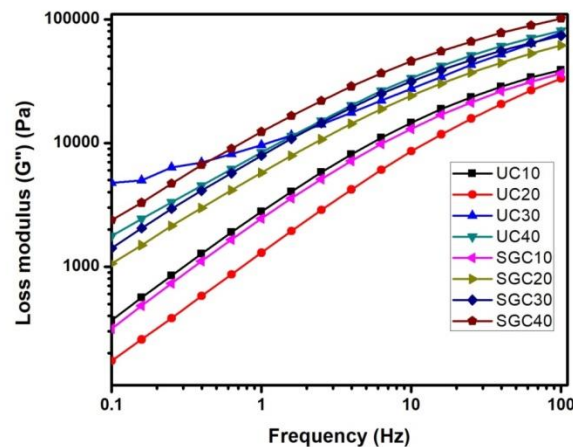


Fig.6.17. Frequency dependence of loss modulus in PP/EPDM/Coir composites

Frequency dependence of storage & loss modulus in PP/EPDM/Coir composites are shown in **Fig.6.16** and **Fig.6.17**. The storage as well as loss modulus of the composites are found to increase with increasing concentration of coir fibers. The higher values of storage modulus of FAS coated coir filled composites points to its capacity to hold stored energy in it. The higher values of loss modulus of FAS coated coir filled composites with filler loading points to its effectiveness in dissipating energy upon impact.

6.7 Non-isothermal crystallisation kinetics of PP/EPDM7.5/Coir composites

Table 6.3 shows important crystallisation parameters such as crystallisation peak (T_c), onset temperature (T_o), Normalised enthalpy (ΔH_c), melting peak (T_m) and under cooling, ΔT_c (where $\Delta T_c = T_m - T_c$) temperatures of uncoated coated coir filled PP/PDM7.5 composites

Table 6.3 Non isothermal crystallisation exotherms of PP/EPDM7.5/Coir composites

Sample ID	Cooling rate ($^{\circ}\text{C}/\text{min}$)	T_o ($^{\circ}\text{C}$)	T_c ($^{\circ}\text{C}$)	ΔH_c (Jg^{-1})	T_m ($^{\circ}\text{C}$)	ΔT_c ($^{\circ}\text{C}$)
UC10	10	120.93	115.5	78.9	163.5	48
	15	118.7	113	75.36	163.25	50.25
	20	117.09	111	75.24	163	52
	25	115.82	109.17	74.31	162.92	53.75
	30	114.71	108	71.32	163	55
UC20	10	122.33	115.67	59.52	163.33	47.66
	15	119.61	113.5	57.33	162.25	48.75
	20	118.09	112	56.53	161.67	49.67
	25	117	110.42	54.87	161.25	50.83
	30	116.09	109	53.78	161.5	52.5
UC30	10	123.45	116.67	47.98	163.17	46.5
	15	121.17	114	47.51	162.75	48.75
	20	119.58	112	46.41	163	51
	25	118.39	110.42	45.97	162.92	52.5
	30	117.31	108.5	45.52	162.5	54
UC40	10	123.58	117.5	50.28	164.5	47
	15	121.72	115.25	49.98	163.75	48.5
	20	120.43	113.67	49.04	163.33	49.66
	25	119.34	112.5	48.01	162.92	50.42
	30	118.44	111	48.28	162	51
SGC10	10	119.72	114	77.69	162.83	48.83
	15	117.59	111.5	77.46	162.75	51.25
	20	116.1	109.67	76.4	162.33	52.66
	25	114.94	108.75	74.99	162.08	53.33
	30	114	107.5	74.21	161.5	54
SGC20	10	121.53	115.33	60.14	166	50.67
	15	119.27	112.75	58.95	165.75	53
	20	117.64	110.67	58.54	165.67	55
	25	116.3	108.75	58.47	165.83	57.08
	30	115.14	107	57.33	166	59
SGC30	10	122.43	115.5	53.29	166.5	51
	15	120.24	113.25	52.82	166.5	53.25
	20	118.63	111	52.08	166.33	55.33
	25	117.3	109.58	51.49	166.25	56.67

	30	116.21	108	51.58	165.5	57.5
SGC40	10	122.84	117.17	56.18	165.83	48.66
	15	120.76	114.75	55.75	166.5	51.75
	20	119.17	113	54.42	165.33	52.33
	25	117.86	111.25	53.71	165.42	54.17
	30	116.21	110	53.46	165.5	55.5

Table 6.4 shows the average crystallinity values of PP /EPDM7.5/Coir composites obtained using DSC analysis.

Table 6.4 % crystallinity of PP/EPDM7.5/Coir composites blends

Sample ID	Crystallinity (%)
UC10	42.5
UC20	34.7
UC30	31
UC40	34.2
SGC10	43.2
SGC20	36.1
SGC30	34.7
SGC40	39

The effect of crystallinity values on cooling rate of crystallisation is shown in figure Fig.6.18

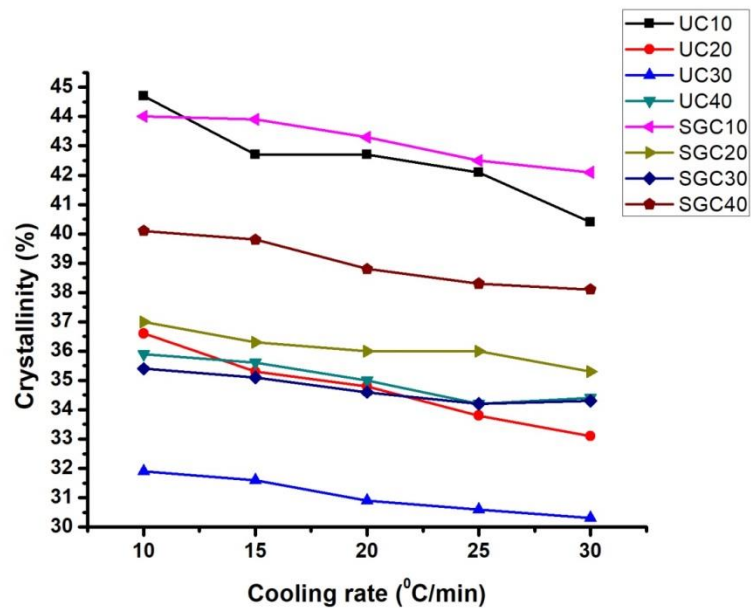
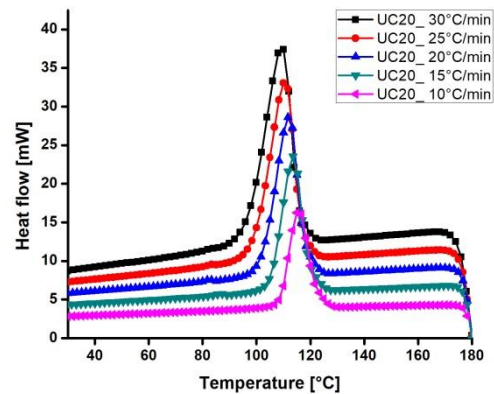
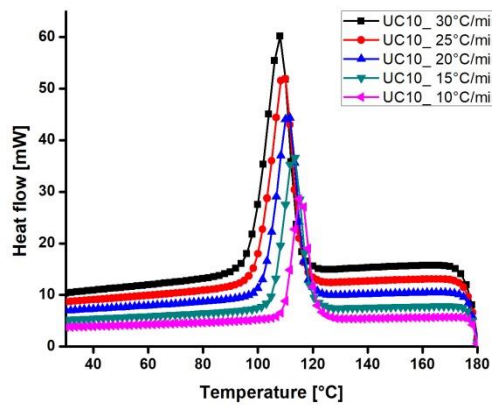


Fig.6.18 % crystallinity versus cooling rate of PP/EPDM7.5/Coir composites

It is clearly seen from the plot that, FAS coated coir filled composites shows comparatively good % crystallinity values with reference to uncoated coir filled composites. This is due to the reason that, the extremely hydrophobic coating using fluoroalkyl functional siloxane given to coir fiber surface helps in imparting crystallinity to it comparing with elementary coir fibers. However upon increasing the volume fraction of coir fibers the crystallinity value found to be decreasing. The results follow statement “in the case of semi crystalline polymers, the crystallinity value decreases upon addition of compounding ingredients.” % crystallinity values show a decreasing trend upon increase in cooling rate of crystallisation. This is due to the fact that, at higher cooling rates, crystallisation time is not sufficient for the composites to complete crystallisation process which is further explained in relative crystallinity versus temperature/time plots. As the crystallinity decreases the strength properties may decrease unless the interphase adhesion compensates for the loss of crystallinity. The coir fibers are composed of cellulose, hemicellulose and lignin. The cellulose is known to be a crystalline material whereas hemicellulose and lignin are amorphous. In PP/EPDM/COIR system, the crystallinity shows a decreasing trend as we increase the parts of coir from 10pph to 30pph of coir fibers and shows a slight increase at 40pph of coir fibers. The DSC exotherms of PP/EPDM7.5/Coir composites at five different cooling rates (10, 15, 20, 25, 30⁰C min⁻¹) are presented in figure Fig.6.19. & Fig.6.20.



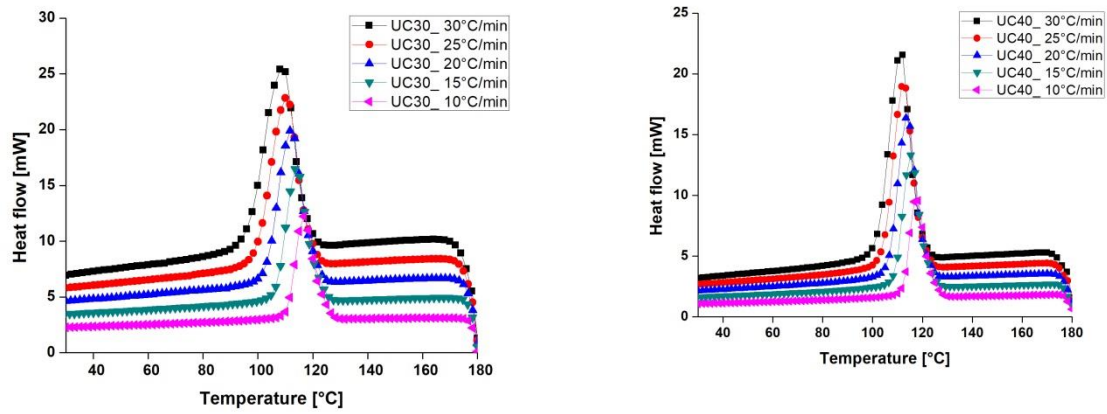


Fig6.19 Non-isothermal crystallization curves of PP/EPDM/Uncoated coir composites at different cooling rates (10, 15, 20, 25, 30⁰C min⁻¹)

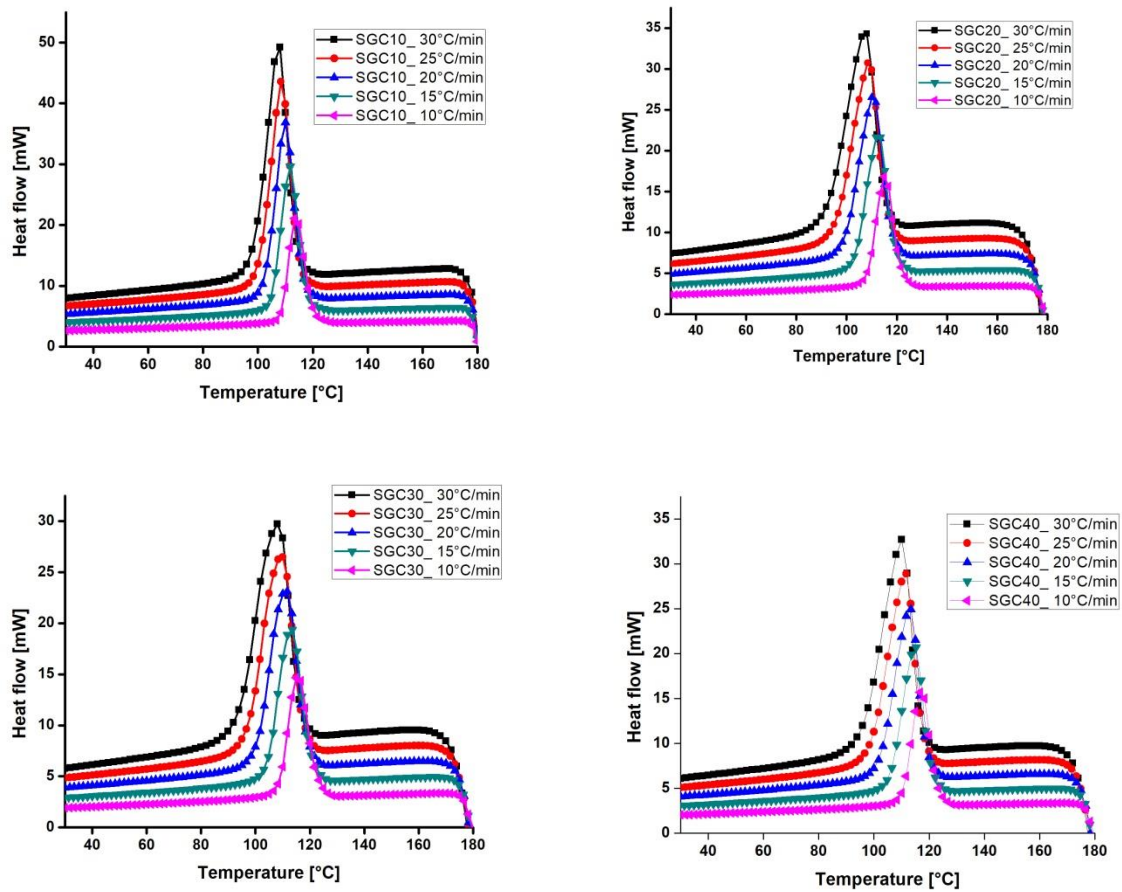


Fig6.20 Non-isothermal crystallization curves of PP/EPDM/FAS coated coir composites at different cooling rates (10, 15, 20, 25, 30⁰C min⁻¹)

From the above DSC crystallisation exotherms, the values of relative crystallinity, X_t were calculated using equation 5.1 given in chapter 5. Fig.6.20 & Fig.6.21 illustrates that both uncoated as well as FAS coated coir filled PP/EPDM composites showed single and sharp exotherms in the temperature range from 90°C to 125°C which vary with cooling rates. The exotherms of the composites widened and shifted to lower temperature for different cooling rates. The variations of relative crystallinity, X_t versus temperature of uncoated and FAS coated coir filled PP/EPDM composites at different cooling rates are shown in figure Fig.6.21 and Fig.6.22.

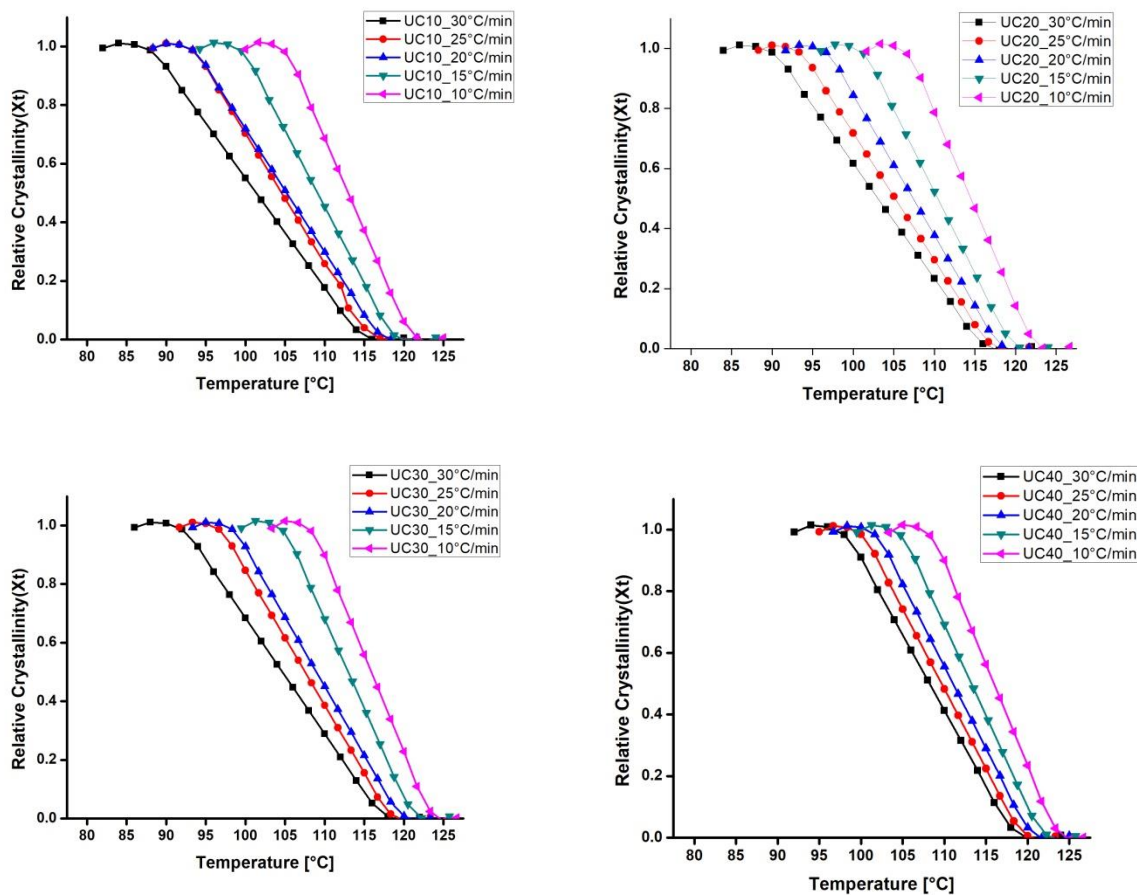


Fig.6.21 Relative crystallinity (X_t) versus Temperature of PP/EPDM/Uncoated Coir composites at different cooling rates (10, 15, 20, 25, 30°C min⁻¹)

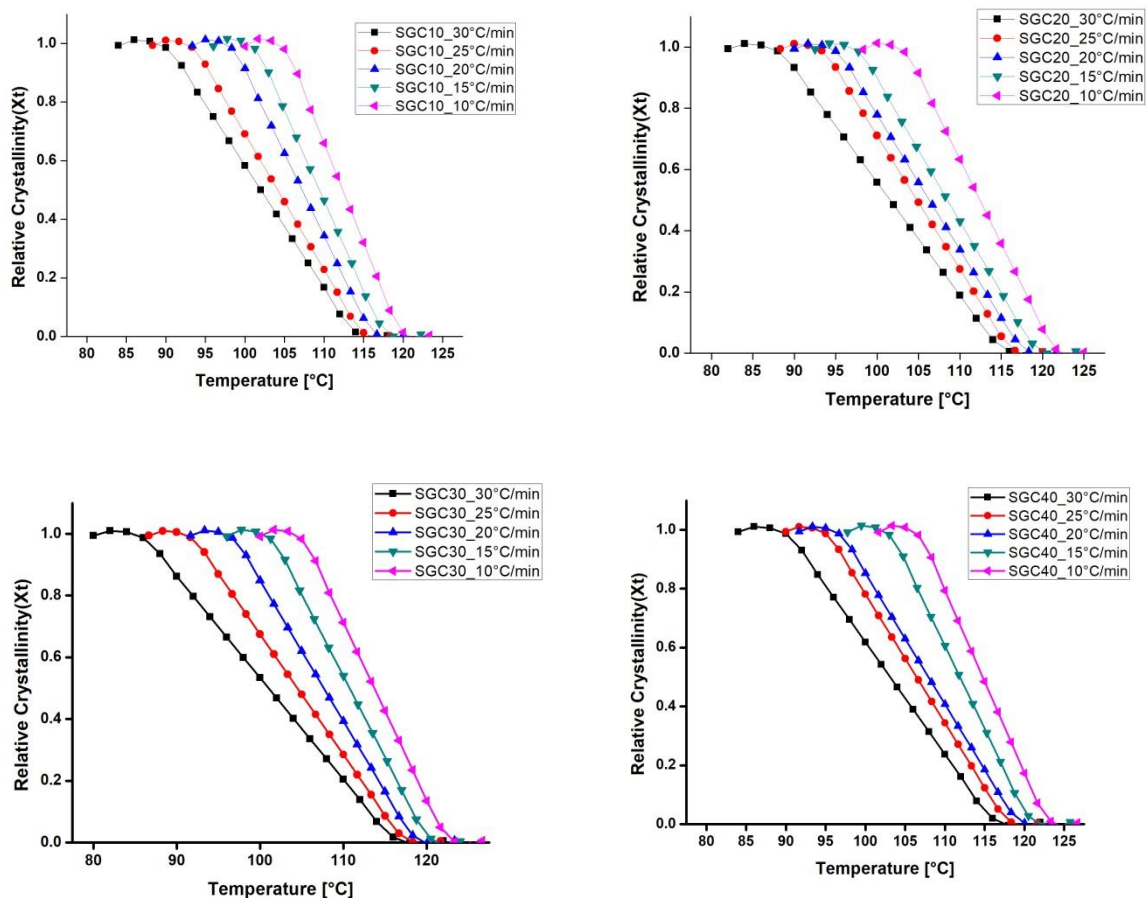


Fig.6.22 Relative crystallinity (X_t) versus Temperature of PP/EPDM/FAS coated Coir composites at different cooling rates (10, 15, 20, 25, 30⁰C min⁻¹)

From the plots Fig.6.22 and Fig.6.23 it can be inferred that the curves exhibits a reverse sigmoidal shape which indicates a lag effect of cooling rate on crystallization in uncoated as well as coated coir based PP/EPDM composites [6].

The temperature axis in Fig.6.21 and Fig.6.22 can be converted into time scale using equation 5.2 (please refer Chapter 5) and is re-plotted in figure Fig.6.23 and Fig.6.24.

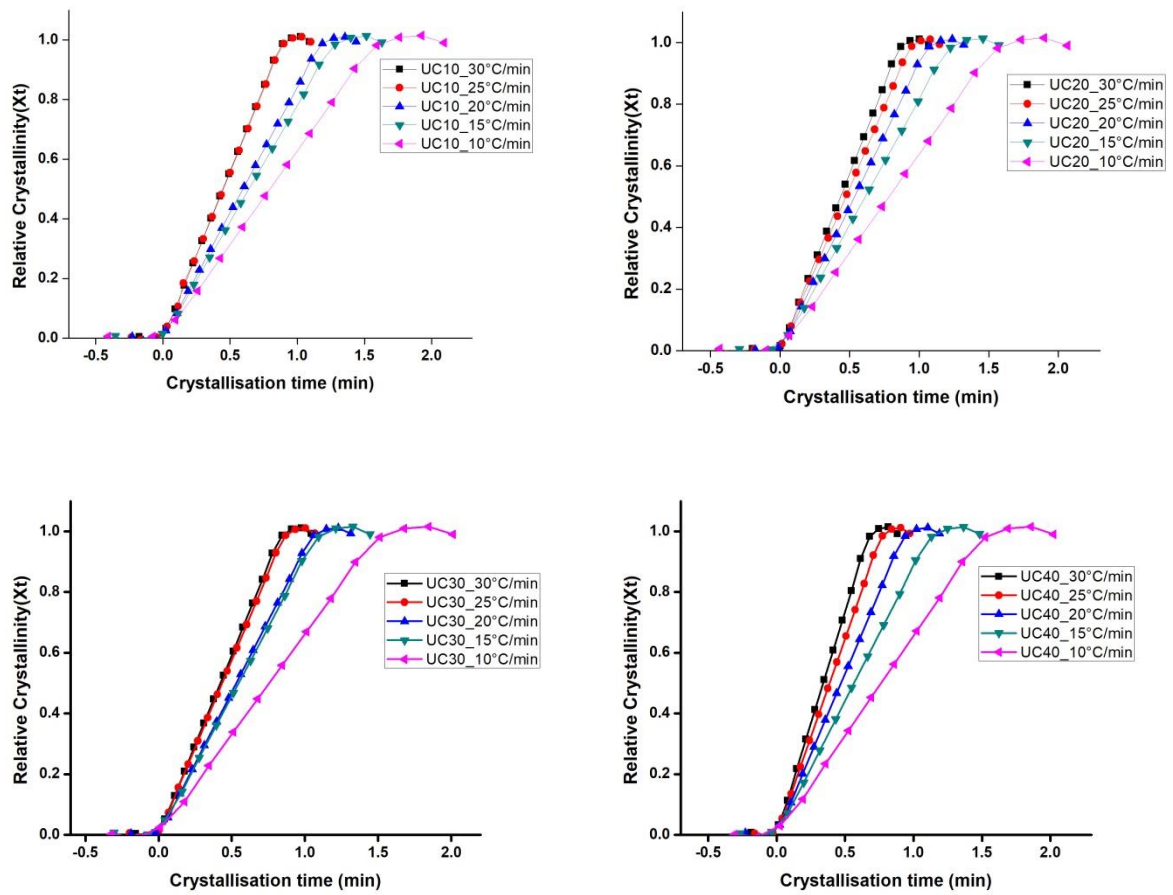
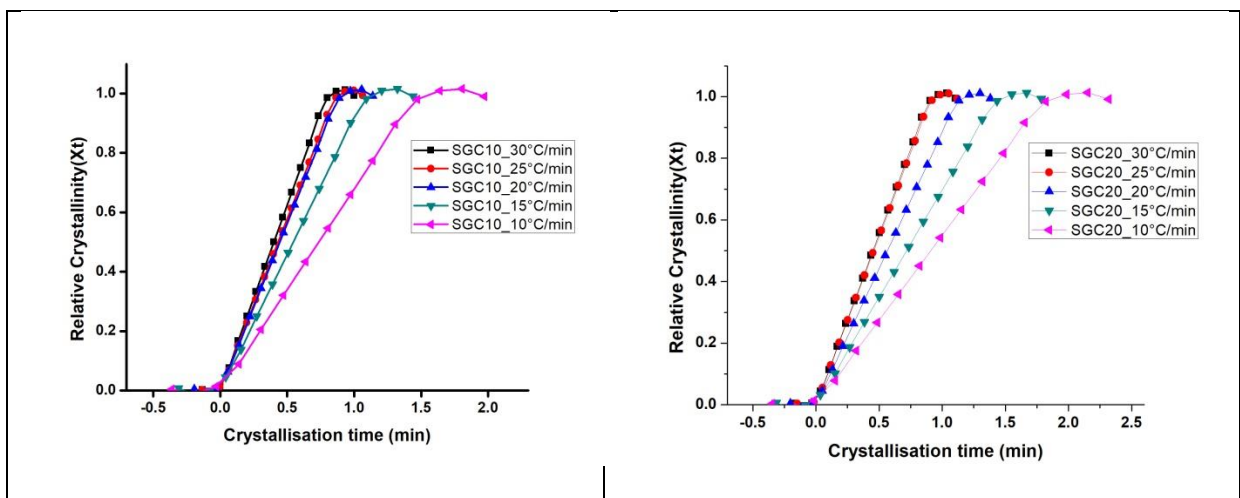


Fig.6.23 Relative crystallinity (Xt) versus Time of PP/EPDM/Uncoated Coir composites at different cooling rates (10, 15, 20, 25, 30°C min⁻¹)



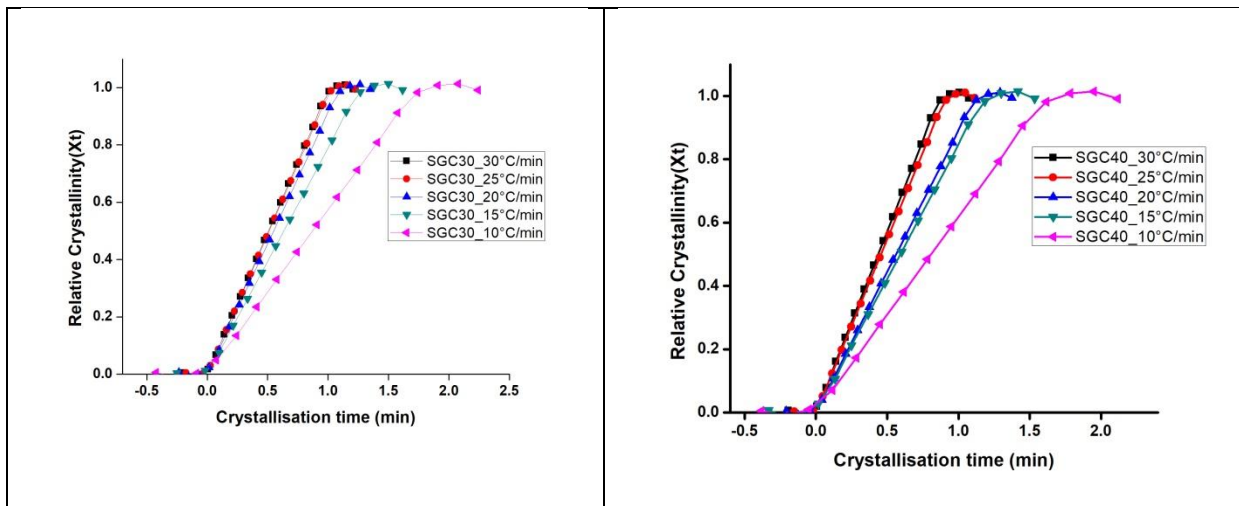


Fig.6.24 Relative crystallinity (X_t) versus Time of PP/EPDM/ FAS coated Coir composites at different cooling rates ($10, 15, 20, 25, 30^{\circ}\text{C min}^{-1}$)

It can be seen from the plots that, all curves are S shaped and at higher cooling rates, shorter time is required to complete crystallisation process. Crystallisation half time, $t_{1/2}$, the time at which crystallinity reaches 50 % can be calculated directly from Fig.6.24 and Fig.6.25. It can be inferred from the Table 6.7, Fig.6.23 and Fig.6.24 that the values of T_0 , T_c and $t_{1/2}$ decreases whereas ΔT_c increases as we move from lower to higher cooling rates. It can be due to the fact that, at higher cooling rates, polymer chains do not get sufficient time to crystallise, which in turn results in initiation of crystallisation at higher under cooling (high value of ΔT_c). Also at higher cooling rates, the polymer chain mobility is destroyed and resulting in incomplete crystallisation process. However, compare with PP/EPDM blends, the PP/EPDM coir composites shows lesser under cooling (low value of ΔT_c) values. FAS coated coir filled composites possess higher enthalpy of fusion (ΔH_c) values compares with uncoated coir filled composites which in turn indicates the higher thermal stability of FAS coated coir filled composites. For a particular cooling rate, the data of T_0 , T_c and $t_{1/2}$ have higher values while ΔT_c is lower for uncoated coir filled composites comparing with pure polypropylene as well as PP/EPDM7.5 blend. The FAS coated composites gives higher values of T_0 , T_c and $t_{1/2}$ and lower values of ΔT_c compare with uncoated coir filled composites as well as PP/EPDM blends. It shows that comparatively higher time is available for the polymer chains to crystallise at higher rates of cooling in the case of FAS coated coir filled composites than uncoated ones and PP/EPDM blends. It can be due to the surface provided by the FAS coated coir for the crystallisation of polypropylene. However the phase interaction and geometrical constraints of coir fiber hinder the crystallisation process and as a result the net effect will be the decrease of crystallinity of polypropylene in the composites [7,8,9].

6.7.1 Nucleation Activity

The nucleation activity of uncoated as well as FAS coated coir in PP/EPDM7.5/Coir composites was determined by Dobrev and Gutzowa method. The value of B or B* was obtained from the slope of Log (R) vs. $1/\Delta T_c^2$ shown in figure Fig.6.26 and are listed in Table 6.5.

Table 6.5 Nucleation activity values by Dobrev and Gutzowa method for PP/EPDM/Coir composites

Sample ID	Slope (B or B*)	Slope (B or B*)	Nucleation activity
EPDM7.5	B	3.48	1
UC10	B*	3.92	1.13
UC20	B*	5.69	1.63
UC30	B*	3.55	1.02
UC40	B*	6.52	1.87
SGC10	B*	5.18	1.49
SGC20	B*	3.55	1.02
SGC30	B*	4.32	1.24
SGC40	B*	4.15	1.19

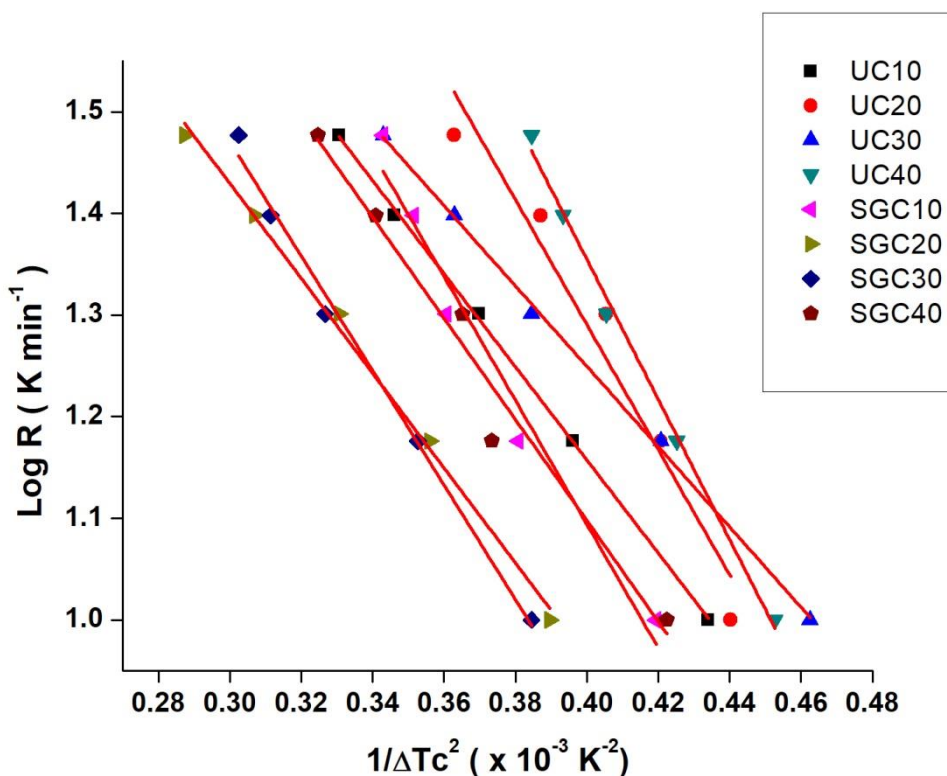


Fig.6.26 Nucleation activity by Dobрева and Gutzowa approach for various PP/EPDM/Coir compositions

The value of nucleation activity is 1 for PP/EPDM7.5 and above 1 for all PP/EPDM/Coir compositions which indicates that uncoated/FAS coated coir is not acting as a nucleating agent at these compositions.

6.7.2 Glass transition temperature

The glass transition temperature obtained using DSC analysis for PP/EPDM/Coir composites are shown in Table 6.6.

Table 6.6 Glass transition temperature values of PP/EPDM/Coir composites

Sample ID	Glass transition temperature (°C)	
PP	-9.77	
EPDM 7.5	-10.10	-53.39
UC10	-10.13	-49.08

UC20	-10.09	-46.06
UC30	-9.81	-42.10
UC40	-9.84	-44.45
SGC10	-9.80	-39.76
SGC20	-9.79	-44.42
SGC30	-9.78	-46.41
SGC40	-10.14	-41.43

Two inflection points observed corresponds to two glass transition temperatures exist in the system. Compare with PP/EPDM blends, no significant change in glass transition temperature of PP/EPDM/Coir composite was observed. However in the case of composites, the difference of two glass transition temperatures decreases which in turn can be an indication of reducing the immiscible nature of PP/EPDM /Coir system.

6.8 Thermo gravimetric (TGA) analysis

Table 6.7 shows the values of thermo gravimetric analysis (maximum degradation temperature, T_{max} and % weight loss of sample) of PP/EPDM/Coir composites

Table 6.7 Thermo gravimetric analysis (T_{onset} , T_{max} and T_f) of PP/EPDM/Coir composites

Sample ID	T_{max1} ($^{\circ}$C)	Weight (loss %) at 700$^{\circ}$C	T_{max2} ($^{\circ}$C)	Weight (loss %) at 700$^{\circ}$C
PP	-	-	463.29	99.88
EPDM7.5	-	-	464.08	99.87
UC10	349.73	6.88	468.23	90.55
UC20	359.51	12.14	468.46	83.49
UC30	353.60	16.98	469.03	76.47
UC40	349.27	19.15	468.92	73.66
SGC10	354.96	5.89	467.21	92.03
SGC20	331.91	9.24	467.28	79.71
SGC30	335.43	10.94	467.92	73.96
SGC40	350.01	12.93	467.67	69.97

Unlike PP/EPDM blends, all the composites exhibit two step degradation. The maximum degradation temperature tabulated between 330-360⁰C shows the maximum degradation temperature of coir fibers whereas the maximum degradation temperature tabulated between 463-468⁰C shows the degradation temperature of PP/EPDM blends. By varying 20pph to 40pph of coir fiber content in PP/EPDM blends, the uncoated composites shows a decreasing trend in maximum degradation temperature value whereas the FAS coated composites showed an increasing trend of maximum degradation temperature value. It can be inferred from the results that, as the coir filler content are increased, the FAS coated coir filled PP/EPDM composites showed an increasing trend in thermal stability than uncoated ones. At 40pph of FAS coated coir filled composites, the lowest loss % of sample weight was observed. Comparing with PP/EPDM blends, all the composites show a slight increase in maximum thermal degradation temperature value. The sample weight loss % is also found to be decreased in the case of composites.

6.9 Conclusions

Based on optimizations of fiber characteristics and blend formulations, PP/EPDM7.5 as the matrix and the coir fiber content was varied from 10pph to 40pph to fabricate the PP/EPDM/Coir composites. It can be inferred from the results that the FAS coated fiber reinforced composites shows significant improvement in impact strength and impact energy values compare with uncoated fiber reinforced composites. The influence of constituent properties on impact response of composites was studied. The extremely high hydrophobic nature of FAS coated coir fibers were linked to the impact, tensile and flexural behaviour of composites. It can be inferred from the SEM images that post-debond fiber sliding is the primary energy absorbing mechanism in FAS coated fiber filled composites whereas fiber pull-out is responsible for contributing toughness in fiber filled composites.

Low shear rate rheology points to the shear thinning behaviour of PP/EPDM/Coir composites. The complex viscosity found to be decreases with increase in frequency which shows the melt is in pseudo plastic state. The storage modulus (G') and loss modulus (G'') of composites shows an increasing trend with oscillatory frequency analysis. Non-isothermal crystallisation kinetics studied using DSC analysis shows a lag effect of cooling rate on crystallization in PP/EPDM/Coir composites. No specific nucleation activity of uncoated/FAS coated coir was observed in PP/EPDM based composites. The high value of maximum degradation temperature and low sample weight loss % obtained using TGA

analysis indicates the stability of composites to withstand high operating temperatures for long periods.

6.10 REFERENCES

1. Brahmakumar, M., Pavithran, C., & Pillai, R. M. (2005). Coconut fiber reinforced polyethylene composites: effect of natural waxy surface layer of the fiber on fiber/matrix interfacial bonding and strength of composites. *Composites Science and technology*, 65(3-4), 563-569.
2. Hancox, N. L. (1971). Izod impact testing of carbon-fiber-reinforced plastics. *Composites*, 2(1), 41-45.
3. Chamis, C. C., & Sinclair, J. H. (1985). Impact resistance of fiber composites: energy-absorbing mechanisms and environmental effects. In *Recent Advances in Composites in the United States and Japan*. ASTM International.
4. Kozawa, E., Nakajima, Y., & Kim, J. K. (2015, May). Silane cross-linkable ethylene-propylene elastomer compositions prepared by reactive processing. In *AIP Conference Proceedings* (Vol. 1664, No. 1, p. 090003). AIP Publishing.
5. Beaumont, P. W. (1979). Fracture mechanisms in fibrous composites. In *Fracture Mechanics* (pp. 211-233).
6. Sharma, R., & Maiti, S. N. (2015). Effects of crystallinity of polypropylene (PP) on the mechanical properties of PP/styrene-ethylene-butylene-styrene-g-maleic anhydride (SEBS-g-MA)/teak wood flour (TWF) composites. *Polymer Bulletin*, 72(3), 627-643.
7. Sharma, R., & Maiti, S. N. (2015). Effects of SEBS-g-MA copolymer on non-isothermal crystallization kinetics of polypropylene. *Journal of materials science*, 50(1), 447-456.
8. Wang, B., Hu, G., & Wei, L. (2008). Melting behavior, nonisothermal crystallization kinetics, and morphology of PP/nylon 11/EPDM-g-MAH blends. *Journal of applied polymer science*, 107(5), 3013-3022.

CHAPTER 7
CONCLUSIONS AND FUTURE WORK

7.1 Conclusions

In this thesis coir based PP/EPDM composites with improved impact resistant properties were developed for various applications. This thesis is summarised with a set of outcomes. The first outcome is the development of the low pressure oxygen plasma surface modification as an effective treatment method to functionalise the lignocellulosic natural coir fibers with hydroxyl groups which in turn convert it into extremely hydrophilic surface. The water absorption studies showed an increase in water absorption from 39% to about 100%. The morphological study using SEM analysis also confirmed changes in the surface topography after plasma treatment. The topographic measurements done using atomic force microscopy showed etching of fiber wall which influences the higher water absorption. XPS analysis reveals that oxygen content measured for samples treated at 50 Pa increased from initial 18 at% to about 32 at%. This study finds that, by controlling the plasma parameters and by understanding the plasma chemistry, the plasma treatment can be developed as a viable technique for surface modification of natural fibers.

The second outcome is the development of hydrophobic coating on the plasma treated coir fiber surface. In this work, the surface modification of lignocellulosic coir fibers was done with the use of low-pressure oxygen plasma, followed by the application of a spray-dry-cure sol-gel coating with the water and oil repellent organic-inorganic hybrid precursor fluoroalkyl-functional siloxane (FAS), with the aim of creating the hydrophobic coir fiber surface. The plasma pre-treatment increased the effective concentration of the FAS network on the lignocellulosic coir fibers. The noticeable increase in water contact angle and decrease in surface free energy value as well as thermodynamic work of adhesion confirms the transformation to hydrophobic behaviour of coated fibers. With the aid of atomic force microscopy and scanning electron microscopy, it was found that the plasma pre-treatment helps in imparting the nanoscopic topography which leads to the formation of a dual micro to nano-structured composite fiber surface with a high content of air pockets, which significantly decreased the interfacial area between the water and the fibers after the sol-gel coating was applied and imparted the extremely high “hydrophobic effect” to the sample. A slight increase in surface roughness value is also validates this finding. The spectroscopic analysis using XPS shows that the characteristic bands F 1s and Si 2p, were detected on the FAS coated coir samples, accompanied by a significant decrease in the carbon and oxygen concentrations, which confirmed that the FAS coating was covered the lignocellulosic coir

fiber surface. The water absorption studies indicates that , in the case of FAS coated coir fibers , the time for fibers spent in water is infinite and because there is no water uptake. The tensile tests performed on elementary as well as FAS coated coir fibers shows that the average breaking force, breaking strength, modulus and elongation at break of FAS coated coir fibers was found to be higher than uncoated coir fibers.

The third outcome is the development of optimized PP/EPDM blend formulation for the fabrication of coir based PP/EPDM composites. Firstly the blends of polypropylene (PP) with various concentrations of ethylene-propylene-diene rubber (EPDM) were prepared. The EPDM was blended with polypropylene with the aim of developing an impact resistant polymer system. Among pure polypropylene as well as PP/EPDM blend formulations, 7.5 parts of EPDM in PP (PP/EPDM7.5) registers highest impact strength value and also comparable tensile and flexural properties with other blend formulations. It was found that one possible reason for increase in impact strength could be the decrease in average diameter of dispersed particles at lower EPDM content leading to better dispersion EPDM in PP matrix. The decrease in impact strength after 7.5pph may be due to the formation of narrower ligaments than critical ligament thickness (interparticle distance). The large area under the stress strain curves of PP/EPDM blends at EPDM content swathe less than or equal to 7.5 pph shows the strain energy capacity of the material. Scanning electron microscopy observations shows that the mechanically induced cavitation behaviour is responsible for the impact resistance of PP/EPDM blends. Low shear rate rheology points to the shear thinning behaviour of PP/EPDM blends. The complex viscosity found to be decreases with increase in frequency which shows the melt is in pseudo plastic state. The storage modulus (G') and loss modulus (G'') of blends shows an increasing trend with oscillatory frequency analysis .Non-isothermal crystallisation kinetics of PP/EPDM blends were studied using differential scanning calorimetry (DSC) analysis. The curve obtained by plotting relative crystallinity (X_t) vs. temperature (T) exhibits a reverse sigmoidal shape which indicates a lag effect of cooling rate on crystallization in PP and PP/EPDM blends. No specific nucleation activity of EPDM was observed in PP/EPDM blends. The high value of maximum degradation temperature obtained using TGA analysis outlines the stability of PP/EPDM blends to withstand high operating temperatures.

The fourth outcome is the development of coir based PP/EPDM composites with varying concentrations of coir fibers (10 to 40pph) for improved impact resistance properties. 100pph

of polypropylene and 7.5pph of EPDM was selected for the composite preparation because it registered highest impact strength and also gives highest pull-out stress value with coir fibers. From the critical fiber length measurements, it is found that, the minimum length (critical length) required holding the coir fiber in PP/EPDM 7.5 matrix will be equal to .25mm. The results shows that the FAS coated fiber reinforced composites shows significant improvement in impact strength and impact energy values compare with uncoated fiber reinforced composites. During internal melt mixing of polypropylene, EPDM and FAS coated coir fibers in Brabender, the fluoro alkyl functional siloxane (FAS) coated coir fibers are melt grafted specifically on EPDM sites. This could be due to the unsaturation in diene monomer exists in EPDM, which creates some additional reactive sites for silane grafting to occur (The grafting can also occur by abstraction of secondary hydrogen from a polypropylene sequence of EPDM). The influence of fiber properties on impact response of composites was studied. It was found that the failure strength of FAS coated coir fibers higher than the uncoated coir fibers which points to the improvement of impact response of composites with FAS coated fibers. Strain energy absorbing capacity of FAS coated coir fibers found to be 75% higher than the uncoated coir fibers which again points to the reason for significant improvement in impact response of FAS coated coir fiber reinforced composites. It can also be inferred from the SEM images that fiber pull-out, fiber fracture and fiber matrix debonding are the primary energy absorbing mechanism in FAS coated fiber filled composites. The rheological properties of the composites were obtained using parallel plate rheometry. Low shear rate rheology points to the shear thinning behaviour of PP/EPDM/Coir composites. The complex viscosity found to be decreases with increase in frequency which shows the melt is in pseudo plastic state. The storage modulus (G') and loss modulus (G'') of blends shows an increasing trend with oscillatory frequency analysis .Non-isothermal crystallisation kinetics of PP/EPDM/Coir composites were studied using differential scanning calorimetry (DSC) analysis. The curve obtained by plotting relative crystallinity (X_t) vs. temperature (T) exhibits a reverse sigmoidal shape which indicates a lag effect of cooling rate on crystallization in composites. No specific nucleation activity of EPDM was observed in PP/EPDM blends. The high value of maximum degradation temperature and low sample weight loss % obtained using TGA analysis indicates the stability of composites to withstand high operating temperatures for long periods.

The resulting composites possess high impact strength properties and comparable tensile and flexural properties. The extremely high hydrophobic behaviour of coir fibers obtained using

low-pressure oxygen plasma, followed by the application of a fluoroalkyl-functional siloxane (FAS) based spray-dry-cure sol–gel coating, is a contribution of this thesis to the engineering sciences to overcome the moisture intake of natural fibers, which is known to be an unsolved problem exist in the scientific literatures. Another scientifically relevant information is the advent of new technique involving the melt grafting of FAS coated coir fibers on to EPDM chain in the internal mixer, which is more attractive due to various industrial advantages.

7.2 Future work

The results obtained in this study are helpful in formulating the objectives for future research work. Following objectives are proposed

1. By utilizing the combination effect of low-pressure plasma and spray-dry-cure sol–gel coating, different organofunctional siloxanes based hybrid precursors can be coated on the natural coir fibers to tailor it for specific applications.
2. Extraction of nano lignin and nano cellulose from the lignocellulosic natural coir fibers and tuning of its surface morphology using low-pressure plasma and spray-dry-cure sol–gel coating.
3. Improving the impact properties of polypropylene using other type of elastomers.
4. Investigation of the fracture behaviour prepared composites using experimental and modelling techniques.
5. The technique mentioned in Objective 1 can be further extended to study its effect of other natural fibers (such as Flax fiber, Pineapple leave fiber (PALF), Jute fiber, Banana fiber etc.) and its polymer based composites.
6. Objective 2 can be further extended to study in other natural fibers (such as Flax fiber, Pineapple leave fiber (PALF), Jute fiber, Banana fiber etc.) and its polymer based composites.
7. Investigation of objectives 1, 2, 3 and 4 in biopolymer (such as PLA, PHA etc) systems.

LIST OF FIGURES

Figure No.	Illustration	Page No.
Fig.1.1	Schematic illustration of contact angle measurement	6
Fig.1.2	Schematic of the surface modification of plastic in a gas plasma reactor	10
Fig.1.3	Surface modification process of plasma treated glass fibers	14
Fig.1.4	Organofunctional siloxanes as molecular bridges	17
Fig.1.5	Chemical structure of fluoroalkyl functional siloxane	18
Fig.1.6	Cross sectional view of coir fiber	19
Fig.2.1	Schematic illustration of oxygen plasma treatment of coir fiber surface	31
Fig.2.2	Large Plasma chamber used for treatment of coconut fibers	32
Fig.2.3	Small Plasma chamber used for treatment of coconut fibers	33
Fig.2.4	Scheme of the spray-dry-cure sol–gel -coating process	36
Fig. 2.5	Numerically controlled cutting machine “Fraiseuse”	41
Fig.2.6	Schematic of the pull-out specimen	42
Fig.3.1	Schematic representation of Oxygen plasma treatment of coir fibers	49
Fig.3.2	An optical spectrum acquired in the small discharge system at the absence of coir	50
Fig.3.3	An optical spectrum acquired in the small system loaded with coir after 14 s of plasma treatment	51
Fig.3.4	Time evolution of the O-atom lines at 777 and 845 nm and selected lines of CO Angstrom band	52
Fig.3.5	SEM analysis of untreated-pristine coconut fibers (a, b), 10 s plasma treated at 50 Pa (c, d) and 10s plasma treated at 75 Pa (e, f) coconut fibers.	55
Fig.3.6	SEM analysis of untreated-pristine coconut fibers (a,b), 30 s plasma treated (c,d) and 60s plasma treated (e,f) coconut fibers	57
Fig. 3.7	AFM height and phase images done on 5x5 and 2x2 μ m area of untreated and 30 s treated coconut fibers	58
Fig. 3.8a	XPS Spectrum for Untreated coir fiber when small chamber is	60

	used for plasma generation	
Fig. 3.8b	XPS Spectrum coir fiber after 10s of plasma treatment at 50 Pa	60
Fig. 3.8c	XPS Spectrum coir fiber after 10s of plasma treatment at 75 Pa	61
Fig.4.1	Water absorption test for uncoated and FAS coated coir fibers	74
Fig.4.2	Scanning Electron Microscope (SEM) images of untreated and FAS coated coir fibers	76
Fig.4.3	AFM topography of uncoated and FAS coated coir fiber surfaces	77
Fig.4.4	Micro to nano-structured composite fiber surface with a high content of air pockets	78
Fig.4.5	Examples of surface survey spectra for untreated fibers (top), only plasma treated fibers (middle), and plasma treated and sol-gel coated fibers (bottom)	80
Fig.4.6	Examples of the deconvolution spectra of high-resolution XPS spectra of untreated fibers (top), only plasma treated fibers (middle), and plasma treated and sol-gel coated fibers (bottom).	82
Fig.4.7	Coir fibers images of diameter measurement using optical microscope	84
Fig.4.8.	Coir fibers loaded in MTS machine for tensile testing	85
Fig.4.9	Stress versus strain curve for uncoated & FAS coated fibers	86
Fig.5.1	Impact strength of pure PP and PP/EPDM blend	92
Fig.5.2	Impact energy of pure PP and PP/EPDM blend	92
Fig.5.3 a	Tensile strength of pure PP and PP/EPDM blends	93
Fig.5.3 b	Modulus of pure PP and PP/EPDM blends	94
Fig.5.3 c	% deformation of pure PP and PP/EPDM blends	94
Fig.5.4	% stress strain diagram of pure polypropylene and PP/EPDM blends	94
Fig.5.4 a	Flexural strength of pure PP and PP/EPDM blends	96
Fig.5.4 b	Flexural Modulus of pure PP and PP/EPDM blends	96
Fig.5.4 c	% deformation of pure PP and PP/EPDM blends under flexural loading	96
Fig.5.5	TEM micrographs of PP/EPDM blends	97
Fig.5.6	SEM micrographs of impact fractured PP/EPDM blends	99

Fig.5.7	Viscosity versus shear rate of PP/EPDM blends	100
Fig.5.8	Frequency dependence of complex viscosity in PP / EPDM blends	101
Fig.5.9	Frequency dependence of storage modulus in PP / EPDM blends	102
Fig.5.10	Frequency dependence of loss modulus in PP / EPDM blends	102
Fig.5.11	% crystallinity versus cooling rate	105
Fig.5.12	Non-isothermal crystallization curves of PP/EPDM blends at different cooling rates and various parts of EPDM: (a) 0 pph, (b) 2.5 pph, (c) 5pph, (d) 7.5pph, (e) 10 pph, (f) 20 pph and (g) 30 pph,.	106
Fig.5.13	Relative crystallinity (X _t) versus Temperature of PP/EPDM blends at different cooling rates and various parts of EPDM: (a) 0 pph, (b) 2.5 pph, (c) 5pph, (d) 7.5pph, (e) 10 pph, (f) 20 pph and (g) 30 pph	108
Fig.5.14	Relative crystallinity (X _t) versus Time of PP/EPDM blends at different cooling rates and various parts of EPDM: (a) 0 pph, (b) 2.5 pph, (c) 5pph, (d) 7.5pph, (e) 10 pph, (f) 20 pph and (g) 30 pph	110
Fig.5.15	Nucleation activity by Dobрева and Gutzowa approach for various PP/EPDM blend compositions	111
Fig.6.1	Impact strength of PP/EPDM/Coir composites	120
Fig.6.2	Impact energy of PP/EPDM/Coir composites	120
Fig.6.3	Tensile strength of PP/EPDM/Coir composites	121
Fig.6.4	Modulus of of PP/EPDM/Coir composites	121
Fig.6.5	% deformation of PP/EPDM/Coir composites	121
Fig.6.6	Flexural strength of PP/EPDM/Coir composites	123
Fig.6.7	Flexural modulus of PP/EPDM/Coir composites	123
Fig.6.8	Flexural deformation of PP/EPDM/Coir composites	123
Fig.6.9	Pullout Experiment	124
Fig.6.10 a	Pull-out stress of uncoated fibers with PP/EPDM blends	125
Fig.6.10 b	Pull-out stress of FAS coated fibers with PP/EPDM blends	125
Fig.6.11	Morphology of impact fractured pure PP and PP/EPDM7.5 blend	127
Fig.6.12	Morphology of impact fractured PP/EPDM7.5/Uncoated coir composites	128
Fig.6.13	Morphology of impact fractured PP/EPDM7.5/FAS coated coir composites	128

Fig.6.14	Viscosity versus shear rate of PP/EPDM/Coir composites	129
Fig.6.15	Frequency dependence of complex viscosity in PP/EPDM/Coir composites	130
Fig.6.16	Frequency dependence of storage modulus in PP/EPDM/Coir composites	131
Fig.6.17	Frequency dependence of loss modulus in PP/EPDM/Coir composites	131
Fig.6.18	% crystallinity versus cooling rate of PP/EPDM7.5/Coir composites	133
Fig.6.19	Non-isothermal crystallization curves of PP/EPDM/Uncoated coir composites at different cooling rates (10, 15, 20, 25, 30 ⁰ C min ⁻¹)	135
Fig.6.20	Non-isothermal crystallization curves of PP/EPDM/FAS coated coir composites at different cooling rates (10, 15, 20, 25, 30 ⁰ C min ⁻¹)	135
Fig.6.21	Relative crystallinity (X _t) versus Temperature of PP/EPDM/Uncoated Coir composites at different cooling rates (10, 15, 20, 25, 30 ⁰ C min ⁻¹)	136
Fig.6.22	Relative crystallinity (X _t) versus Temperature of PP/EPDM/FAS coated Coir composites at different cooling rates (10, 15, 20, 25, 30 ⁰ C min ⁻¹)	137
Fig.6.23	Relative crystallinity (X _t) versus Time of PP/EPDM/Uncoated Coir composites at different cooling rates (10, 15, 20, 25, 30 ⁰ C min ⁻¹)	138
Fig.6.24	Relative crystallinity (X _t) versus Time of PP/EPDM/ FAS coated Coir composites at different cooling rates (10, 15, 20, 25, 30 ⁰ C min ⁻¹)	139

LIST OF TABLES

Table No.	Illustration	Page No.
Table 1.1	Physical properties and chemical composition of coir fiber	18
Table 2.1	Properties of Polypropylene	29
Table 2.2	Properties of Keltan 9565Q DE	30
Table 2.3	Properties of Coir fibers	30
Table 2.4	PP/EPDM blend formulations	40
Table 2.5	PP/EPDM/Coir composite formulations	40
Table 3.1	Average water absorbency time and water absorptive capacity of coir fibers according to plasma treatment	52
Table 4.1	Average values (n=30) of the contact angle of the different conditions of coir fibers (untreated, and FAS coated)	70
Table 4.2	Surface energy components (mJ/m^2) γ_s , γ_s^d and γ_s^p of untreated as well as sol-gel coated coir fibers were calculated by using Owens-Wendt formula (based on geometric mean approach)-All dimensions are in “mN/m”	71
Table 4.3	Surface energy components (mJ/m^2) of untreated as well as sol-gel coated coir fibers were calculated by the acid–base method using three probe liquids [water (polar), ethylene glycol (polar) and tricresylphosphate (TCP-nonpolar)] -All dimensions are in “mN/m”	72
Table 4.4	Average water absorbency time and water absorptive capacity of uncoated and FAS coated coir fibers	73
Table 4.5	Sample's surface composition in at. % (average of two measurements)	79
Table 4.6	Tensile measurements of uncoated and coated fibers	85
Table 5.1	Average diameter of EPDM spherical particles measures using Image J	98
Table 5.2	Non isothermal crystallisation exotherms of PP and PP/EPDM blends	103
Table 5.3	% crystallinity of PP and PP/EPDM blends	104
Table 5.4	Nucleation activity values by Dobrevá and Gutzowa method for PP/EPDM blends	111
Table 5.5	Glass transition temperature values of PP/EPDM blends	112

Table 5.6	Thermo gravimetric analysis (T_{onset} , T_{max} and T_f) of PP/EPDM blends	113
Table 6.1	PP/EPDM/Uncoated coir composite formulations	119
Table 6.2	PP/EPDM/FAS coated coir composite formulations	119
Table 6.3	Non isothermal crystallisation exotherms of PP/EPDM7.5/Coir composites	132
Table 6.4	% crystallinity of PP/EPDM7.5/Coir composites blends	133
Table 6.5	Nucleation activity values by Dobrev and Gutzowa method for PP/EPDM/Coir composites	140
Table 6.6	Glass transition temperature values of PP/EPDM/Coir composites	141
Table 6.7	Thermo gravimetric analysis (T_{onset} , T_{max} and T_f) of Composites	142

PUBLICATIONS

International / National Journal publications

- Praveen, K. M., Sabu Thomas, Yves Grohens, Miran Mozetič, Ita Junkar, Gregor Primc, and Marija Gorjanc. "Investigations of plasma induced effects on the surface properties of lignocellulosic natural coir fibers." *Applied Surface Science* 368 (2016): 146-156.
- Praveen K.M , Gregor Primc, Barbara Simončič, Marija Gorjanc, Isabelle Pillin, Bastien Seantier, Alenka Vesel, Miran Mozetič, Yves Grohens, Sabu Thomas, Nandakumar Kalarikkal "Investigations of fluoroalkyl functional siloxane (FAS) based hydrophobic coating induced effects on surface and mechanical properties of lignocellulosic natural coir fibres" (Communicated)
- Praveen K.M , Khadidja Taleb, Isabelle Pillin, Antoine Kervoelen ,Yves Grohens, Sabu Thomas, Nandakumar Kalarikkal," Investigations on the effect of EPDM content on mechanical, morphological, rheological and thermal properties of PP/EPDM blends" (Communicated)
- Praveen K.M , Khadidja Taleb, Isabelle Pillin, Antoine Kervoelen ,Yves Grohens, Sabu Thomas, Nandakumar Kalarikkal,"Investigations on the effect of FAS coated coir on mechanical, morphological, rheological and thermal properties of PP EPDM based composites" (Communicated)

Books edited

- Co-Edited a Book titled "*Nanotechnology-Driven Engineered Materials New Insights*" Published by Apple Academic Press jointly with CRC Press, Taylor & Francis Group
- Co-Edited a Book titled "*Engineering Technologies for Renewable and Recyclable Materials Physical-Chemical Properties and Functional Aspects*" Published by Apple Academic Press jointly with CRC Press, Taylor & Francis Group
- Co-Edited a Book titled "*Engineered Carbon Nanotubes and Nanofibrous Material Integrating Theory and Technique*" Published by Apple Academic Press jointly with CRC Press, Taylor & Francis Group
- Co-Edited a Book titled "*Physical Chemistry for Engineering and Applied Sciences Theoretical and Methodological Implication*" Published by Apple Academic Press jointly with CRC Press, Taylor & Francis Group
- Co-Edited a Book titled "*Theoretical Models and Experimental Approaches in Physical Chemistry*" Published by Apple Academic Press jointly with CRC Press, Taylor & Francis Group

- Co-Edited a Book titled “*Modern Physical Chemistry Engineering Models, Materials, and Methods with Applications*” Published by Apple Academic Press jointly with CRC Press, Taylor & Francis Group
- Co-Editing a Book titled “*Non-Thermal plasma Technology for Polymeric Materials*” Published by Elsevier

Books Chapters

- Communicated a Chapter *entitled “FIBER REINFORCED COMPOSITES: MACRO TO NANOSCALES”* to Springer Handbook of Functional Polymers Published by Springer
- Communicated a Chapter *entitled “Relevance of Plasma Processing on polymer materials and interfaces”* to a book entitled “Non-Thermal plasma Technology for Polymeric Materials” published by Elsevier

Papers presented in International /National Conferences

- Oral Presentation (Contributory Lecture) on “PLASMA SURFACE MODIFICATION EFFECTS ON THE INTERFACIAL PROPERTIES OF COIR FIBERS” at National Conference on Material Science and Technology” (NCMST-2015) Indian Institute of Space Technology, Trivandrum, Kerala, India

Posters presented in International /National Conferences

- Poster presentation entitled “*SEM and AFM evidencing the plasma modification effects on the surface features of coir fibers*” at Mahatma Gandhi University, Kottayam, Kerala, India on October 2015.
- Poster presentation entitled “*Polymer composites for neutron shielding applications*” at International Conference on Macromolecules: Synthesis, Morphology, Processing, Structure, Properties and Application (ICM 2016) held at Mahatma Gandhi University, Kottayam, Kerala, India on May 2016
- Poster presentation entitled “*Effect of HAF carbon black on Curing and Mechanical properties of Natural rubber-LDPE composites*” at International conference on Polymer Processing and Characterization (ICPPC – 2017) held at Mahatma Gandhi University, Kottayam, Kerala, India on December 2016
- Poster presentation entitled “*Investigation on Curing and Mechanical properties of Natural rubber-LDPE-Nano B4C composites for neutron shielding applications*” at Fourth International Conference on Nanostructured Materials and Nanocomposites (ICNM 2017) held at Mahatma Gandhi University, Kottayam, Kerala, India on February 2017.

